Winter 2011

Balloon Borne Mars Research Platforms

Sean Michael Hancock
Old Dominion University

BALLOON BORNE MARS RESEARCH PLATFORMS

by

Sean Michael Hancock
B.S. May 2008, Old Dominion University

A Thesis Submitted to the Faculty of
Old Dominion University in Partial Fulfillment of the
Requirement for the Degree of

MASTER OF SCIENCE

AEROSPACE ENGINEERING

OLD DOMINION UNIVERSITY
December 2011

Approved by:

_____
Robert L. Ash (Director)

_____
Colin P. Britcher (Member)

_____
Brett A. Newman (Member)

ABSTRACT

BALLOON BORNE MARS RESEARCH PLATFORMS

Sean Michael Hancock
Old Dominion University, 2008
Director: Robert L. Ash

Aerial platforms can fill a measurement gap between orbiters and rovers, providing planetary scale high resolution *in situ* measurements, access to scientifically interesting terrain that is either inaccessible or hazardous to rovers, and serve as a planet-wide delivery platforms to deploy surface probes and rovers to areas inaccessible given existing entry, descent, and landing systems. A permanent robotic outpost on the Martian surface can utilize locally-derived hydrogen as a lifting gas for balloon systems deployed from Mars. That approach can simplify the inflation and launch of aerial vehicles while allowing for a long duration deployment campaign that is not constrained by Earth-launch windows. The purpose of this thesis is to provide a high level evaluation of the size, type, instrumentation, and number of aerial vehicles necessary for a successful long duration planetary scale balloon mission. A series of "small" meteorological balloons (1,800 m^3) with radio sonde instrumentation similar to contemporary terrestrial meteorological sounding balloons can provide year round *in situ* vertical profile atmospheric measurements of pressure, temperature, humidity, and wind speed up to 20 km altitude, for verification of global circulation models. Larger (35,200 m^3 – 38,800 m^3) heavy payload balloons can provide long duration, planetary scale missions expanding atmospheric measurements and enabling high resolution geological, geochemical, and geophysical data – with a single balloon carrying a 100 kg payload floating at nominally 10 km above Mars reference surface altitude, capable of circumnavigating the planet more than three times during a conservative 20 sol mission. Incorporating buoyancy control into heavy payload balloon systems

may provide sufficient lateral control to enable the investigation of specific features of Mars or

even delivery of payloads to locations that are inaccessible to entry, descent, and landing systems.

This thesis is dedicated to my wife Debbie, who inspired me to pursue my dreams and tirelessly loved, supported, and motivated me through my efforts. Thank you.

ACKNOWLEDGMENTS

This thesis could not have been written without the untiring efforts of Dr. Robert Ash, who provided hours of consultation and direction during my research and throughout the editing of this manuscript. Deborah Fairbrother deserves special acknowledgement her technical guidance in balloon design, fabrication, and launch and for sharing her experiences with NASA's balloon program. I would like to thank Carl Justus, who provided the necessary expertise to utilize the Mars-GRAM 2005 software, and I extend my heartfelt gratitude to Saito Yoshitaka who shared his experience and knowledge in the development and utilization of ultra-thin balloon films. Lastly, I would like to thank my committee members for their guidance and contributions to the successful completion of this thesis.

NOMENCLATURE AND ABBREVIATIONS

a	acceleration, $kg \cdot m / s^2$
a	planetary albedo
c	distance between balloon tendons, m
d	diffusion rate
f	free lift ratio
g	acceleration of gravity, $kg \cdot m / s^2$
h	convective heat transfer coefficient, $W / m^2 \cdot K$
m_b	mass of balloon – including payload support structure, kg
m_g	mass of lifting gas in the balloon, kg
$m_{payload}$	mass of balloon payload, kg
m_{sys}	mass of balloon system, kg
n	number of gores
p	partial pressure of gas across balloon film, kPa
r_{gore}	pumpkin balloon gore radius curvature, m
r_{sphere}	radius of spherical balloon, m
s	manufactured gore width
t	thickness, m
t	time, s
u	balloon velocity relative to local atmosphere, m / s
z	geopotential altitude, m
A_{proj}	balloon projected area, m^2
A_{surf}	balloon surface area, m^2

C_D		drag coefficient
D		balloon diameter, m
D		drag force, N
F		free lift force, N
F_B		buoyant force, N
I_{sun}		solar constant, W/m^2
L_s		solar longitude, deg
P_∞		ambient atmospheric pressure, kPa
R		ideal gas constant, $J/kg \cdot K$
S		reference area, m^2
T_b		mean temperature of balloon, K
T_g		temperature of lifting gas, K
T_p		temperature of planetary surface, K
T_s		temperature of space and upper atmosphere, K
T_∞		ambient atmospheric temperature, K
V_b		balloon volume at any given altitude, m^3
V_{max}		fully inflated balloon volume, m^3
$\dot{Q}_{abs-g}$		rate of radiative energy absorbed by lifting gas, W
$\dot{Q}_{conv-atm}$		rate of convective heat transfer between balloon film and atmosphere, W
$\dot{Q}_{conv-g}$		rate of convective heat transfer between balloon film and lifting gas, W
$\dot{Q}_d$		direct solar heat rate, W
$\dot{Q}_{i-g}$		rate of internally generated heat, W

$\dot{Q}_r$	reflected solar heat rate, W
$\dot{Q}_{rad-Mars}$	rate of energy radiated to Mars, W
$\dot{Q}_{rad-space}$	rate of energy radiated to space, W
$\dot{Q}_s$	scattered solar heat rate, W
W	weight, N
α	lobe half angle, deg
α	solar absorptivity of balloon envelope
δ	film permeability
ε	infrared emissivity of balloon envelope
σ_{hoop}	pumpkin balloon skin hoop stress, kPa
σ_{skin}	balloon skin stress, kPa
σ	Stefan-Boltzman constant, 5.6704×10^{-8} W/ m$^2 \cdot$ K^4
ρ_g	lifting gas density, kg / m^3
ρ_∞	local ambient atmospheric density, kg / m^3
ρ^*	ambient atmospheric density at float altitude, kg / m^3
ζ	cosine of local solar zenith angle
Δp	balloon superpressure, kPA
CMET balloons	Controllable Meteorological balloons
DCI	Dust Cover Index
EDL	entry, descent, and landing
FMI	Finnish Meteorological Institute
GCM	Global Circulation Model
GFSK	Gaussian Frequency Shift Keying

GISS	Goddard Institute for Space Studies
IR	Infrared Radiation
ISAS	Institute of Space and Astronautical Science
JAXA	Japan Aerospace Exploration Agency
LTST	Local True Solar Time
MABS	Mars 2001 Aerobot-Balloon System
MABVAP	Mars Balloon Validation Program
MAP	Mars Aerial Platform
Mars-GRAM	Mars Global Reference Atmospheric Model
MDO	Machine Direction Orientation
MEPAG	Mars Exploration Program Analysis Group
MET balloons	Meteorological Balloons
MGCM	NASA Ames Mars General Circulation Model
MGS	Mars Global Surveyor
MOLA	Mars Orbital Laser Altimeter
MRO	Mars Reconnaissance Orbiter
MTGCM	University of Arizona Mars Thermospheric General Circulation Model
NASA	National Aeronautics and Space Administration
PBO	Poly(p-Phenylene-2,6-BenzobisOxazole)
PET	Polyethylene Terephthalate
TAO	Take-off, Ascent, and Orbit Insertion
TDO	Transverse Direction Orientation
TES	Thermal Emission Spectrometer
UHF	Ultra High Frequency
ULDB	Ultra Long Duration Balloon
UTC	Coordinated Universal Time

UV	Ultraviolet Radiation
VL1	Viking Lander 1
VL2	Viking Lander 2

TABLE OF CONTENTS

LIST OF TABLES

LIST OF FIGURES

CHAPTER 1
INTRODUCTION

Exploration of Mars has proceeded from the early flyby missions, capable of conducting observations for a few days at the closest approach, to orbiters, capable of observing the planet for months or years at a relatively close range, and finally to landers and rovers operating on the surface and making *in situ* observations. Despite the successes enjoyed to date by the Mars exploration program, a resolution gap exists in measurements between orbiters and surface landers and rovers.

The geography and atmosphere of Mars is complex and includes physical and chemical properties that vary over large temporal and geographic scales. A thorough understanding of these geographic and atmospheric features is necessary for the scientific understanding of the origins of Mars as well as the success of future manned missions to Mars. Mars displays a varied geological history, including evidence of impact, volcanic, and tectonic processes and wind and liquid water erosion. The 2008 Mars Exploration Program Analysis Group (MEPAG) report entitled *Scientific Goals, Objectives, Investigations, and Priorities* (MEPAG, 2008), known as the "Goals Document," prioritizes understanding the Martian climate, including understanding the current atmosphere and climate, understanding recent climate history, and understanding ancient climate history. To thoroughly understand the varied environment, extended duration, high resolution, multipoint, *in situ* measurements are needed.

Orbiters can provide full planetary scale low to medium resolution remote imagery. Landers and rovers can provide high resolution imagery and *in situ* measurements, including atmospheric measurements made during entry, but only in their immediate vicinity. The restrictions on the mobility of rovers were made evident by *Sojourner*, *Spirit*, and *Opportunity* – realistic travel distances are limited to tens of kilometers per year at relatively obstacle free sites while large areas of Mars are inaccessible altogether. Aerial platforms can complement and

extend orbital and landed measurements by filling the resolution gap between orbiters and surface

rovers and landers, providing planetary scale *in situ* measurements with image resolution orders

of magnitude greater than orbiters while providing access to scientifically interesting terrain that

is either inaccessible or too hazardous for surface rovers and landers, serve as a planet-wide

delivery systems to deploy surface probes and rovers to areas inaccessible given existing entry,

descent, and landing systems, and allow for *in situ* atmospheric measurements for durations

significantly longer than entry probes.

Aerial platforms have been proposed that range from powered aircraft, gliders,

helicopters, and lighter-than-atmosphere (LTA) systems (Wright et al., 2004). Flight duration for

gliders is heavily dependent on wind and updrafts which are not well understood, especially

locally. Powered aircraft and gliders require significant energy expenditure to generate lift which

constrains flight time. LTA system (i.e. balloon) performance at float altitude can be understood

and modeled to the degree of knowledge available characterizing the ambient and radiative near-

surface environment of Mars and offer the potential for extended flight duration over long

traverses utilizing a relatively simple system. The development of aerial vehicles capable of

operating in the Mars environment has been of interest to many scientists since the successful

Soviet Venera-Vega flights in the atmosphere of Venus in 1985 demonstrated the technical

feasibility of deploying a balloon at another planet and utilizing it as a platform for scientific

observations. That mission consisted of two identical 3.4 m diameter helium inflated

superpressure balloons, each carrying a 6.7 kg gondola and floating at a nominal 54 km altitude.

A Soviet-French-American experiment tracked the balloons for two Earth days collecting

pressure, temperature, and wind speed data until the onboard batteries ran out of power (Sagdeev

et al., 1986). The actual duration of the floating balloon platforms is unknown.

Terrestrially, balloons are routinely used as aerial platforms for scientific observations.

In the past, planetary balloon missions were hampered, because the science return was small

when compared to landers and rovers due to mission lifetime. Today, technological

improvements in balloon materials and fabrication, payload miniaturization, and demonstrated

performance of terrestrial unmanned aerial vehicles (UAVs) and planetary autonomous

operations (rovers) make autonomous balloon systems for planetary exploration a viable concept.

Conceptual designs for Mars balloons have been proposed and some even tested utilizing aerially

deployed balloons.

Building on the experience gained from the Venera-Vega mission, Soviet and French

scientists began work on a Mars balloon mission for the 1994 Mars opportunity. The system

consisted of a 6-micron Mylar balloon suspending a guiderope from the gondola. During

daylight the balloon would be overpressured. At night, the balloon would descend and rest on the

surface on the guiderope, with the mass of the guiderope on the surface relieving the night time

loss in balloon buoyancy so the gondola instrument platform would not touch the surface. The

mission was projected to last about 10 days, constrained by gas leakage from the balloon

(Tarrieu, 1993). The collapse of the Soviet Union resulted in the delay of the planned mission to

1996 and eventually to the 1998 launch opportunity. Programmatic and technical problems

eventually resulted in program cancellation.

In 1994, under the NASA Discovery Program, the Mars Aerial Platform (MAP) mission

was proposed. The MAP mission was to consist of three 12-micron, biaxial nylon 6,

superpressure balloons. Each balloon would suspend a 7 kg gondola and be designed to float at a

nominal 6 km constant density altitude. The three balloons were to be deployed during descent

by three identical entry capsules in the northern, southern, and equatorial zones. The MAP

mission succumbed to a lack of technology readiness, primarily with balloon envelope design.

(Greeley et al., 1996)

In late 1995, the Mars Aerobot/Balloon Study (MABS) was initiated by NASA in

conjunction with the NASA stratospheric balloon research program at NASA's Wallops Flight

Facility (WFF). The MABS study built on the work of the MAP mission and achieved great

advancements in applicable superpressure balloon design and fabrication technologies, including

supporting the formulation of NASA's Ultra-Long Duration Balloon (ULDB) project, a 100 day terrestrial scientific stratospheric balloon, through WFF. The MABS study baselined aerial deployment of a superpressure balloon. The MABS study pushed planetary balloon technology, both in envelope materials and balloon geometry, to a level that makes Mars superpressure balloon systems feasible today (Nock et al., 1997).

In 1997, the Mars Balloon Validation Program (MABVAP) was established with the primary objective of validation of the aerial deployment and inflation of thin-film light-gas balloons in Martian-like environment. The program included laboratory, wind tunnel, and vacuum chamber tests of system components. Tropospheric and stratospheric flight tests of deployment and inflation of light film balloons in a relevant Martian environment were also conducted. The program culminated in the first aerial deployment and inflation of a small Mars-like superpressure balloon in Earth's stratosphere (Kezhanovich et al., 2004). Aerial deployment continues to be a challenge requiring improved risk reduction strategies, while being complicated further by severe mass limitations on the balloon coupled with the rarefied Martian atmosphere and the balloon loads experienced during aerial deployment. Entry, descent, and deployment (EDD) of the Mars Exploration Rover missions, which included inflation phases, lasted approximately six minutes (Steltzner et al., 2003). This provides minimal time for balloon deployment and inflation. Aerial deployment places tight constraints on balloon and payload size and mass.

A permanent robotic outpost on the surface incorporating surface-launched balloon systems could simplify the inflation and launch of aerial vehicles while simultaneously allowing for a long duration balloon-based exploration campaign consisting of both MET sounding balloons and large scientific exploration balloons. Furthermore, the near-surface availability of water ice on Mars between the poles and mid-latitudes has now been documented to the point where water can be considered as a feed stock for *in situ* resource production (see Byrne, et al., 2009, and Mathieu, Forget and Mustard, 2010, for example). Since Mars atmosphere is more

than 95% carbon dioxide by volume, the use of hydrogen produced by electrolysis of local water is a logical and appropriate lifting gas. The systems needed to locate, then extract water ice from Mars regolith, along with the hardware required to separate and possibly purify water for electrolysis are not yet defined. However, there are no apparent technology gaps that would need to be overcome in order to develop and qualify those systems for Mars applications. Consequently, it is assumed that replenishable hydrogen will be available for exploration systems deployed from a fixed Mars surface outpost.

In June, 2004, the MEPAG chartered Mars Human Precursor Science Steering Group concluded one of the highest priority Mars investigations that would have a significant effect on reducing the cost and risk of the first human mission to Mars is to determine the variation of atmospheric properties between the surface and 90 km which would affect entry, descent, and landing (EDL) and take-off, ascent, and orbit insertion (TAO) for both normal ambient conditions and also during dust storms, because during both EDL and TAO, any atmospheric abnormalities in density or unexpected wind forces could result in significant variations from planned trajectories (Beaty et al., 2005). There are two regions where atmospheric uncertainties can cause significant risk to both EDL and TAO. Between 0 and 20 km, the significant risk is turbulence derived wind forces in the planetary boundary layer caused by convective systems and topographically driven winds. In this same regime, turbulence and the electrical fields created by dust storms are not well understood and pose significant risks. Between 30 and 60 km, the significant risk is density anomalies that occur while entry and ascent vehicles are at maximum dynamic pressures, experiencing maximum acceleration. Martian atmospheric densities between 0 and 20 km can provide sufficient buoyancy to support planetary balloons. Terrestrial scientific balloons have regularly been flown to altitudes greater than 50 km (Saito et al., 2006) where atmospheric conditions are comparable to Mars ambient conditions 20 km above the reference surface altitude. An extended duration MET sounding balloon campaign could provide valuable information in the 0 to 20 km regime on the planetary boundary layer and the exchange of heat,

mass, and momentum from the surface to the upper atmosphere, serving to validate remote measurements from orbiting spacecraft, while providing baseline and boundary condition data for atmospheric Global Circulation Models (GCM). Those measurements could also facilitate GCM validation directly. In addition, long term *in situ* measurements could provide seasonal and diurnal trend data for atmospheric flows and atmospheric dust transport.

Large scientific balloons offer the capability of high resolution surface imaging, *in situ* measurements of the atmosphere, radar soundings of the subsurface, and/or gravity and magnetic measurements, and these measurements can be made at a planetary scale over terrain that is inaccessible to rovers or landers. Depending on the season, a balloon could potentially circumnavigate the planet in approximately a week, driven by winds, with no fuel expenditure. Additionally, heavy payload balloons offer the capability for lifting and moving instrumented packages and small rovers from one surface location to another. Current EDL technology constrains landed payload mass to well below a metric ton with landing footprints on the order of hundreds of kilometers while limiting simultaneously landing sites to low altitudes with respect to the reference MOLA areoid in order to provide sufficient atmospheric depth to accommodate deceleration (Clark et al., 2009). Inclusion of a balloon platform buoyancy control system could potentially allow sufficient lateral trajectory control to enable the investigation of specific regions of Mars with delivery of payloads to locations that are inaccessible using current EDL technology.

The goal of this thesis is to present a high level system engineering analysis for a Mars surface exploration element utilizing locally-deployed balloons. Analysis includes balloon sizing and design, payload considerations, and a conceptual launch system. Two balloon systems have been considered in this study – small MET balloons for atmospheric sounding, and large scientific balloons for planet-wide surface science.

CHAPTER 2

MARS BALLOON FLIGHT ENVIRONMENT

2.1 PRESSURE

Mars atmospheric composition was measured accurately during the Viking mission and is summarized in Table 1, where it can be seen that CO_2 constitutes more than 95% of the atmosphere (Alexander, 2001). The high percentage (by volume) of carbon dioxide and Mars' low average surface temperature result in the condensation and sublimation of significant quantities of carbon dioxide at the poles between winter and summer, producing significant seasonal winds along with large variations in local ambient pressure. Due to its elliptic orbit, the seasonal transport rate of carbon dioxide between the poles differs significantly, and Mars surface pressure varies annually by as much as 20% from the annual mean (Hourdin et al., 1993). The Earth does not have an equivalent cycle, because the primary volatile components of Earth's atmosphere, H_2O and CO_2, represent only 0.4% and 0.038% of the total composition respectively. Seasonal variations in the ambient pressures measured at the Viking I and Viking II lander sites are shown for one Mars year in Figure 1. As atmospheric carbon dioxide condenses during fall/winter at one pole, the atmospheric CO_2 sublimates at the opposite pole (spring/summer). This process leads to a decrease in atmospheric pressure at the fall/winter pole, and an increase in atmospheric pressure at the spring/summer pole, driving mass flow from the warm pole to the cold one.

From Figure 1, it can be seen that the pressure minimum during late winter in the southern hemisphere is lower than the pressure minimum during the corresponding late winter period in the northern hemisphere. Concurrently, the pressure maximum during southern early summer is higher than the pressure maximum during northern early summer. The disparity between the northern and southern polar CO_2 condensation –

sublimation cycles is a result of the eccentricity of Mars' orbit, resulting in a shorter, less

cold northern winter than southern winter.

Atmospheric Composition of Mars as measured by Viking Landers	
Carbon Dioxide	95.32%
Nitrogen	2.7%
Argon (40)	1.6%
Oxygen	0.13%
Carbon Monoxide	0.07%
Water Vapor	0.03%
Argon (36), Neon, Krypton, Xenon, Ozone, Methane	trace

Table 1: Atmospheric Composition of Mars as Measured by Viking Landers.
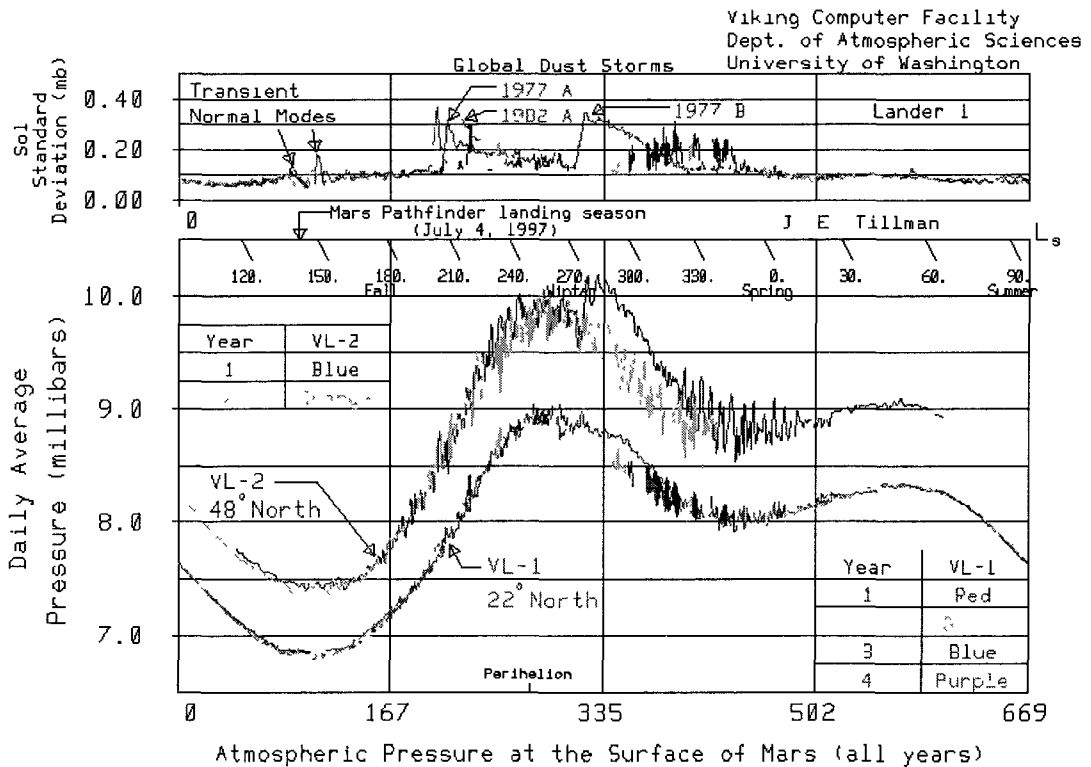
Figure 1: Surface Pressure at Mars as Measured by Viking Landers (Courtesy of J. E. Tillman, University of Washington, Dept. Atmospheric Sciences).

Figure 1 also shows sol to sol variations in ambient pressure which can represent significant deviations from the sol mean. Shorter period pressure cycles can be attributed to frontal weather activity, including dust storms and global oscillations. Frontal activity is indicated by large sol to sol variability. Pressure variations due to dust storms tend typically to have longer periods with reduced or minimal sol to sol variation (Zurek, 1976). Global pressure oscillations are seasonal and are believed to be temperature dependant (Tillman, 1988) with a nominal period of one sol.

The surface pressure, as measured by Viking Lander 1 at 22°N follows the same trend as that measured by Viking Lander 2 at 48°N; however the sol mean surface pressure at the Viking Lander 2 site is higher than that at the Viking Lander 1 site. Figure 1 demonstrates that the annual pressure cycle varies greatly with Mars location. This is believed to be due to Martian orography and geostrophic winds (Hourdin et al., 1993).

2.2 TEMPERATURE

Like ambient pressure, Mars surface temperatures are subject to periodic cycles. These cycles include seasonal variations, sol to sol variations that may be caused by frontal activity or dust storms, and varying diurnal cycles. The low overall absolute temperatures are a result both of the distance from the sun and the thin Martian atmosphere, which is insufficient to support significant greenhouse heating effects.

The diurnal temperature cycle measured at the Pathfinder and VL1 landing sites is displayed in Figure 2. It can be seen that the near surface temperature can vary by about 65 K during a single sol. By superimposing VL1 data (measured at 1.6 m above the surface) over Pathfinder data (measured at 0.25 m, 0.5 m, and 1.0 m above the surface), measured at similar latitude and longitude, Tillman (1998) was able to show that the atmospheric temperature decreases significantly with height above the surface. Because the atmosphere is so thin, it has minimal thermal inertia, resulting in large temperature variations due to changes in heat input and

mechanical forcing from the regolith. Diurnal temperature variations are controlled primarily by

solar heating and night time infrared cooling of the surface to the atmosphere and into space.

Heat exchange between the atmosphere and the surface occurs in the planetary boundary layer

whose local night time thickness varies from tens to hundreds of meters, and during the day time

is on the order of 5 km thick (Savijärvi and Sili, 1993). Within this layer, the exchange of

momentum, heat, and moisture between the surface and the atmosphere are due primarily to wind

and turbulence, strongly affecting the thermal profile of the atmosphere.
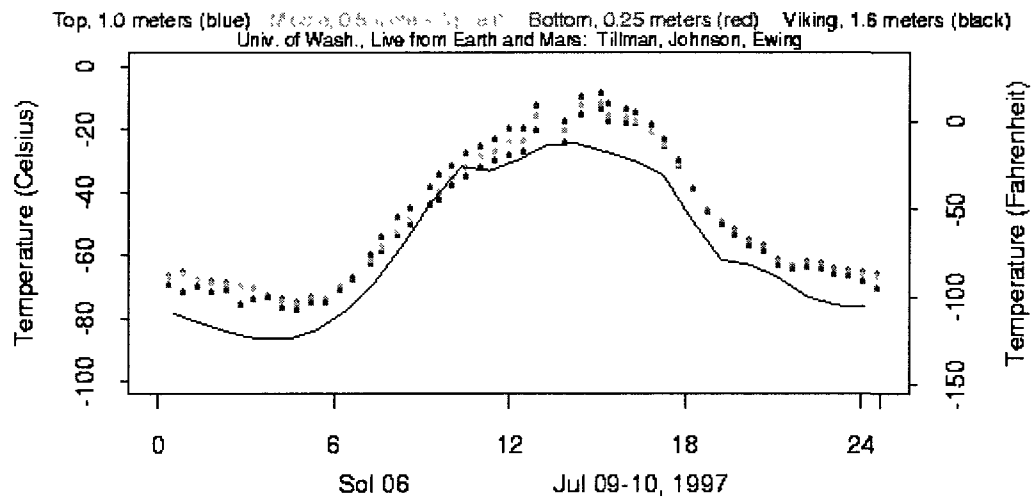
Figure 2: Diurnal Temperature Variation on Mars as Measured by VL1 and Pathfinder (Courtesy of J. E. Tillman, University of Washington, Dept. Atmospheric Sciences).

2.3 HUMIDITY

While water vapor on average only makes up approximately 0.03% of Mars' atmosphere,

during most seasons, the night time atmosphere is saturated over much of the planet. During

daytime, the relative humidity is much lower. The exception to this is the southern hemisphere

during summer. During southern arctic summer, the absolute humidity rises only until it equals

the amount of water vapor in the atmosphere in the equatorial region even though the atmosphere

is capable of holding substantially more water. While the northern arctic region has sufficient

local water sources to saturate the atmosphere at night, southern arctic water vapor is transported through the atmosphere from the equatorial region (Davies, 1979). Even though there is insufficient water vapor to impact atmospheric density, high relative humidity can lead to ice-water clouds or fog around mountains, and contributes to morning fog as well. Additionally, the visible North Polar Hood is made of water ice clouds (Cattermole, 2008). These clouds and fog can impact the balloon radiation environment.

2.4 WINDS

Currently, wind is the primary transport process shaping the surface of Mars. Martian winds are created by the global sublimation-condensation cycle driving mass flow from the warm pole to the cold one, and infrared heating and cooling causing warm atmosphere to rise, cold atmosphere to sink, and dense atmosphere at the surface to move towards areas where warm atmosphere is displaced upward. The Coriolis Effect results in average wind directions that are nearly parallel to the equator.

Martian winds have generally been measured *in situ*, ranging from breezes of up to 10 m/s, while increasing to near 30 m/s during strong frontal activity in fall and winter. Winds can occasionally rise to over 50 m/s, especially near the poles (Tillman, 1985; 1988). The winds lift small dust particles from the surface and those particles can impact larger regolith particles, ejecting them into the atmosphere (via saltation) and these wind-dust interactions sometimes produce dust storms that engulf the entire planet.

Dust devils are a common atmospheric feature on Mars as well and they have been observed at almost all elevations (Balme and Greeley, 2006). Dust devils are thermally driven vortices that contribute significantly to overall dust transport and atmospheric haze. As a result, dust devils impact atmospheric temperature by affecting solar heating and infrared cooling. The low pressure core of this type of vortex has proven to be very effective at lifting even fine-grained particles; however the overall contribution of dust devils to atmospheric dust loading is still not

fully understood. Terrestrial dust devil observations have demonstrated that terrestrial dust devils occur in late morning and afternoon, with peak activity occurring between 1300 and 1400 h, then ending after 1700 h local solar time (Sinclair, 1969), and *Spirit/Pathfinder* data have compared favorably with the terrestrial observations (Stanzel et al., 2008). Dust devils cores can range in size up to a few hundred meters in diameter and the axial vortex column can extend up to several kilometers in height, while moving with the general circulation. Although it was expected that the dust devil season was confined to the summer seasons for both hemispheres, observations from the Mars Express High Resolution Stereo Camera have detected a clear peak of dust devil activity in the southern hemisphere summer, but a majority of northern hemisphere dust devils have been observed to occur in the spring (Stanzel et al., 2008).

Viking Lander wind observations indicated regular slope winds which are attributable to the large diurnal surface temperature gradient, a result of the predominantly infrared nature of the atmospheric heat transfer coupling with the surface. Daytime anabatic upslope winds result when the sun heats topographic slopes, creating warmer, less dense atmosphere that rises up the slopes. At night, as the slopes cool, katabatic downslope winds result from the falling cooler and more-dense atmosphere flowing into less dense atmosphere. Katabatic downslope winds tend to be stronger than anabatic upslope winds. Conditions for slope winds are favorable on Mars in summer (Savijärvi and Sili, 1993).

Since the atmospheric pressure at the surface of Mars is less than 1% of Earth ambient surface pressure, the wind forces (dynamic pressure) on Mars are lower by a factor of 100 than the wind forces caused by a comparable terrestrial wind velocity. Currently, the lack of knowledge of near-surface Martian winds and their variability is the dominant error source in predicting entry trajectories. Because winds will serve as the primary motive force for balloon motion, analysis of balloon trajectories will provide significant insight into atmospheric winds. The variable nature of atmospheric winds will be discussed further in Chapter V as a means of controlling exploration balloon trajectories.

2.5 DENSITY

The linear dependence of aerodynamic forces on density makes it essential to have an accurate vertical profile of atmospheric density. The composition of Mars' atmosphere lends itself to the use of an ideal gas model as a very accurate engineering model for estimating atmospheric density variation. Furthermore, atmospheric density is subject to the same variations that affect atmospheric pressure, i.e. temperature, and composition – including geographic, diurnal, sol to sol, and seasonal influences – and is highly dynamic.

The difficulty in accurately predicting the local density of Mars atmosphere was demonstrated by the aerobraking behavior of the Mars Reconnaissance Orbiter (MRO). MRO accelerometer-derived densities showed that periapsis density from orbit to orbit could vary significantly. Atmospheric densities calculated from accelerometer measurements aboard the MRO differed by up to 200% from the Mars Global Reference Atmospheric Model (Justh et al., 2006). Mars-GRAM is an engineering level atmospheric model. The current version, Mars-GRAM 2010, is based on the NASA Ames Mars General Circulation Model (MGCM) approximating atmospheric behavior from the surface up to 80 km, and on the University of Arizona Mars Thermospheric General Circulation Model (MTGCM) for altitudes greater than 80 km. The Mars-GRAM model is updated regularly to ensure agreement with measurements (Justus et al., 2002). Additionally, *in situ* measurements have shown strong latitudinal and seasonal variability in atmospheric density and the significant impact of dust storms, further-complicate atmospheric density predictions (Barlow, 2008). The dynamic nature of atmospheric density will play an important role in balloon sizing and overall system design in Chapters IV and V.

2.6 DUST

Airborne dust plays a significant role in atmospheric heating and dynamics. Dust acts as a moderator in the global climate system by increasing the optical depth of the atmosphere and thus reducing solar and thermal radiation coupling with the surface, thereby impacting the heating rates of the surface and atmosphere and impacting the planetary atmospheric circulation (Szwast et al., 2006).

Analysis of Mars Global Surveyor (MGS) and Viking Orbiter observations by Szwast *et al.* (2006) has shown a correlation between albedo and surface dust. High albedo was indicative of significant accumulations of surface dust. Removal of dust from the surface which is typically darker than the dust, lowers the albedo (Szwast et al., 2006). Figure 3 represents a visual comparison of the MGS Thermal Emission Spectrometer (TES) dust cover index (DCI) with albedo. The DCI is a method created by Ruff and Christenson (2002) to map fine-grained silicates using thermal infrared spectra, and is defined as the average emissivity, measured at wave numbers between 1350 and 1400 cm^{-1}. It should be noted that while albedo correlates well with dust coverage on year-to-year timescales, short term and seasonal changes in albedo do not appear to be related to dust coverage.

It is generally believed that there is a seasonal "dust cycle" on Mars, but this cycle is complex with significant year-to-year variations that are neither well understood nor predictable. Based on MGS observations, global dust storms are responsible for the largest changes in dust concentration. Seasonal winds, local and regional dust storms, and extra-tropical cyclones also contribute significantly to dust concentration dynamics; however dust devils and small-scale dust lifting events do not appear to be significant overall contributors (Szwast et al., 2006).

From the balloon design perspective, high dust optical depth reduces diurnal variations in atmospheric radiation, minimizing the diurnal variation in balloon envelope superpressure levels. However, the balloon envelope has to be designed to tolerate the more-extreme superpressure

variations, which will occur at a nominal optical depth of zero. Additionally, dust deposition can result in added mass to a balloon and generally represents a threat to balloon and payload survival.
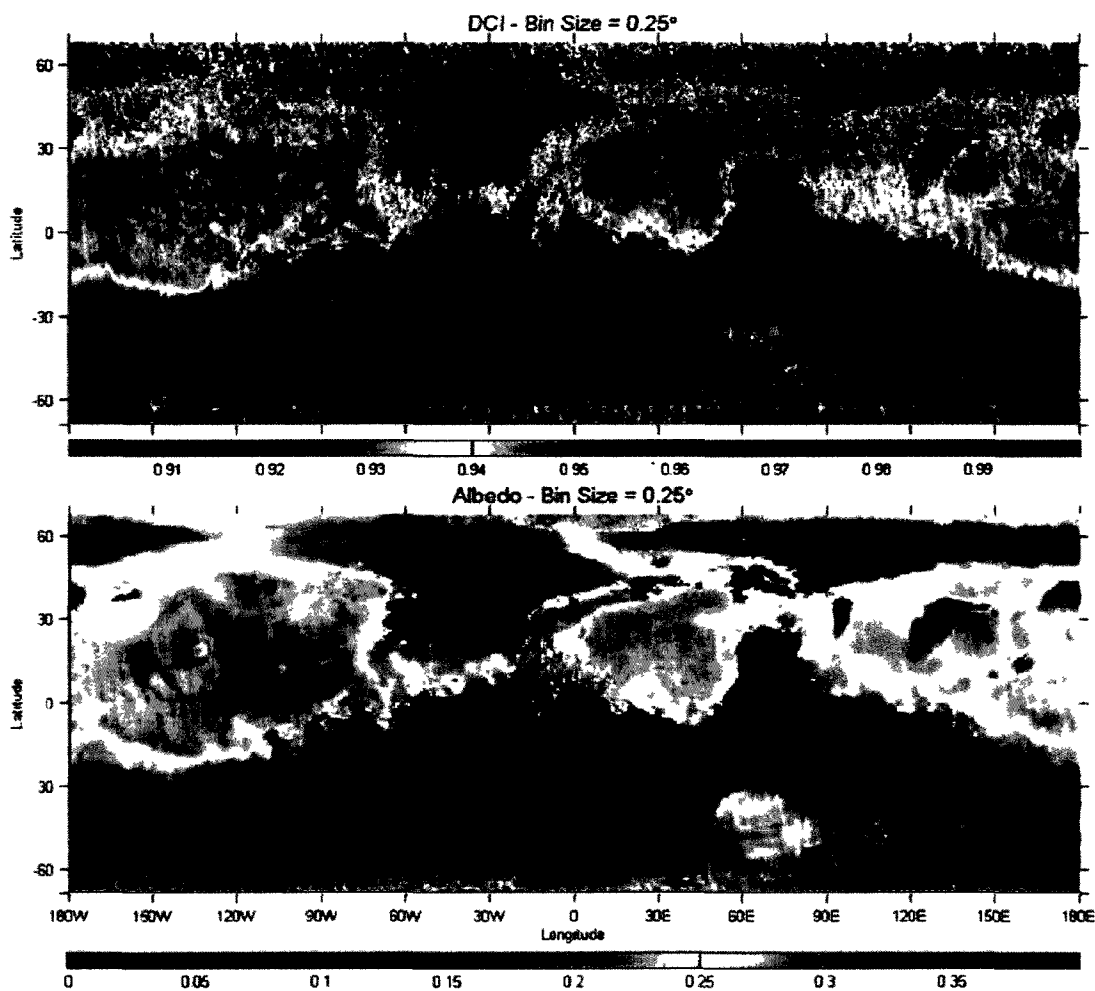
Figure 1: MGS TES DCI Versus Albedo. Both are Binned by 0.25 of Latitude and 0.25 of Longitude and Averaged over the Entire MGS Mission (Szwast et al., 2006).

CHAPTER 3

BALLOON DESIGN CONSIDERATIONS

3.1 ZERO-PRESSURE AND SUPERPRESSURE BALLOON BASICS

Terrestrial high-altitude balloon technology has benefitted from recent developments in envelope materials, fabrication techniques and overall system designs, requiring a review of the state-of-the-art in terms of potential for Mars applications. The three most common types of scientific and meteorological research balloons are: extensible, zero-pressure, and superpressure balloons. Recently, solar heated Montgolfier balloons have also been proposed as aerial platforms for Mars research (Jones et al., 1999).

Extensible balloons are generally used terrestrially as radio-sonde atmospheric sounders. Those balloons are inflated with a lifting gas (hydrogen, helium, ammonia, or methane), sealed, and allowed to rise. As the balloon ascends and the atmospheric pressure decreases, the balloon envelope – often latex - stretches, and the balloon volume increases until the balloon film ultimately ruptures.

Zero-pressure balloons utilize non-extensible, light-weight material to contain a fixed mass of buoyant fluid. Zero-pressure balloon systems carry scientific instruments to a predetermined density altitude where the buoyant fluid has expanded in response to the local ambient pressure (Yajima et al., 2009). The balloon is partially filled with lifting gas at launch. As the balloon ascends, the lifting gas expands until the envelope becomes fully inflated – the altitude of initial full inflation. At this point, these balloon systems utilize a balloon duct control valve to vent excess lifting gas, preventing balloon pressurization. The resulting lifting gas mass decrease lowers its gas density, resulting in additional buoyancy-derived lift. The balloon continues to rise via this venting process until it reaches its design constant-density equilibrium floating altitude where the buoyant force equals the total system weight and the pressure differential between the balloon lifting gas and the surrounding atmosphere is zero. These

balloons float at this altitude until the ambient conditions change. At typical float altitudes the ambient environment is controlled primarily by the thermal radiation environment. If the temperature increases, more gas is vented, however the balloon stays fully inflated. If the temperature decreases, the lifting gas contracts and the balloon volume decreases causing the balloon to descend, where the ambient pressure is higher, causing the balloon volume to decrease further. Consequently, the balloon can continue to descend toward the ground unless it achieves another equilibrium altitude or until ballast is released. Zero-pressure balloons cannot be used for long duration flights, because of the loss of buoyancy associated with night-time cooling – this affect would be magnified in Mars' thin atmosphere. They are, however, very effective for short duration, heavy payload flights.

Solar heated Montgolfier balloons are a special class of zero-pressure balloons that use the ambient atmosphere as the lifting gas and radiant heating of the lifting gas to provide the necessary buoyancy. Solar heated Montgolfier balloons have an opening at the envelope bottom for filling the balloon. A control vent at the top of the balloon can release envelope gas, allowing the balloon to descend or, when closed, allow the envelope gas to be heated radiantly and thus expand causing the balloon to rise. In this way, solar heated balloons can achieve somewhat controlled flight and even controlled soft-landings. Solar heated balloons have been proposed for short-duration flights at Mars with the possibility of multiple landings for controlled roving/landing and also as an entry decelerator (Jones et al., 1999).

Superpressure balloons also utilize non-extensible envelope materials, but the balloon film is designed to tolerate the pressure differential required to float at a constant density altitude where the internal pressure of the lifting gas is greater than the ambient atmosphere. Superpressure balloons are partially inflated with the lifting gas and sealed, prior to launch. As the balloon ascends, the lifting gas expands in much the same way as a zero-pressure balloon, increasing the balloon volume until the envelope becomes fully inflated. From the initial full-inflation altitude, the balloon continues to rise, progressively converting excess free lift to internal

pressures greater than the ambient pressure until the constant-density equilibrium floating altitude is reached. Unlike the zero-pressure balloon, the buoyancy of the superpressure balloon is not affected by changes in the radiation environment (Yajima et al., 2009). A properly designed superpressure balloon withstands internal temperature fluctuations by accommodating the associated variations in internal pressure, thus maintaining a constant balloon volume and associated buoyant force, enabling the balloon to continue to float at its constant-density altitude. During the day, the effective balloon temperature increases by absorbing solar energy, and that increase in temperature results in a proportional increase in internal pressure and superpressure. The tensile strength of the balloon envelope limits the maximum allowable pressure differential between the lifting gas and the ambient atmosphere. As a result, a relief valve is incorporated in the balloon system to prevent the balloon pressure from exceeding its predetermined design limit. The pressure can increase either until the temperature stops increasing or until the preset pressure differential is reached. If the temperature continues to increase, valving will continue until the gas temperature reaches its maximum. The balloon will not release gas again unless the previous temperature maximum is exceeded. At night, the balloon temperature drops rapidly due to infrared radiant cooling (to the atmosphere and into space), and the balloon pressure drops proportionally. For the balloon to maintain constant altitude, sufficient lifting gas must remain after the daytime temperature maximum has been reached so that the balloon pressure remains above ambient atmospheric pressure. Because a super-pressure balloon only loses lifting gas mass through valving, leaking, or diffusion of the lifting gas through balloon envelope, super-pressure balloon systems are particularly well suited for long duration flights.

3.2 BALLOON GOVERNING EQUATIONS FOR BUOYANCY AND LIFT

The buoyant force on a balloon is based on Archimedes' Principal which states that the buoyant force on an object is equal to the weight of the fluid displaced by that object:

$$F_B = \rho_\infty V_b g \,, \tag{1}$$

where ρ_∞ is the local atmospheric density, V_b is the volume of the balloon, and g is the local gravitational constant. Balloon free lift is defined as the total buoyant force of the balloon minus the total weight of the balloon system, i.e.:

$$F = F_B - W \tag{2}$$

where W is the weight of the total balloon and payload system. The free lift ratio, f, is defined as the ratio of free lift to the weight of the total system:

$$f \equiv \frac{F}{m_{sys} g} \tag{3}$$

where m_{sys} is the total system mass defined as:

$$m_{sys} = m_b + m_{payload} + m_g \tag{4}$$

with m_b defined as the balloon mass, $m_{payload}$ as the mass of the payload, and m_g as the mass of the lifting gas within the balloon. A force balance on the balloon, assuming no vertical wind component and that the balloon is in equilibrium and neutrally buoyant yields:

$$F = \rho_\infty V_b g - m_{sys} g = 0 \tag{5}$$

A neutrally buoyant balloon will float at a constant density altitude without rising or falling. For the balloon to rise, $F > 0$. In that case, the balloon system will be accelerated upward and, assuming the shape of the balloon is rigid and neglecting any dynamic coupling between forces on the balloon and payload (see Figure 4), the equation of motion becomes:

$$F_B - W - D = m_{sys}a \qquad (6)$$

or

$$\rho_\infty V_b g - m_{sys}g - \frac{1}{2}\rho_\infty u^2 C_D S = m_{sys}a \qquad (7)$$

where D is the drag force, u is the relative velocity (with respect to atmosphere motion) of the rising balloon, C_D is the drag coefficient, S is the reference area of the balloon cross section, and a is the acceleration of the balloon.
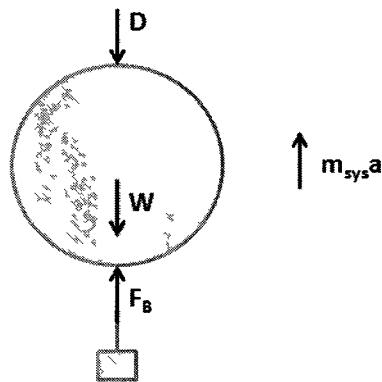
Figure 4: Balloon Free Body Diagram.

From Equation (7), a differential equation can be developed to express the vertical motion of a balloon rising through the atmosphere:

$$a = \frac{du}{dt} = \frac{\rho_\infty V_b g}{m_{sys}} - g - \frac{1}{2} \frac{\rho_\infty u^2 C_D S}{m_{sys}} \qquad (8)$$

It should be noted that ρ_∞, V_b, u, C_D, and S are all functions of time. However, while C_D changes with altitude, and therefore time, because of expansion of gas, assuming a constant C_D of 0.8, close to that of a flat disk of equal cross-sectional area normal to the flow, is a reasonable approximation. Also, while an ascending, partially-filled balloon is not a perfect sphere, it can be treated as a sphere in terms of the fidelity of this first-order dynamic altitude model.

3.3 BALLOON GEOMETRIC CONSIDERATIONS

The three most common balloon shapes are cylindrical, spherical, and pumpkin. Balloon shape is integral to balloon design. The balloon shape dictates the surface area available for thermal/radiative energy exchange with the environment which drives the altitude of a zero pressure balloon and the overpressure for a superpressure balloon. The balloon shape also controls the envelope structural loads that will be experienced by the balloon material thereby influencing material strength requirements and selection. Large thermal energy exchange rates can result in large superpressure differentials between the maximum and minimum mean effective balloon temperatures. This pressure differential impacts the structural requirements of the envelope material. Larger structural loads lead to heavier balloon envelope requirements, thus increasing the balloon size required for a given payload capacity. Balloon shape also affects the means by which payloads are suspended and the associated localized stress distribution.

A cylindrical balloon shape is not efficient from an overall mass perspective. For an equivalent volume, the surface area of a cylindrical balloon is larger than a spherical, and the surface area relative to a corresponding sphere surface area increases even more rapidly for larger length to diameter ratios (Smith et al., 1997). Cylindrical balloons have the advantages of ease of

fabrication, a lower drag force in the direction of ascent, relative to an equivalent sphere, and ease of reefing (Nock et al., 1997). Additionally, because balloons are thermally driven, for a superpressure balloon flight at high latitudes with sun angles where solar illumination is primarily from the side, a cylindrical balloon with a matched height to diameter ratio can be desirable. Likewise, for a superpressure balloon near the equator where solar illumination is primarily the top of the balloon, a cylindrical balloon with a large height to diameter ratio can have advantages (Smith et al., 1997). The Soviet/French Mars'96 mission baselined a cylindrical balloon (Tarrieu, 1993).

Spherical balloons are fabricated from flat gores taped or bonded together at their edges to approximate the spherical shape. A spherical balloon is the most efficient geometry in terms of lifting force per unit of surface area, and it provides a uniform pressure-based stress distribution over the entire surface. However, the circumferential stress of a spherical balloon is proportional to its (large) radius and dictates the need for a high strength envelope material in order to handle the required payload lifting forces:

$$\sigma_{skin} = \frac{1}{2} \frac{r_{sphere} \Delta p}{t} \tag{9}$$

where σ_{skin} is the stress on the envelope, r_{sphere} is the radius of the sphere, Δp is the balloon superpressure, and t is the film thickness. It is also difficult to attach the payload to the balloon because of the localized stress concentrations produced at the attachment points. When tapes are employed to seal the gores, they can provide additional meridional strength, and the use of directionally oriented or composite films for the envelope can provide the necessary envelope film strength with minimal mass penalty. Because of their simplicity, efficiency, stability, and manufacturability, spherical balloons have a long design heritage, including Carrier, Boomerang, Sky Anchor, MAP, MABS, and Vega (Smith et al., 1997).

"Pumpkin", natural shape, or elastica balloon designs, are characterized by surface "lobing effects" produced by excess circumferential envelope material. These surface lobes limit the circumferential balloon envelope stresses by reducing the radius of curvature associated with the overall envelope surface (Yajima et al., 2009) :

$$\sigma_{hoop} = \frac{r_{gore}\Delta p}{t} \tag{10}$$

where σ_{hoop} is the stress on the envelope, r_{gore} is the radius of curvature of the gore, Δp is the balloon superpressure, and t is the film thickness. High-strength meridional tendons at the edges of each gore are longer than the envelope gore length allowing the tendon to carry the meridional loads. It has been shown that there is a limit to the lobing for a given number of gores before the balloon envelope buckles, resulting in a cleft (Smith and Rainwater, 2002). This buckling phenomenon is shown in Figure 5 for a fully inflated, full-scale Ultra Long Duration Balloon (ULDB) flown from Australia in March, 2001. As the number of gores was increased, the allowable amount of built-in lobing decreased.
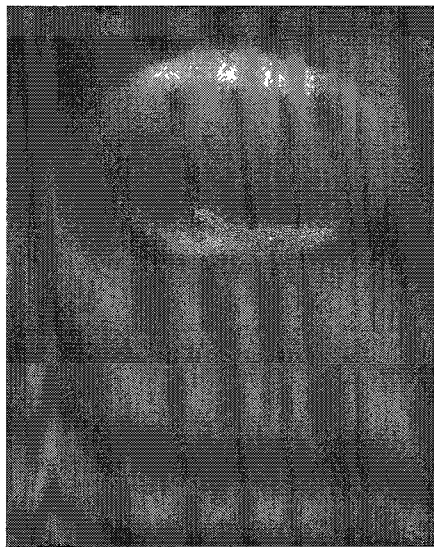
Figure 5: Full-Scale ULDB with Undeployed Material (Smith and Rainwater, 2002).

Calladine (1988) has developed a semi-empirical lobing limit relationship utilizing the

characteristic lobe geometry represented in Figure 6, given by:

$$n < 47 / \alpha^{2.5} \tag{11}$$

where α is the half-angle, in radians, of the lobed gore and n is the number of gores. The

maximum manufactured gore width is s, and the maximum distance between tendons is c.

Rearranging this equation and utilizing simple geometry, Smith and Rainwater (2004) were able

to develop a relationship for the maximum half-lobe gore angle and maximum width ratio given

by

$$\alpha_{max} = \left(47 / n\right)^{0.4} \tag{12}$$

$$s / c_{max} = \alpha_{max} / \sin \alpha_{max} \tag{13}$$
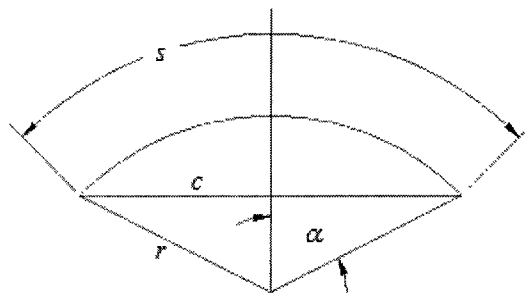
Figure 6: Lobed Gore Geometry.

The ULDB project tested this relationship by manufacturing a series of 48 gore model

balloons of various gore designs. The results of this test are plotted in Figure 7 along with data

for previous ULDB flight tests. Balloons with constant lobe angles and varying lobe radius

behaved according to the Calladine relationship. Those with constant lobe radius did deploy

completely with an s/c greater than that expressed by the Calladine relationship. While the

Phase IV-A balloon had s/c at the equator greater than that defined by the Calladine

relationship, it did fully deploy, because the majority of the balloon was below the Calladine

s/c_{max} ratio.
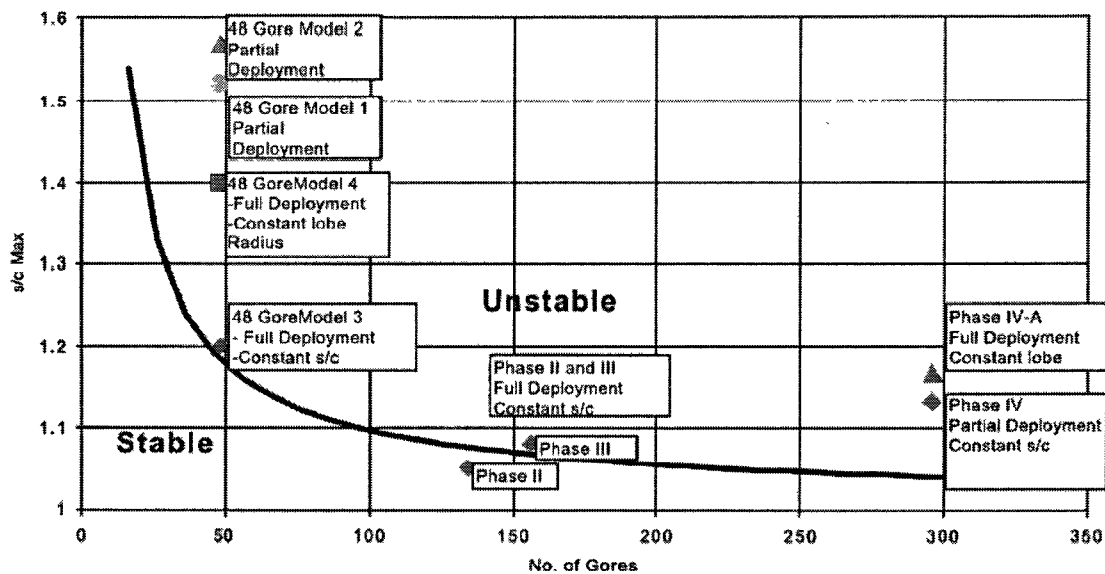
Figure 7: Comparison of ULDB Test Balloons with Calladine Relationship
(Smith and Rainwater, 2004).

3.4 BALLOON MATERIAL CONSIDERATIONS

The Martian atmosphere is thin and, as such, has low thermal inertia. Balloons, by

nature, are thermally driven. The mean temperature of a Mars balloon depends primarily on the

thermal radiation environment in the vicinity of the balloon, which varies significantly over a

diurnal cycle. Additionally, balloon radiant energy exchange varies seasonally, geographically,

with atmospheric dust load, and with balloon altitude. The balloon temperature maximum and

minimum control the diurnal maximum and minimum float altitude of zero pressure balloons and

control the differential pressure range required to maintain a superpressure balloon at constant volume. The pressure differential multiplied by the maximum balloon radius of curvature determines the maximum stress level experienced by the envelope material, and that ratio of stress to the film material strength should be sufficiently less than unity to maintain an appropriate Margin of Safety.

The low density of Mars' atmosphere, combined with large temperature swings translates to large balloon envelope volumes, constructed from light-weight, high-strength film material. The material specification is strongly coupled to balloon geometry. For a spherical superpressure balloon, the only way to increase the allowable maximum envelope differential pressure is to increase the film thickness which increases the empty balloon mass, necessitating even larger balloons, and thus increasing the envelope stresses for the same differential pressure. In a spherical superpressure balloon, the envelope carries most of the load which translates to significant meridional and circumferential design stresses. This often makes the mechanical properties of the envelope material the limiting factor controlling balloon size and its associated maximum payload mass. Despite this drawback, due to their simplicity and volumetric efficiency, lightly loaded spherical balloons using bilaminated polyester film for the envelope material (Letrenne et al., 1999) or Mylar film (Rand and Crenshaw, 1996) have been flown successfully at high altitudes in Earth's atmosphere for many years.

The design limitations for spherical superpressure balloons just summarized prompted further investigation into how to increase the volume and payload capacity of a Mars balloon without increasing the thickness of the film material. The result was the pumpkin balloon, made up of a series of lobes created by excess circumferential material between high strength tendons at the edge of each gore. The tendons off-load the meridional stress load from the film to the tendon. Circumferential stress in the skin is reduced by the smaller radii of curvature associated with the surfaces of the lobe elements. This allows the utilization of envelope material with

strengths significantly lower than that of the load tendon, but with sufficient strength to tolerate high localized stresses.

The load tendons require a light weight, high stiffness material in order to support the meridional loads. Zylon – poly(p-phenylene-2,6-benzobisoxazole) (PBO) has been used successfully for tendons in past superpressure balloons, including NASA's Ultra Long Duration Balloon (ULDB) program (Seely et al., 2004). However, strength degradation of Zylon due to aging and sensitivity to ultraviolet at a minimum requires controlled material handling and may warrant using another material altogether. Table 2 compares possible tendon material candidates.

Material:		Kevlar	Carbon	Zylon
Tensile Strength	(gpd)	22	23	42
Elongation at Break	(%)	2.4	1.5	2.5
Tensile Modulus	(gpd)	850	1480	2000

Table 2: Material Properties of Balloon Tendon Materials.

Pumpkin balloons have demonstrated the ability to withstand five times the pressure loads of a spherical balloon with an equivalent volume (Rand et al., 1999). However, while the weight penalty is less than for a corresponding spherical balloon, the pumpkin balloon overall tends to be heavier than the corresponding spherical balloon.

In addition to ultimate strength, the envelope film must have an appropriate modulus of elasticity in the temperature range characterizing the float altitude. This can be critical, because a relatively low modulus of elasticity material responds to superpressures by stretching, thus increasing the envelope volume and buoyancy of the balloon. If that is the case, the balloon can continue to ascend to higher altitudes and potentially burst. The higher the modulus of elasticity of the balloon film, the more stable the balloon float altitude.

The very large areas of thin film material required to fabricate balloons with dimensions anticipated for Mars applications result in some rather unique design considerations. It is not possible to manufacture and handle that much material without creating small "pinholes"

scattered randomly over the elemental structural areas. However, because of the very low ambient and balloon differential pressures, small numbers of these holes can be tolerated. Long duration flights require the balloon film to be resistant to pinholing and to have a low permeability to the lifting gas. Assuming that the lifting gas is hydrogen, the very small cross section of hydrogen atoms means that those molecules can migrate through some types of thin film materials with relative ease and that permeability is an important consideration. In addition to low permeability to the lifting gas, it is also desirable to have a low permeability to the constituents of Mars ambient atmosphere in order to insure that there is no appreciable diffusion of atmospheric carbon dioxide (with a molecular weight of 44.01, compared with hydrogen's molecular weight of 2.016) into the balloon volume at any point during the flight. Long duration flight systems must experience minimal degradation resulting from exposure to ultraviolet (UV) radiation. It is possible that UV exposure must be considered during the transit to Mars and during the balloon flight through Mars atmosphere. Because the intensity of solar radiation for Mars' atmosphere is about half of Earth's, it is likely that any stratospheric balloon material used for high-altitude terrestrial applications will have sufficient UV resistance at Mars.

For maximum volumetric efficiency with the least impact on overall spacecraft bus size, it will be necessary to pack these deployable balloon systems to high packing densities. Consequently, the balloon envelope material must first withstand the packing and associated creasing stresses, along with possible plastic deformation and uncontrolled thermal processing that could occur as a result of transit to Mars and finally, while on the surface of Mars, the material will be subject to ionizing radiation and temperature extremes. The balloon material must tolerate abrasion caused by chafing during packing and storage, as well as during deployment. Creases in the film material can cause tears, and abrasion can cause pinholes at random points of contact. These problems are magnified at elevated temperatures. The balloon material must maintain its integrity after being exposed to large temperature gradients. Additionally, it will be necessary to assess material recovery capabilities related to of exposure to

transient spacecraft temperature extremes during Earth-Mars transit that could exceed the design temperature range. The material sensitivity to temperature could necessitate an onboard thermal management system requirement during transit. The effect of long term exposure (on the order of a year or greater) to ionizing radiation should also be considered.

Sterilization will be required to prevent Mars contamination by microorganisms from Earth. Methods of sterilization will need to be evaluated to determine their effect on the balloon material and balloon reliability. Sterilization should not weaken or plastically deform the material. Lastly, the balloon must exhibit reliable manufacturability, and any gores should be sealed gas tight with seal strengths equal to or greater than the parent film.

Film mass per unit area of film material is also an important selection criteria. The requisite mechanical properties for terrestrial superpressure balloons are attained through film material orientation – either machine direction orientation (MDO), transverse direction orientation (TDO), or a combination of MDO and TDO, known as biaxial orientation. The physical properties of two materials used currently in superpressure balloons are summarized in Table 3. Mylar – polyethylene terephthalate (PET) – is a common superpressure balloon film manufactured by DuPont-Teijin Films. The thinnest standard gauge Mylar film is 6 μm. Dartek is a 6,6 nylon MDO film produced by DuPont. The high strength in the machine direction and high elongation in the tear direction provides increased tear strength. Both of these materials are sufficiently ductile at low temperatures to be viable for use in the Martian environment. Dartek is hydroscopic, which requires material handling considerations during manufacturing; however the trace moisture levels, even in humid Martian atmospheric conditions, should not impact material performance (Rand and Crenshaw, 1996).

Material:		Mylar (PET)	Dartek
Specific Gravity	(g/cc)	1.39	1.14
Tensile Strength	(MPa)		
Machine Direction		200	295
Transverse Direction		235	49
Elongation at Break	(%)		
Machine Direction		116	25
Transverse Direction		91	169
Modulus	(GPa)		
Machine Direction		4.8	3.1
Transverse Direction		5	2.7
0.2 % Offset Yeild Stress	(MPa)		
Machine Direction		91	79
Transverse Direction		87	76

Table 3: Material Properties of Thin Balloon Films.

Mylar and Dartek both have shortcomings justifying consideration of a composite film

Mars balloon envelope design. Mylar is prone to pinholes resulting from folding and storage.

Improved manufacturing techniques have ameliorated the problem, but the potential still exists.

Mylar is also subject to crack propagation, particularly at temperatures below -80°C. Nylon

Dartek balloons fail at their seams, likely due to adhesive failure. The superpressure 2001 Mars

Aerobot/Balloon System (MABS) design proposed using a five layer composite material,

consisting of a 3.5 micron Mylar film for substrate stiffness, a layer of polyester based adhesive, a

55 denier Kevlar scrim in an orthogonal pattern with 160 yarns per meter (to meet the strength

requirements with minimal weight penalty), another layer of polyester adhesive, and a 6 micron

layer of polyethylene film (Stratofilm 372) for pinholing resistance and inhibition of crack

initiation and propagation. The adhesive layers provide bonding between the primary layers

while also providing additional pinholing resistance (Nock et al., 1997). The layup for this

composite structure is shown schematically in Figure 8.
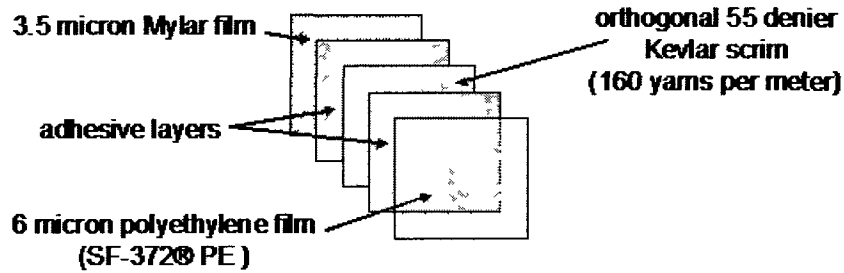
Figure 8: MABS Composite Structure Layup (Nock et al., 1997).

The predicted mechanical properties for this composite over the expected flight environment temperature range are summarized in Table 4. The composite is sealed with a Mylar heat activated tape with seam strength equal to 88 percent of the parent material at 23°C and 98 percent at -140°C. In addition to improved fracture strength over standard Mylar and Nylon films, the composite showed no sign of degradation after exposure to 2 Mrads of gamma ray radiation, indicating suitability for sterilization. The estimated composite film mass per unit area can be reduced from 19.66 g/m² to approximately 13 g/m² by reducing the amount of adhesive between layers or by eliminating adhesive entirely and embedding one component of the composite into the other, and/or using a thinner PE component (Smith et al., 1997).

Areal Density	(g/m²)	19.66
Strength (23°C to -140°C)	(N/m)	> 2500
Tear Toughness 23°C	(N)	12
-140°C	(N)	43
Seam Strength (23°C to -140°C)	(N/m)	> 2500
Radiation Effect		No degredation in strength for radiation levels of 2 Mrads
Adhesive Performance		No observed component or adhesive delamination or embirttlement down to -198°C

Table 4: Mechanical Properties Predicted for the Mars Aerobot Balloon System.

	Thickness (μm)	Ultimate Strength (kg/cm^2)		Ultimate Elongation (%)	
		MD	TD	MD	TD
25°C	3.4	410±40	370±30	520±50	960±60
	3.0	360±20	270±10	570±20	720±30
	2.8	340±20	250±20	610±20	790±20
-40°C	3.4	610±80	460±20	330±30	570±30
	3.0	420±20	310±20	360±20	310±40
	2.8	440±10	440±30	400±10	460±70
-80°C	3.4	690±50	640±70	220±20	380±30
	3.0	490±40	520±60	230±60	230±30
	2.8	660±40	460±20	230±20	210±30

Table 5: Mechanical Properties of Ultra-Thin Polyethylene Films
(Saito et al., 2002; 2006).

Unlike a superpressure balloon, the meridional stresses associated with supporting the payload are more important than are the circumferential stresses in a zero-pressure balloon. In addition to not being subject to the strength requirements associated with superpressure, the lack of an imposed overpressure relaxes requirements for a high modulus of elasticity envelope material, as well as the transparency to solar and albedo radiation requirement. Also, because the flight duration for zero-pressure balloons is typically short, they are not that sensitive to permeability and resistance to pinholing issues. Zero-pressure balloons are, however, subject to the other material requirements described. The Balloon Group at the Institute of Space and Astronautical Science (ISAS), within the Japan Aerospace Exploration Agency (JAXA), has successfully flown ultra-thin polyethylene zero-pressure balloons terrestrially with payloads up to 10 kg to altitudes greater than 50km (Saito et al., 2006). The ambient atmospheric conditions at these altitudes are comparable to ambient Mars conditions at 20 km. The mechanical properties for the films used in these balloons are summarized in Table 5.

3.5 SUSPENSION GEOMETRY

A challenge for spherical balloon systems is the mechanical attachment of the payload; a concentrated load normal to the envelope surface results in an "infinite" stress at the point of application, and a vertical force tangent to the sphere at the point of application results in a significant stress concentration (Smalley, 1975). Because of this, payloads are often supported by means of a harness of load lines which interface with the spherical balloon at locations where load line discontinuity stresses are low enough to be compatible with the balloon envelope material--30 degrees below the equator of a spherical balloon. Another method for suspending payloads is by attaching the payload to a bottom fitting which is secured to a center load line, shorter than the balloon diameter, and attached to an apex fitting. This method transfers the suspended load to the apex fitting. Both of these methods for payload attachment create operational problems during balloon deployment (Rand and Crenshaw, 1996). For very light payloads, it is possible to attach the payload directly to the base of the balloon as shown in Figure 9.
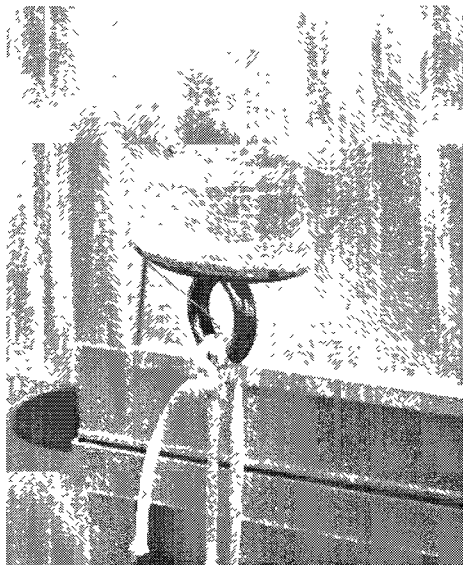
Figure 9: Spherical Balloon Base Payload Attachment Fitting.

In the case of pumpkin balloon designs, the meridional stress loads are carried by the tendons, and it is possible to attach the payload directly to the bottom fitting as shown in Figure 10, showing how potential attachment pins are incorporated into the base fitting, securing the tendons.
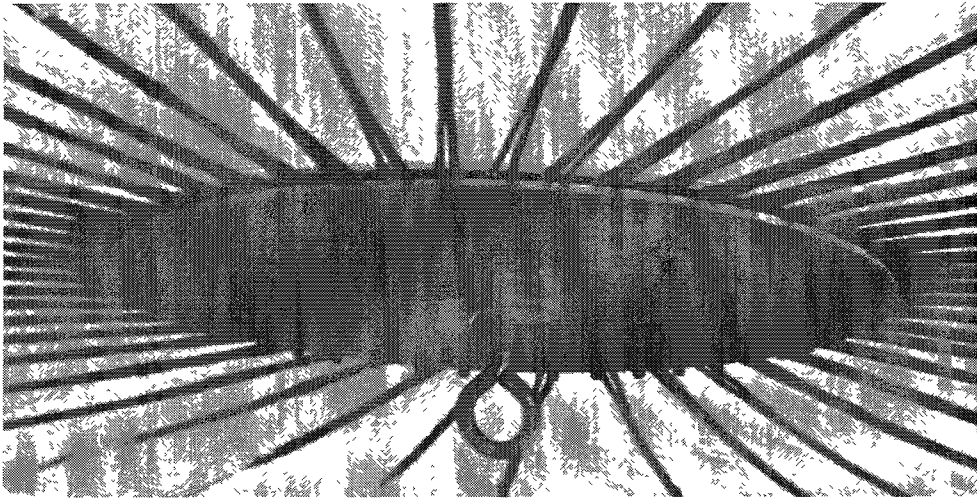
Figure 10: Pumpkin Balloon Payload Attachment Fitting.

3.6 BALLOON THERMAL EFFECTS

Lifting-gas temperature is a key driving factor governing the behavior of balloons in flight. During ascent, as a result of lifting gas expansion and potential energy reductions, the gas temperature can decrease, resulting in a significant loss of lift. If this occurs, balloon ascent rates can decrease or even cease until ambient energy exchange enables the balloon system to approach thermal equilibrium with respect to the ambient environment. Because of this restorative effect, temporary loss of lift can retard the ascent rate, but is not a significant factor overall during initial ascent. However, once float altitude is achieved, effective balloon temperature is the primary parameter controlling balloon altitude. T_{g-max} and T_{g-min}, the maximum and minimum effective balloon temperatures are controlling design parameters in both zero pressure and superpressure balloon design, impacting the lifting gas mass loss and ballast requirements for zero pressure

balloons, and the design (maximum) balloon over-pressure level for superpressure balloons. For a planet like Mars, with a thin atmosphere and large diurnal temperature swings, this influence is magnified.

Balloon films identified in earlier analyses for Mars applications are sufficiently thin that film thermal resistance due to heat conduction does not require a meaningful temperature drop. Hence, the film thermal resistance between the lifting gas envelope and the atmosphere can be ignored, and quasi-equilibrium thermal loading can be estimated using the balloon energy balance:

$$\dot{Q}_d + \dot{Q}_r + \dot{Q}_s + \dot{Q}_{l\text{-}g} + \dot{Q}_{conv\text{-}atm} + \dot{Q}_{conv\text{-}g} + \dot{Q}_{abs\text{-}g} = \dot{Q}_{rad\text{-}Mars} + \dot{Q}_{rad\text{-}space} \qquad (14)$$

where $\dot{Q}_d$ is the direct solar heat rate, $\dot{Q}_r$ is the reflected solar heat rate received from the planet, $\dot{Q}_s$ is the scattered solar heat rate due to particulate matter in the atmosphere, $\dot{Q}_{l\text{-}g}$ is the internally generated heat rate, $\dot{Q}_{conv\text{-}atm}$ is convective heat transfer rate between the balloon film and the atmosphere, $\dot{Q}_{conv\text{-}g}$ is convective heat transfer rate between the balloon film and the lifting gas, $\dot{Q}_{abs\text{-}g}$ is the rate of radiative energy absorbed by the lifting gas, $\dot{Q}_{rad\text{-}Mars}$ is the rate of energy radiated to Mars, and $\dot{Q}_{rad\text{-}space}$ is the rate of energy radiated to space. It can be assumed that no heat is generated within the balloon by lifting gas radiant absorption. Because of the low thermal inertia of the atmosphere, convective heat transfer between the balloon and the atmosphere is negligibly small and can also be neglected. Hydrogen lifting gas has negligible radiant absorption for wavelengths up to approximately 1200 Å (Harrison et al., 1948), which spans part of the ultraviolet spectrum. Based on the fact that hydrogen is used to wash out and fill vacuum spectrographs because of its near-perfect transparency (Harrison et al., 1948), the $\dot{Q}_{abs\text{-}g}$

term can be neglected. Therefore the heat load on the balloon can be estimated by equating the sum of the convective heat transfer rate from the balloon film to the lifting gas and the direct, reflected, and scattered solar heat rates to the sum of the radiated heat rate from the balloon to Mars' surface and the balloon to space (Heun et al., 1997).

The large variation in radiant heating and cooling experienced by the balloon, varying from the top of the balloon to the bottom, implies that the thermal analysis should incorporate different gray-body properties for the top and bottom halves of the balloon surface. Applying the simplifying assumptions above and incorporating differences in balloon envelope properties between the top and the bottom of the balloon, Eq. (14) becomes:

$$\dot{Q}_{d(top)} + \dot{Q}_{d(bot)} + \dot{Q}_r + \dot{Q}_s + \dot{Q}_{conv-g(top)} + \dot{Q}_{conv-g(bot)} = \dot{Q}_{rad-Mars} + \dot{Q}_{rad-space} \qquad (15)$$

The individual heating rates can be represented as follows:

$$\dot{Q}_{d(top)} = \alpha_{top} A_{proj(top)} I_{sun} \qquad (16)$$

$$\dot{Q}_{d(bot)} = \alpha_{bot} A_{proj(bot)} I_{sun} \qquad (17)$$

$$\dot{Q}_r = a\alpha_{bot} A_{proj(bot)} I_{sun} \qquad (18)$$

$$\dot{Q}_s = a\alpha_{top} A_{proj(top)} I_{sun} \qquad (19)$$

$$\dot{Q}_{conv-g(top)} = h\frac{A_{surf}}{2}\left(T_g - T_{b(top)}\right) \qquad (20)$$

$$\dot{Q}_{conv\text{-}g(bot)} = h\frac{A_{surf}}{2}\left(T_g - T_{b(bot)}\right) \tag{21}$$

$$\dot{Q}_{rad\text{-}Mars} = \sigma\varepsilon_{bot}\frac{A_{surf}}{2}\left(T_{b(bot)}^4 - T_p^4\right) \tag{22}$$

$$\dot{Q}_{rad\text{-}space} = \sigma\varepsilon_{top}\frac{A_{surf}}{2}\left(T_{b(top)}^4 - T_s^4\right) \tag{23}$$

where α_{top} is the balloon film solar absorptivity for the top hemisphere, α_{bot} is the balloon film solar absorptivity for the bottom hemisphere, ε_{top} is the balloon surface infrared emissivity for the top hemisphere, ε_{bot} is the balloon surface infrared emissivity for the bottom hemisphere, $A_{proj(top)}$ is the projected area of the top hemisphere of the balloon, $A_{proj(bot)}$ is the projected area of the bottom hemisphere of the balloon, A_{surf} is the overall surface area of balloon, I_{sun} is the solar constant, a is the planet albedo, h is the convective heat transfer coefficient between the lifting gas and the balloon envelope, T_g is the temperature of the lifting gas, $T_{b(top)}$ is the mean film temperature for the top hemisphere of the balloon which is assumed to be constant over the entire surface of the hemisphere, $T_{b(bot)}$ is the mean film temperature for the bottom hemisphere of the balloon which is assumed also to be constant for that hemisphere, T_p is the surface temperature of Mars, T_s is the temperature of space and the upper atmosphere which was assumed to be $20K$, and σ is the Stefan-Boltzman constant ($5.67051\times10^{-8}\,W/m^2K^4$).

The balloon surface absorptivities and emissivities are properties of the balloon envelope coatings. The planet albedo, planet surface temperature, and view factors vary diurnally, seasonally, and geographically. The solar constant varies inversely with the square of the radius from Mars to the sun, varying from 492 W/m^2 at aphelion to 715 W/m^2 at perihelion. Because only a portion of the balloon is visible to the sun at any given time, the projected area of the top

and bottom hemispheres of the balloon are functions of the cosine of the local zenith angle of the sun (Heun et al., 1997):

$$A_{proj(top)} = \frac{\pi}{8} D^2 \left(1 + \cos\zeta\right) \tag{24}$$

$$A_{proj(bot)} = \frac{\pi}{8} D^2 \left(1 - \cos\zeta\right) \tag{25}$$

Employing these relations, and assuming that the balloon gas is in thermal equilibrium, equations can be developed to estimate the instantaneous average temperatures of the lifting gas in the upper hemisphere and in the lower hemisphere. Those algebraic equations can be solved numerically, in order to estimate the average absolute temperature of the balloon lifting gas:

$$\frac{\pi D^2}{8}\left(1+\cos\zeta\right)\alpha_{top}I_{sun}\left(a+1\right)+h\frac{\pi D^2}{2}\left(T_g - T_{b(top)}\right) = \sigma\varepsilon_{top}\frac{\pi D^2}{2}\left(T_{b(top)}^4 - T_s^4\right) \tag{26}$$

$$\frac{\pi D^2}{8}\left(1-\cos\zeta\right)\alpha_{bot}I_{sun}\left(a+1\right)+h\frac{\pi D^2}{2}\left(T_g - T_{b(bot)}\right) = \sigma\varepsilon_{bot}\frac{\pi D^2}{2}\left(T_{b(bot)}^4 - T_p^4\right) \tag{27}$$

$$T_g = \frac{T_{b(top)} + T_{b(bot)}}{2} \tag{28}$$

In order to minimize variations in superpressure, it is desirable to minimize the variation in balloon temperature. The surface albedo affects the magnitude of the reflected and scattered solar energy onto the balloon skin, and is highly variable (see Figure 11). Balloon flights over regions with high albedos will result in greater thermal loading (higher heating rates), increasing

the required superpressure, and consequently increasing the stresses on the balloon envelope. While flights over terrain with a low albedo are desirable, balloon flight trajectories are somewhat unpredictable and based on scientific needs. Therefore, the worst case albedo affects must be factored into the balloon design.
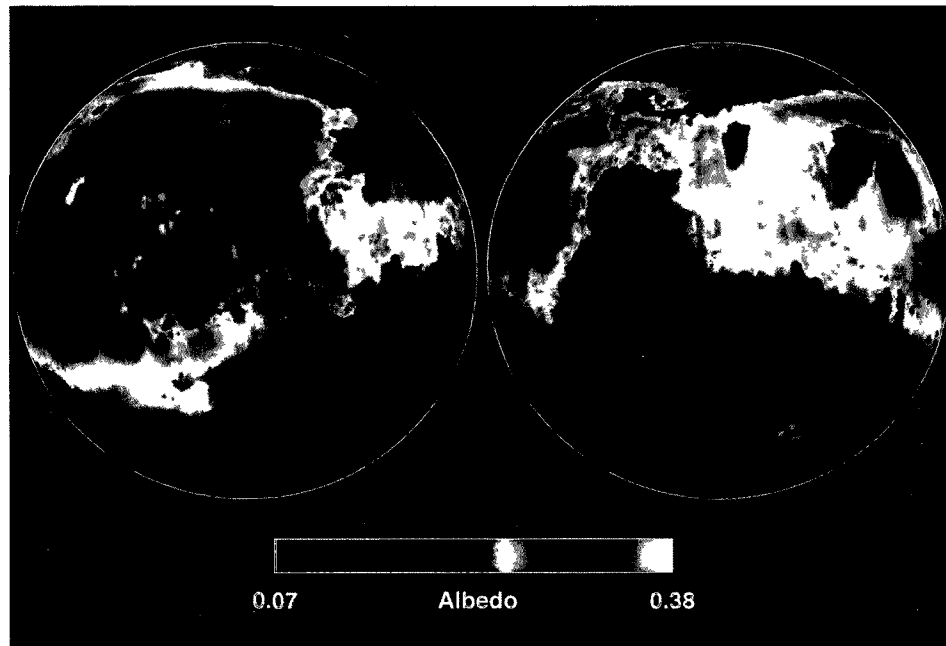
Figure 11: Two Views of Mars Albedo Derived from MGS TES Measurements (Lavoie, 2001).

The thermal-optical radiative properties of the balloon are integral to the overall balloon design. The large diurnal, seasonal, and geographic variations in direct, reflected, and scattered solar energy translates to a preference for an envelope material with a low solar absorptivity. By optimizing the thermal-optical radiative properties of the balloon, it is possible to reduce the maximum superpressure experienced by the balloon during any given flight, thereby reducing the envelope strength requirement, and consequently, the overall balloon mass.

3.7 INFLATION GAS

Balloon buoyancy is governed by the ratio of the lifting gas to ambient atmospheric densities. For a balloon to have lift, the lifting gas must either have a molecular weight much less than that of the ambient atmosphere or be at a temperature much greater than the ambient atmosphere for the same pressure condition. Helium and hydrogen are both candidate lifting gasses. The average molecular weight of Mars' atmosphere is 43.34. Diatomic hydrogen not only has a factor of two molecular weight advantage over helium, it also has a larger molecular cross section and is therefore less susceptible to lifting gas loss. The propensity of helium to leak can result in a greater inflation system mass for gas storage. Lastly, because of the absence of free oxygen in the 95+ % carbon dioxide Martian atmosphere, there is no combustion hazard associated with the use of hydrogen and it can be derived from *in situ* water ice.

3.8 BALLOON LIFE

Balloon life is determined by the envelope's ability to retain the lifting gas for the duration of the flight. During a balloon flight, lifting-gas mass is lost as the gas escapes through the envelope film, either from pinhole leaks, tears, fabric deterioration, or by diffusion.

The leakage rate through a pinhole or tear is a function of the superpressure of the balloon and the size of the holes. For small pinhole leaks, when the mean free path of the lifting gas is greater than the diameter of the hole, the flow is controlled by molecular processes. The leakage rate through a single pinhole is negligible; however multiple pinhole leaks caused by imperfections in the film can lead to significant mass loss. While some materials like Mylar are prone to pinholing, improved manufacturing techniques and the use of composites can reduce the chance of pinhole leaks. Larger tears are possible as a result of creasing due to packing or from damage during deployment. For these leaks, the leak rate per unit of leak area is proportional to the square of the superpressure.

Gas is lost by diffusion through the balloon envelope even when no defects or tears are present, and diffusion losses are a function of the partial pressure of the gas contained within the film enclosure – i.e. the lifting gas molecules migrate through the film and diffuse to the outside. The diffusion rate, d, can be defined as:

$$d = \frac{\delta p A_{surf}}{t} \tag{29}$$

where δ is the film permeability to the lifting gas, p is the difference in partial pressure of the gas across the film, A_{surf} is the surface area and t is the film thickness. The permeability, δ, is a function of envelope material and temperature. Permeability increases typically with increasing temperature. The permeability of Mylar to various gasses over a range of temperatures is plotted in Figure 12.

Composite envelopes that include materials such as Mylar can reduce the diffusion rate and extend balloon life indefinitely when balloon performance is limited solely by diffusion. And, since many pinhole leaks can be avoided through careful film material selection, manufacturing, and testing, the most important limitation to balloon life is damage sustained to the balloon envelope resulting in tears and leaks – either through packing, deployment, or from atmospheric turbulence during flight.
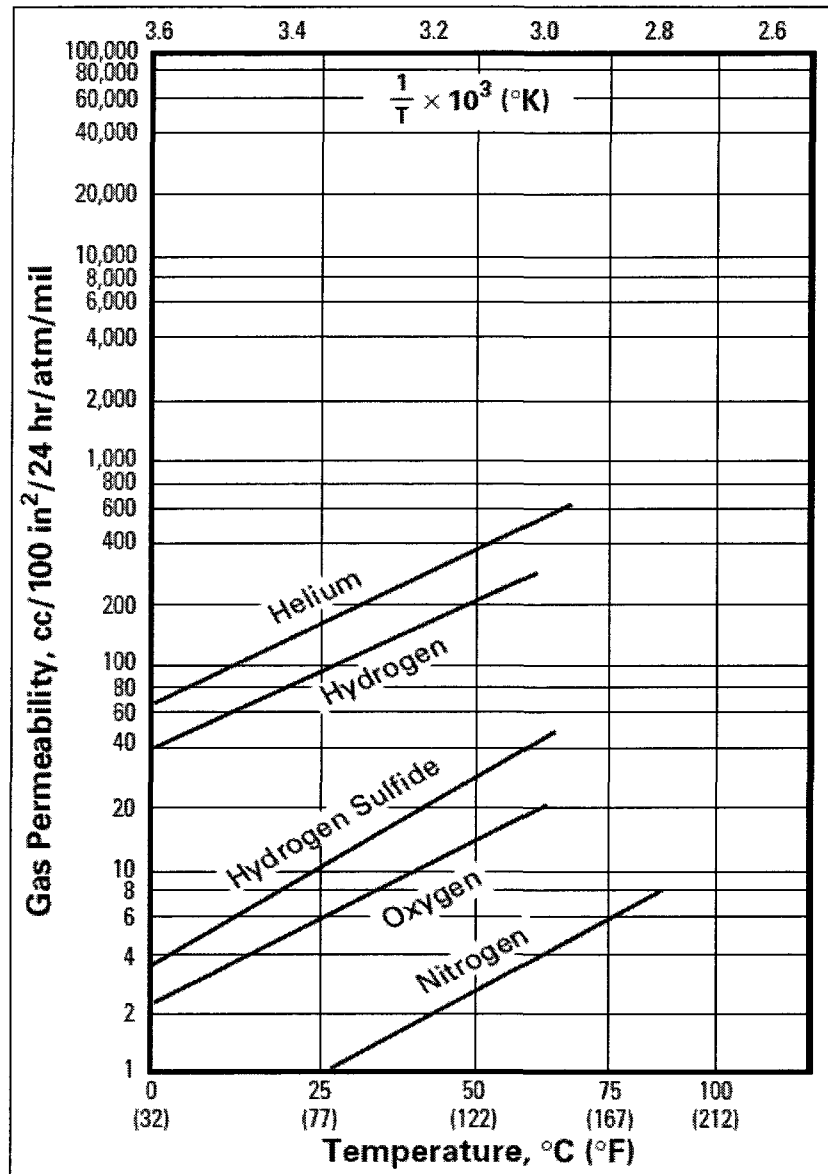
Figure 12: Permeability of Mylar to Various Gases as a Function of Temperature.

3.9 TOPOGRAPHICAL CONSIDERATIONS

The Mars reference areoid is defined as the equipotential surface of the Goddard Mars

Gravity Model, and coincides with a sphere of radius 3,396 km, from the planet's center of mass.

A 30 km local topographical surface variation exists, ranging from elevations 5 km below the

reference areoid at Hellas Planitia to 25 km above the reference areoid at the top of Olympus

Mons in the Tharsis province, extending from the Amazonis Planitia in the west to Chryse

Planitia in the east (Alexander, 2001). There is a roughly 5 km difference in elevation between

the lower northern hemisphere and the higher southern hemisphere. With the exception of the

Tharsis province, most of the Martian surface remains below elevations of 10 km above the

reference ellipse. The Tharsis volcano-tectonic province is centered near the equator in the

longitude range between -60°E to -140°E and contains the following major volcanic shields:

Olympus Mons – 18°N, -135°E, Alba Patera – 42°N,-108°E, Ascraeus Mons – 12°N,-112°E,

Pavonis Mons 0°,-113°E, and Arsia Mons – 9°S, -121°E (see Figure 13). In addition to these

volcanoes, the Tharsis province also contains the large east-west Valles Marineris canyon system,

which is not a direct hazard to balloons, but is of significant geological interest.
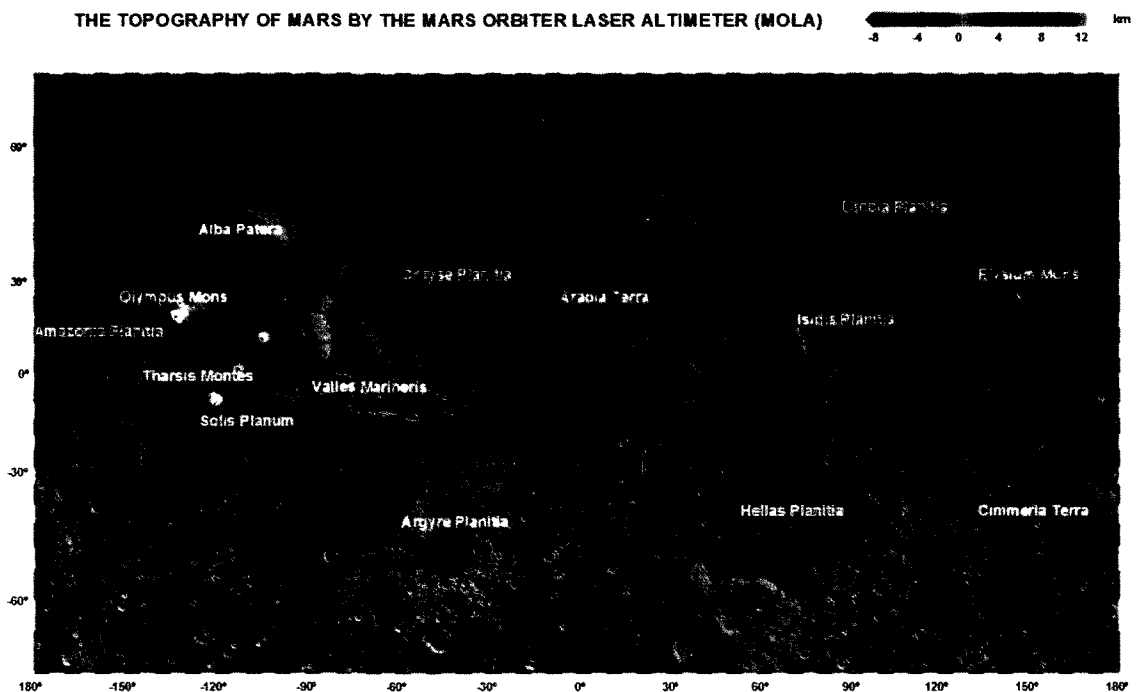
Figure 13: MOLA Topographic Map of Mars (Neumann, 2007).

Because of the thin atmosphere, planetary entry requirements drive landing site selection

toward low elevation locations, in order to exploit the increased atmospheric density (higher

dynamic pressures at given velocities) and utilize as much of the vertical atmospheric column as

possible for deceleration. The low elevation requirement is also advantageous for balloon launches from the surface since the increased atmospheric density reduces the required lifting gas volume necessary to launch a balloon payload.

Large, payload-carrying planetary balloons that can float above the highest terrain or around peaks while travelling great distances, offer exceptional opportunities for planetary exploration. Superpressure balloon systems are the logical designs for long duration flights, and their design float altitude is therefore an important consideration. Superpressure balloon float height above the local ground surface is influenced strongly by diurnal temperature swings. Balloon float trajectories near the surface of high plateaus will necessarily require higher float altitudes, and that means that the atmospheric column above the balloon is thinner, translating to stronger radiative coupling with the Sun and with deep space which can result in higher thermal loading and higher superpressures (Nock et al., 1997).

CHAPTER 4

MARS METEOROLOGICAL BALLOON SYSTEM

4.1 METEOROLOGICAL MEASUREMENT REQUIREMENTS

Near-surface atmospheric sounding data can be enabling for many scientific applications. It is possible to characterize daily, seasonal, annual, and inter-annual variations in Martian weather, including atmospheric oscillations, frontal activity, estimates of atmospheric dust distributions, and the occurrence of local and global dust storms using only surface pressure measurements (Tillman, 1988). Accurate knowledge of atmospheric temperature and pressure variations is essential for defining the Mars surface operational environment. Atmospheric temperature, when coupled with atmospheric pressure data, yields the local atmospheric density. Due to the low ambient pressures and temperatures at Mars, water vapor concentrations are so low that they do not influence density. However, knowledge of local humidity levels provides insight into water vapor transport processes and cloud formation.

Knowledge of local wind speed and direction histories is an important element in understanding the aeolian processes shaping the surface of the planet. From an engineering perspective, accurate and timely knowledge of local instantaneous Martian atmospheric density and wind conditions can reduce substantially the uncertainties in entry trajectory predictions, thereby shrinking the landing ellipse, and enabling precision EDL capabilities. Data on local wind patterns are also critical in developing airborne exploration systems. Since balloons float with the atmosphere, remote tracking of deployed balloons can provide an accurate measurement of horizontal wind speed and wind-direction histories.

The minimum meteorological measurement requirements for a weather balloon carrying a radiosonde are instantaneous pressure, temperature, humidity, wind, altitude, and density. In order to reduce radiosonde mass (and therefore minimize the balloon size and mass), it is only necessary to measure the instantaneous pressure, temperature, and humidity directly.

A standard balloon-borne radiosonde produces vertical profiles of measured properties. Precise altitude determination is essential for accurate vertical atmospheric profiles. Errors in calculated balloon height cannot be distinguished from measurement inaccuracies. Terrestrially, the geopotential altitude of each radiosonde sampling point has been determined using GPS, or more traditionally, calculated using the measured parameters in the hypsometric altitude equation:

$$z_2 - z_1 = \frac{RT_\infty}{g} \ln\left(\frac{P_{\infty-1}}{P_{\infty-2}}\right)$$ (30)

4.2 RADIOSONDE INSTRUMENTATION

Radiosonde sensors that are already space-qualified can greatly reduce cost and risk. From 1989 to 1994, the Finnish Meteorological Institute (FMI) performed space qualification testing on small, lightweight pressure, humidity, and temperature sensors derived from the commercially available Barocap®, Humicap®, and Thermocap® terrestrial sensors manufactured by Vaisala, Inc. as candidate sensors for future Mars missions. The sensors were exposed to temperatures ranging from -135°C to 60°C and impact shocks up to 500g (Harri et al., 1995) during the qualification tests. Performance specifications for the tested sensors are summarized in Table 6, and various derivatives of these sensors have been employed on the Mars-96 Small Stations and Penetrators, the Mars Polar Lander, Beagle 2, and Phoenix missions.

The Barocap® is a capacitive aneroid sensor employing a silicon diaphragm over a miniature vacuum cavity. The Thermocap® is a capacitive wire sensor, and Humicap® consists of two thin film capacitor sensors. The humidity sensors are heated alternately to prevent ice from forming while utilizing measured capacitance to determine relative humidity directly.

Characteristics of FMI Tested Sensors							
Range		Resolution	Accuracy (3 sigma)	Temperature Dependence	Hysteresis	Mass (g)	Dimensions (mm)
min	max						
Barocap® (hPa)							
0	50†	<0.005	<0.02	40 hPa/K	<0.005	3	Ø15x8
Humicap® (%RH)							
0	100	<0.1	<1	-	-	1	4x4x0.2
Thermocap® (K)							
0	370	<0.02	<0.1	N.A.	-	1	Ø1.52x2.4

†Barocap® operating range is 0-1200 hPa

Table 6: Characteristics of the Finnish Meteorological Institute Tested Sensors
(Harri et al., 1995).

In order to reduce radiosonde mass (and therefore minimize the balloon size), only

pressure, temperature, and humidity are measured directly *in situ*. Analog sensor outputs are

digitized and transmitted to the ground station via a UHF transmitter (presumably at 405 MHz)

using a narrowband GFSK (Gaussian Frequency Shift Keying) modulated downlink signal which

carries 2400-bit data frames at a data rate of 2400 bits/second and can transmit to a range of

nominally 750 km. The sonde is powered by a lithium-ion battery with a specific energy density

of 150-250 W-hr/kg. A functional block diagram for the space-qualified radiosonde is displayed

in Figure 14. Based on the component mass and the mass of a similar Vaisala RS92-D

radiosonde, a total mass allowance of 150 g is sufficient for these radiosonde units.

Virtually all balloon envelope materials are transparent to radar. However, a reflective

(to radar) ribbon material can be incorporated in the balloon tether, enabling wind speed and

altitude tracking via ground station radar. As a check, the altitude measurements can be

compared with hypsometric estimates employing the data obtained from sonde measurements.

Density can be calculated using the ideal gas law.

Prior to balloon launch, sonde pressure, temperature, and humidity measurements should be "zeroed" with respect to ground station reference sensors in order to ensure proper operation of the sonde sensors, including reconditioning the humidity sensors, and proper operation of the transmitter. After launch, this candidate sonde package is designed to transmit sensor readings at a rate of 1/s.
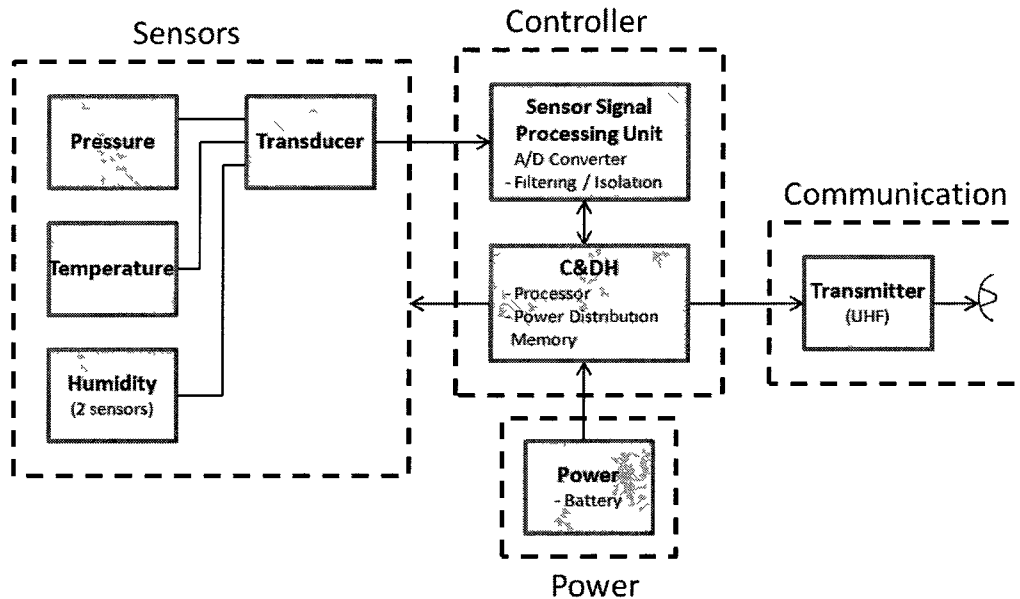
Figure 14: Radiosonde Functional Block Diagram.

4.3 WEATHER BALLOON DESIGN

Undoubtedly, Mars' very thin atmosphere and variable surface winds present the biggest challenges for reliable deployment and launch of these relatively large balloons. Extensible latex balloons are commonly used for terrestrial balloon-borne radiosondes. However, the substantially larger balloon volume required for Mars radiosondes, even at initial inflation, drives the balloon design toward thin films in order to minimize significant envelope mass penalties. The small payload mass and short duration of weather balloon flights make zero-pressure

balloons ideal. Zero-pressure balloons are deployed and flown regularly in the Earth's atmosphere.

Ultra-thin polyethylene zero-pressure balloons with payloads up to 10 kg have been flown on Earth to altitudes greater than 50 km (Saito et al., 2006) where terrestrial atmospheric conditions are comparable to Mars ambient conditions 20 km above the reference surface altitude. A spherical balloon geometry is preferable because of its simplicity and the modest loads produced by the very low payload mass. For reference purposes, a 3.4 μm polyethylene envelope material of the type used in JAXA's ultra-thin film test flights (Yamagami et. al., 2004) utilizing hydrogen lifting gas and capable of lifting a 165 g payload (150 g radiosonde and 15 g suspension line and reflector) to 20 km with a nominal ascent rate of 1 m/s will be assumed and a baseline Mars launch site location in Northeast Amazonis (35°54'N 144°21.6'W -3867 m MOLA height) has been employed.

The required volume for a balloon to be neutrally buoyant at a constant density altitude can be calculated assuming zero free lift. From Equations (4) and (5):

$$\rho^* V_{max} - \left(m_b + m_{payload} + m_g \right) = 0 \tag{31}$$

where ρ^* is the desired float density and V_{max} is the volume of the fully inflated balloon. The mass of the balloon is a function of the fully inflated balloon volume based on the construction of the balloon, $m_b = m_b \left(V_{max} \right)$. Yamagami determined empirically, that for a zero-pressure, spherical balloon using 3.4 μm polyethylene envelope material, this relationship is:

$$m_b = 0.23 V_{max}^{2/3} \tag{32}$$

including the mass of the film, seams, and inflation fittings. In addition, another 50 g of mass can be added for the inclusion of a reefing sleeve. The mass of the inflation gas is also a function of the fully inflated balloon volume:

$$m_g = \rho_g V_{max} \tag{33}$$

where ρ_g is the density of the lifting gas at the equilibrium float condition. Therefore, assuming ρ_g is known, Equation (31) becomes:

$$\rho^* V_{max} - \left(0.23 V_{max}^{2/3} + 0.030 kg\right) - m_{payload} - \rho_g V_{max} = 0 \tag{34}$$

and can be solved for V_{max}.

After inflation, the first requirement of a balloon is to rise rapidly enough to avoid any obstacles. With the mass of the complete balloon system fully defined, it is possible to calculate the mass of lifting gas at launch required to provide the necessary free lift ratio:

$$f = \frac{\rho_\infty V_b}{m_{sys}} - 1 \tag{35}$$

for the desired ascent rate, recognizing that excess lifting gas will be vented at the equilibrium altitude. Solving Equation (35) for the volume of the balloon gives the balloon volume required to provide the buoyant force necessary for the desired free lift:

$$V_b = \frac{m_{sys}(f+1)}{\rho_\infty}$$

(36)

where ρ_∞ is the local atmospheric density at the launch altitude. The mass of lifting gas required

to occupy the lifting gas volume, as established from Equation (36), is:

$$m_g = \rho_g V_b$$

(37)

In order to develop overall MET balloon system specifications, it was necessary to

combine realistic Mars environmental conditions with balloon performance estimates.

MATLAB™ was employed to assist with preliminary design studies for the weather balloon.

The MATLAB™ programs utilized input from two Mars surface weather models - Mars24

Version 6.0.3 (Schmunk, 2008) and the NASA Mars-GRAM 2005 (Justus and Johnson, 2001) -

to simulate flight trajectories. The MATLAB™ code for performance analysis is contained in

Appendix A 1.

Mars24 is a Java application created by Robert B. Schmunk from the NASA Goddard

Institute for Space Studies (GISS). Schmunk's program was utilized to synchronize Coordinated

Universal Time (UTC) and Mars Local True Solar Time (LTST) for the balloon flight trajectory

simulations. Mars24 displays a Mars sunclock, a graphical representation of Mars showing its

sun and night sides, a numerical readout of the time (Earth UTC and local time and Mars MTC

and local time) in 24-hour format, a plot showing the relative orbital positions of Mars and Earth,

and a diagram showing the solar angle for a given location on Mars.

The Mars Global Reference Atmospheric Model (Mars-GRAM 2005) (Justh and Justus,

2007) is an engineering-oriented model of the Martian atmosphere utilizing input data tables from

the NASA Ames Mars General Circulation Model (MGCM) and the University of Arizona Mars

Thermospheric General Circulation Model (MTGCM). Both the MGCM and MTGCM models are fully global, based on first-principles, and both have been fit to measured data from Mariner, Viking, the Mars Pathfinder, and the Mars Global Surveyor missions. From the Mars-GRAM 2005 program, a simulated atmospheric database was created to represent a nominal balloon environment for a given latitude, longitude, altitude and local time.

In addition to the default inputs, user inputs to the Mars-GRAM 2005 model included the assumption of seasonal variation of background dust and use of the MOLA reference areoid. Outputs from the Mars-GRAM 2005 model utilized in the balloon design tools included atmospheric temperature, atmospheric pressure, atmospheric density, albedo, surface temperature, terrain height, north-south wind (meridional) speed, east-west (zonal) wind speed, standard deviation in the wind speed – both north-south and east-west, and the cosine of the local solar zenith angle. These data were generated in 5 degree increments of both latitude and longitude, in 100 m increments in height, hour by hour.

The user inputs to the weather balloon design tool were the overall balloon payload mass, the free lift ratio necessary for a prescribed ascent rate, the desired maximum MOLA altitude, the balloon launch MOLA altitude, the latitude and longitude of the balloon launch, the time of the balloon launch in seconds from UTC midnight on the day of launch, and the trajectory simulation time step. As mentioned previously, the atmospheric database created by the Mars-GRAM 2005 program was referenced to UTC time, while Mars LTST was established using the Mars24 program. The simulation time step had to be sufficiently small to enable the balloon ascent calculations to remain stable – a time step of 1 s was used for the weather balloon design calculations.

With the user inputs, the design tool utilized a Newton-Raphson algorithm and the equations developed previously in this section to calculate the size of the weather balloon for neutral buoyancy at the desired maximum altitude. Subsequently, the MATLAB™ program in Appendix A 1 was used to determine the mass of lifting gas and balloon size necessary to

produce the desired free lift ratio at launch. Once the balloon was sized, the program marched

forward in time to simulate balloon ascent position as a function of time after launch, utilizing the

user-specified time step and the equations of motion described in Equations (6) through (8).

Calculated local (to the balloon) atmospheric properties were the ambient temperature,

pressure, density, wind speed and direction, utilizing the MarsGRAM 2005 atmospheric database.

Computed balloon properties were: balloon volume, diameter, surface area, buoyant force and

free lift at launch. Additionally, MOLA height, vertical velocity, vertical acceleration, latitude,

and longitude were calculated as functions of time. The program assumed that during balloon

ascent, the balloon temperature was equal to the local ambient temperature at each balloon

altitude, which was a reasonable assumption since a zero pressure balloon design was employed.

Also, since buoyancy acts as a righting force, vertical winds were ignored. Finally, the

MATLAB™ program created a balloon trajectory text file.

Four weather balloon deployment scenarios were simulated. Launches were assumed to

occur at the noon local true solar time (LTST) in the northern hemisphere at vernal equinox (Ls =

0°), summer solstice (Ls = 90°), autumnal equinox (Ls = 180°), and winter solstice (Ls = 270°).

The Schmunk (2008) Mars24 Version 6.0.3 was utilized to synchronize local Mars time (see

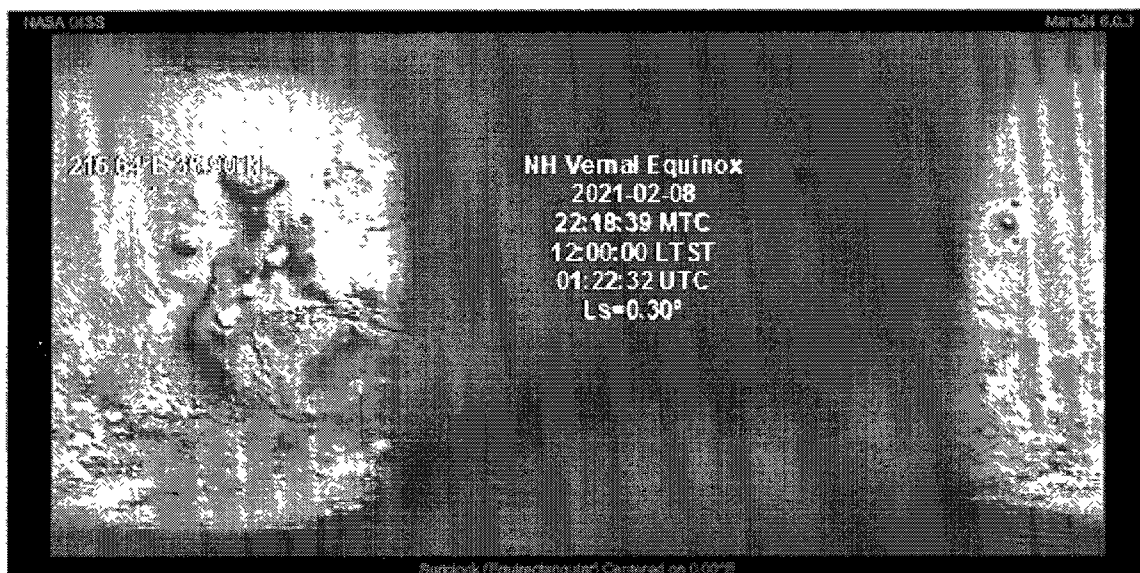Figure 15 through Figure 18) with the Mars-GRAM 2005 model.

Figure 15: MET Balloon Launch Site Northern Hemisphere
Vernal Equinox Launch Time.

Figure 16: MET Balloon Launch Site Northern Hemisphere
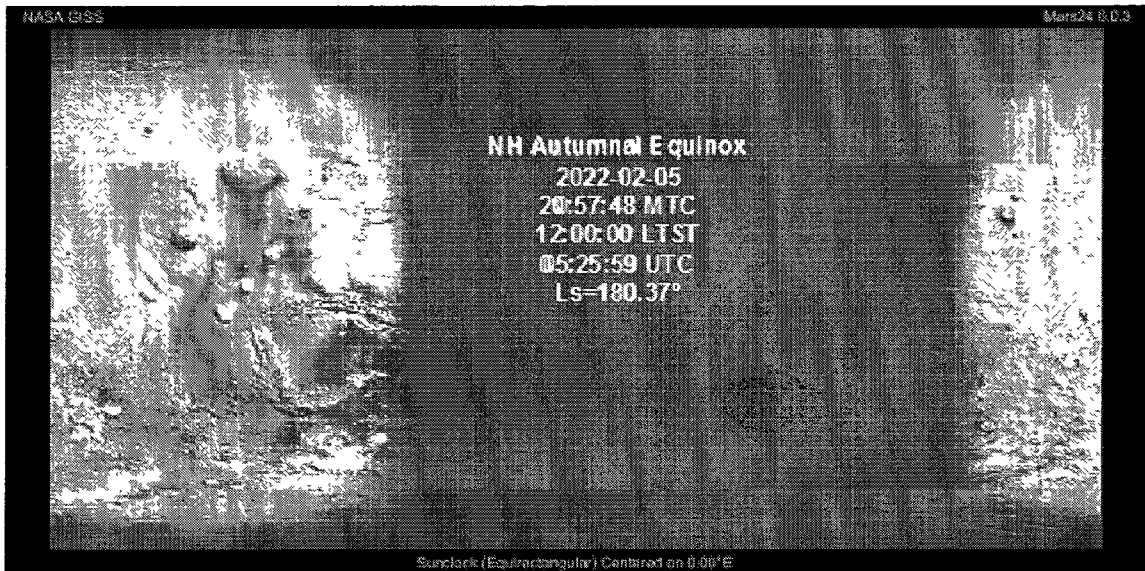Summer Solstice Launch Time.

Figure 17: MET Balloon Launch Site Northern Hemisphere
Autumnal Equinox Launch Time.
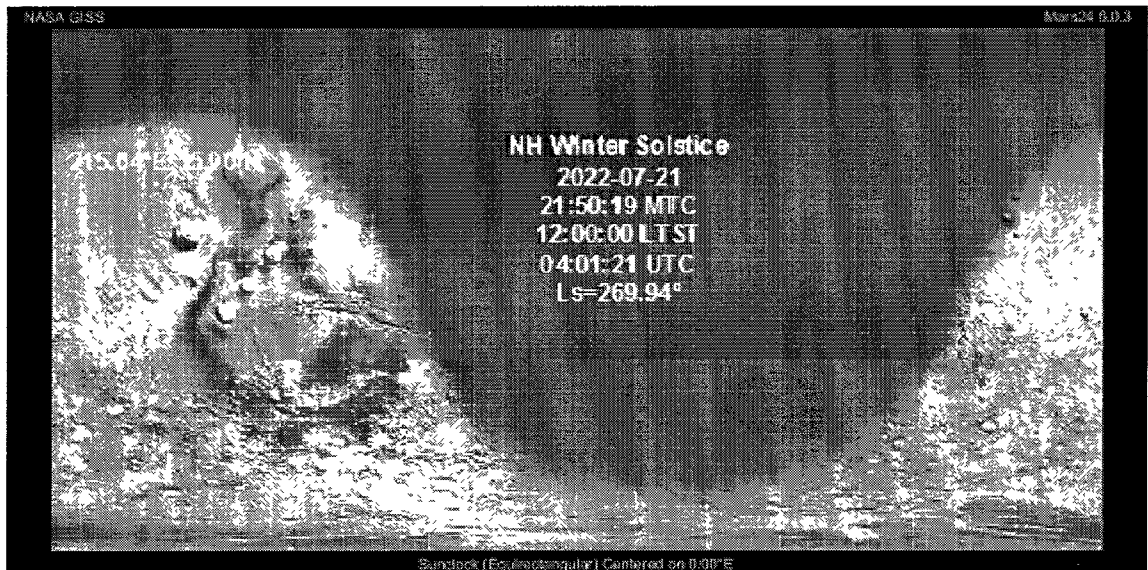
Figure 18: MET Balloon Launch Site Northern Hemisphere
Winter Solstice Launch Time.

The results for the four simulated scenarios are summarized in Table 7. Based on these results, atmospheric conditions dictate that the northern hemisphere autumnal equinox scenario requires the largest balloon for the same maximum balloon altitude and payload specifications. For that scenario, the required balloon volume was 1781.0 m^3 with a total system dry mass of 3.53 kg. There were significant differences between this case and the best case scenario (winter solstice), which only required an estimated balloon envelope volume of 1135.7 m^3 and a total system mass of 2.66 kg. However, because it is necessary to deploy these balloons during all four seasons, the autumnal equinox requirements define the balloon design.

	Ls = 0°	Ls = 90°	Ls = 180°	Ls = 270°
Fully Inflated Volume (m^3)	1517 2	1447 4	1781 0	1135 7
Fully Inflated Diameter (m)	14 26	14 03	15 04	12 94
Launch Volume (m^3)	151 7	162 0	189 3	100 5
Launch Diameter (m)	6 62	6 76	7 12	5 77
Initial Hydrogen Mass (kg)	0 16	0 15	0 17	0 13
Balloon Mass (kg)	3 09	2 99	3 43	2 55
System Dry Mass[†] (kg)	3 19	3 10	3 53	2 66
† DOES NOT INCLUDE: mass of the inflation gas				

Table 7: MET Balloon Design Summary.

Since these weather balloons are designed to ascend to an altitude of 20 km in less than six hours, the balloon ground track is only important in terms of establishing local wind directions and making sure that the radiosondes remain within receiving range of the ground station. Predicted altitude histories (Figure 19) for the four launch scenarios differ only slightly since the balloons were all designed to have the same nominal ascent rates. However, seasonal winds vary a great deal as can be seen in the nominal ground tracks for the four launch scenarios (Figure 20 and Figure 21). The most obvious feature of this plot is that the "summer solstice" balloon trajectory was east to west while the other three balloon trajectories were west to east. Figures 20 and 21 also show that the winter solstice balloon launch scenario traversed the longest distance,

covering a 938 km ground track, in approximately seven hours and thus drives the range

requirements for the radiosonde transmitter and the launch system tracking radar.
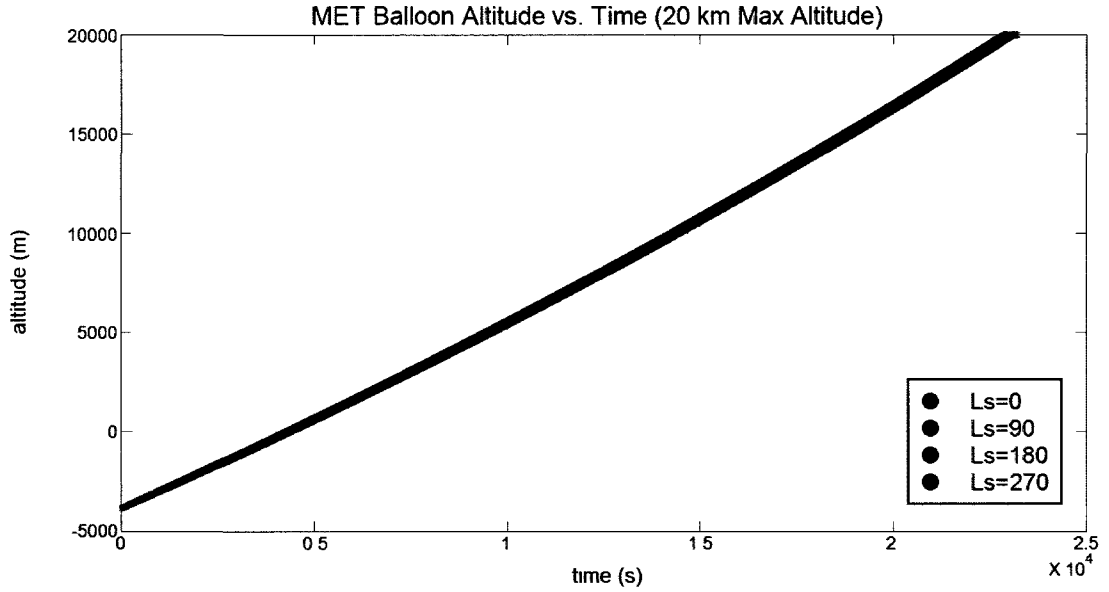
Figure 12: MET Balloon Vertical Flight Profiles.
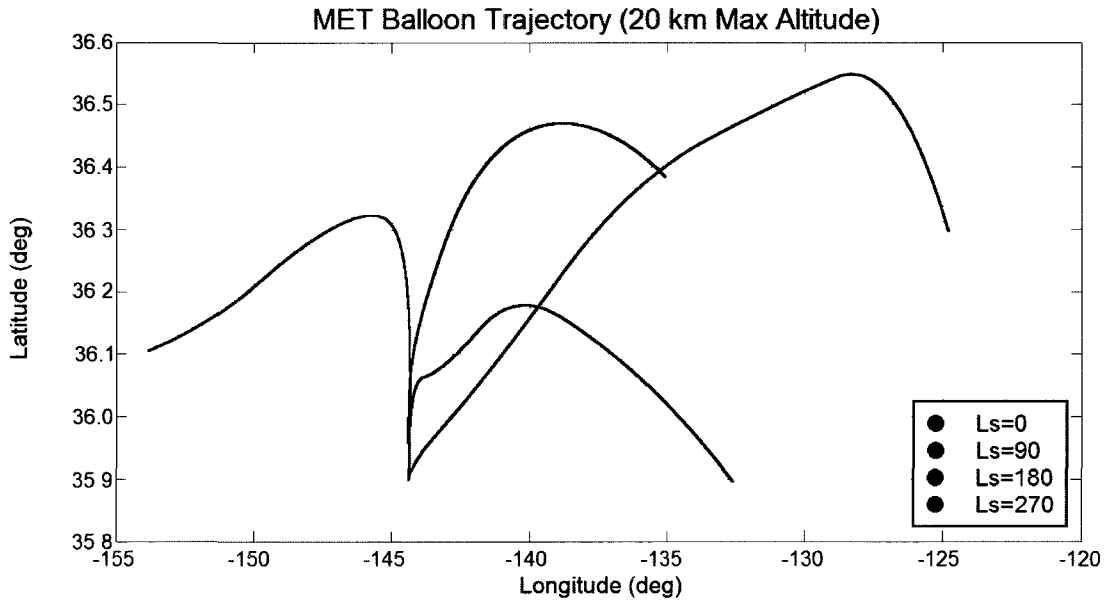
Figure 20: MET Balloon Horizontal Flight Trajectories.
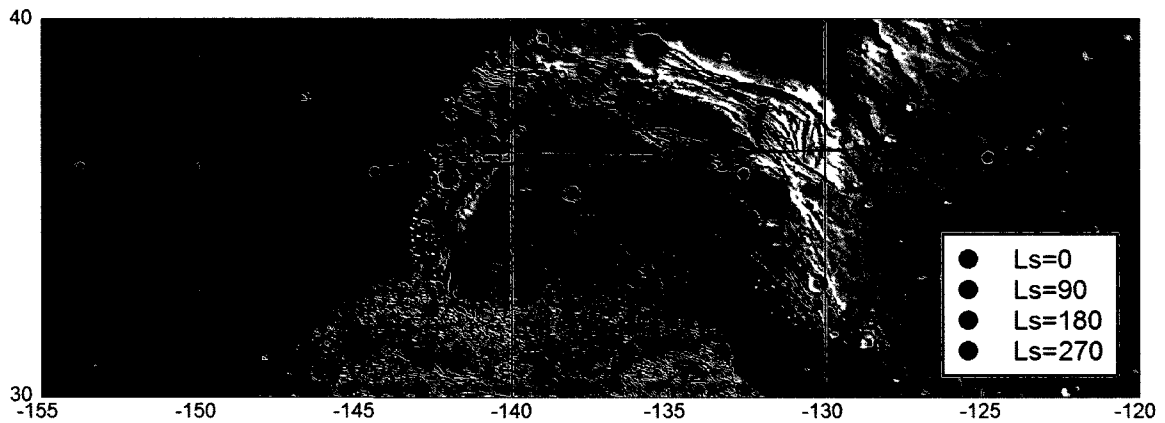
Figure 21: MOLA Overlay of MET Balloon Ground Track.

4.4 MET BALLOON SYSTEM SUMMARY

The MET balloon system can be divided into the following elements: balloon - envelope,

seams, end fittings, and inflation tube; radiosonde; and suspension system. The balloons were

designed to transport a 150 g radiosonde payload to an altitude of 20 km while recording *in situ*

atmospheric measurements. The primary MET balloon system element masses estimated using

the design tool developed for this thesis, in Appendix A 1, are summarized in Figure 22,

including the overall mass budget.

Volume: 1800.0 m³
Diameter: 15.09 m
Balloon Mass: 3.43 kg
Gas Mass: 174 g
Sonde Mass: 150 g
System Dry Mass: 3.53 kg

Material: 3.4um polyethylene
Material Strength: 410±40 kg/cm² MD
370±30 kg/cm² TD
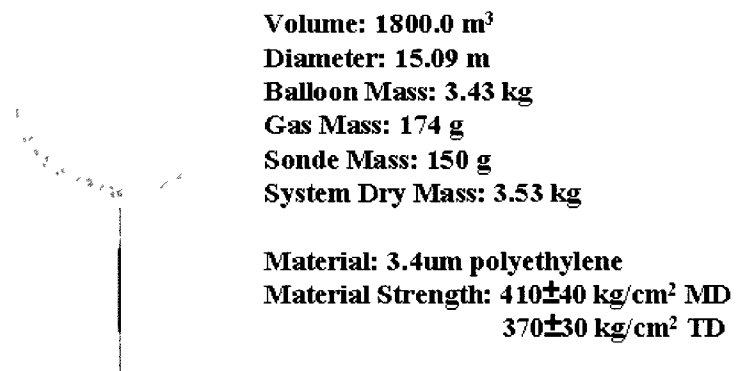
Figure 22: MET Balloon Design Summary.

The balloon envelope was sized for positive buoyancy at 20 km under the worst case conditions – northern hemisphere autumnal equinox – assuming a lifting gas mass that was sufficient to provide free lift at a nominal 1 m/s ascent rate. The balloon is to be inflated through an inflation tube located in the upper hemisphere of the balloon and each balloon is packed by folding. Using the four seasonal launch designs, the initial balloon volume from a launch site located at Northeast Amazonis (35°54'N 144°21.6'W) will be between 100.5 m^3 and 189.3 m^3 (5.77 m < diameter < 7.12 m).

The lengths of the Mars seasons are summarized in Table 8. Assuming a weather balloon launch every eighteen degrees of solar longitude, translates to five launch days per season. It is also desirable for one of the five seasonal launch days to include a morning and evening launch in order to verify diurnal atmospheric changes. If two spare balloons are included, a total of 26 balloons are required with a total estimated mass between 92 and 104 kg. This mass estimate is for the MET balloon systems only, and does not include provisions for inflation or launch.

Season (Northern Hemisphere)	Starting Ls	Length (sols)
Spring	0°	194
Summer	90°	178
Autmumn	180°	142
Winter	270°	154

Table 8: Length of Seasons on Mars.

Packing volumes of nylon decelerators (i.e. parachutes) based on proven packing methods are summarized in Table 9. The biggest risk to damage of the balloon during packing is knife-line creases damaging the fabric on a fold. Assuming a balloon can be packed, without damage, to an equivalent manual hard pack density of 448 kg/m^3, each balloon can be packed into a package of 0.0079 m^3. 26 balloons would require a total volume of 0.2 m^3.

Packing Density of Nylon Decelerators	
Packing Method	Packing Density (kg/m3)
Manual -soft	352
Manual - hard	448
Vacuum or light mechanical press	481
Pneumatic press	561
Hydropress - light	641
Hydropress - medium	738

Table 9: Packing Densities of Nylon Decelerators.

4.5 MET BALLOON LAUNCH SYSTEM

The relatively large size of the Mars balloons represents a significant autonomous launch challenge and is likely the critical risk-limiting step. The balloon launch system must be capable of launching twenty-six MET balloons. It includes the structure, electronics, mechanisms, and inflation system, along with a tracking radar system. In addition, the launch system must include a meteorology package for monitoring the launch environment, with sensors similar to the types used in the MET balloon system radiosondes. The balloon launch system conceptual design is depicted in Figure 23.

An integral part of each launch will be the deployment and inflation of the *launch cone* atop the launcher. The launch cone is employed to stabilize the balloon during inflation and minimize the risk of wind-driven damage or tearing of the balloon envelope. The balloon launch system is designed to sit atop a lander like a turret, and, in preparation for launch, rotate so that the balloon and payload are oriented in the downwind direction from the lander. The balloon payload is then extended from the lander on a jib boom. The consumable hydrogen lifting gas is supplied to each balloon via a common inflation system shown in Figure 24.
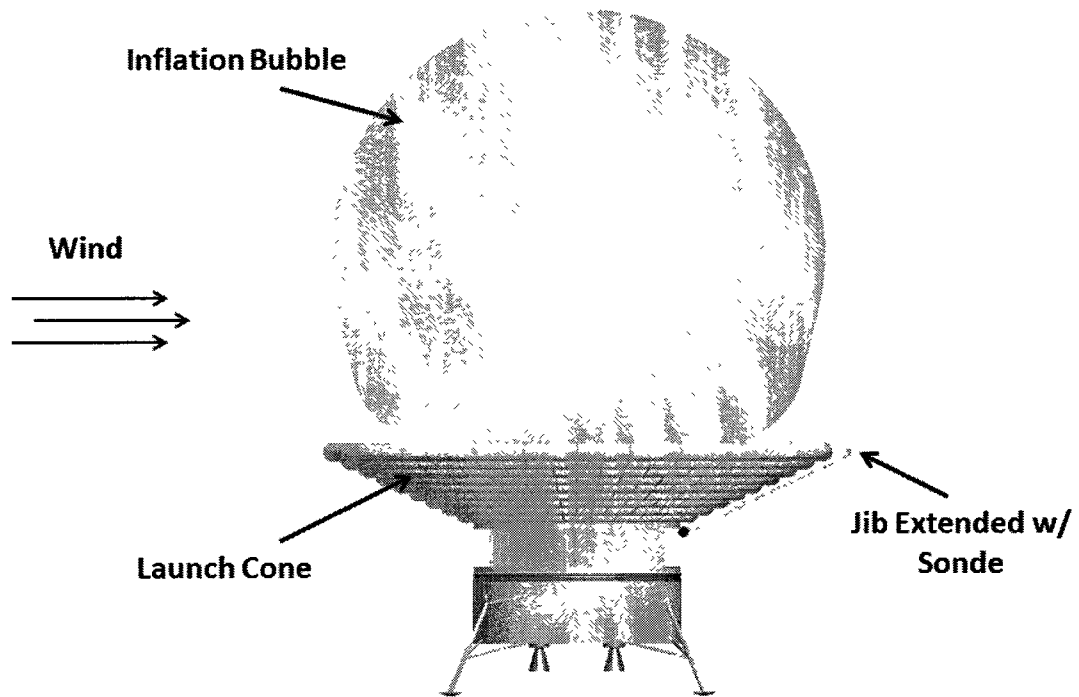
Figure 23: Conceptualization of Balloon Launch System.
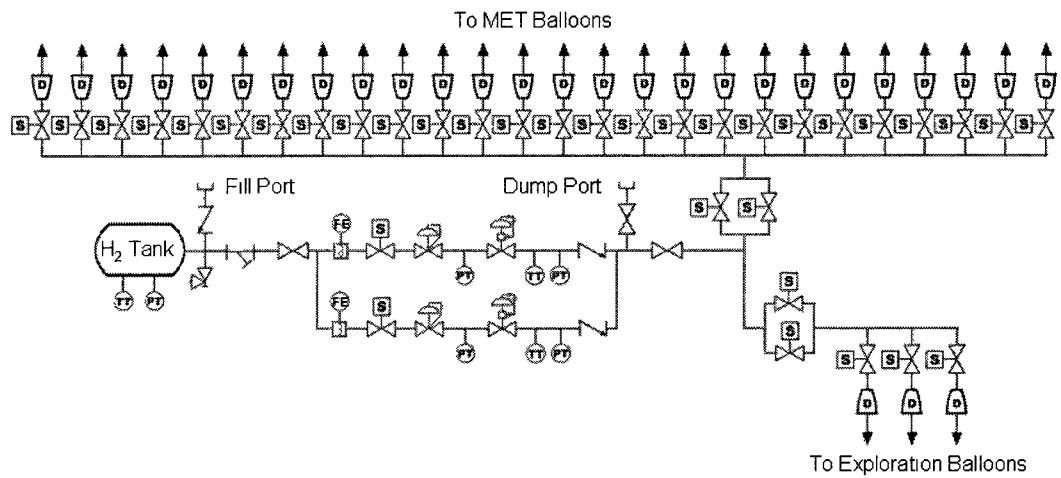
Figure 24: Inflation System Schematic.

The sequence of steps for MET balloon launch operations is depicted in Figure 25. When a MET balloon launch command is initiated, in order to mitigate the risk of damage to the balloon by wind or dust, before inflation is initiated; local go/no-go weather conditions are checked against prescribed launch criteria and the resulting condition transmitted to the Earth monitoring station. Since a terrestrial ground control link can impose up to a 40-minute round trip communication delay, a critical system engineering element will be validation of short-term Mars surface weather forecasting, based on the monitored Mars launch site weather data. Once a "go" condition is authorized for a balloon flight, the launcher system radar and UHF receiver are activated, the MET instrument package is activated and appropriate system checks are performed sequentially. The radiosonde pressure, temperature, and humidity sensor outputs are compared with surface-based environmental sensors to ensure proper operation of the sonde sensors, including recalibrating the humidity sensors, and proper operation of the radio transmitter. Once the system checkouts are successfully completed, the launcher system rotates to place the payload down-wind of the lander, deploys the inflatable launch cone, and extends the sonde on the jib boom as shown in Figure 23. With the cone fully inflated and the launcher in the correct configuration, the MET balloon solenoid valve and the respective balloon solenoid valve are opened. After these valves are verified open, the main hydrogen-supply solenoid valve is opened and the balloon begins to fill, slowly at first to minimize risk of damage to the balloon envelope and then at a higher inflation rate as the *inflation bubble* is established, and controlled, utilizing a control valve.

MET BALLOON LAUNCH OPERATIONS
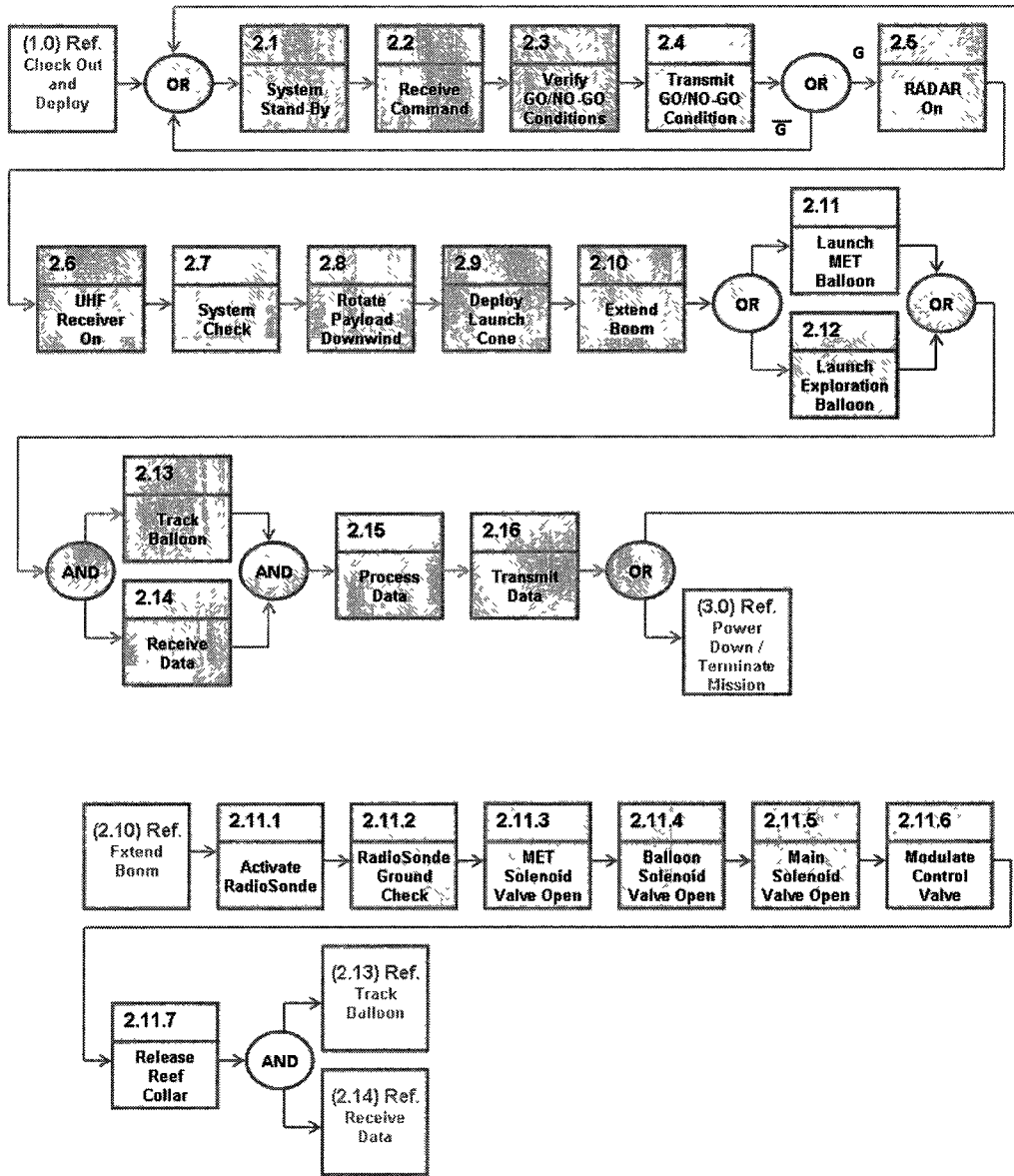
Figure 25: MET Launch Operations Functional Flow Block Diagram.

The balloon is restrained in the launcher by a hutch clutch (see Figure 26). A collar with a tear strip ensures that only the top portion of a balloon is inflated, based on the required deployment volume (for managed ascent) at launch. Once the required lifting gas mass has been supplied to the balloon bubble, the hutch clutch will release and the balloon will begin to rise, unfolding the remaining un-inflated envelope beneath it. As the wind begins to convect the balloon, that motion will snatch the radiosonde away from the launcher (and lander). The un-inflated length of balloon will be wrapped in a reefing sleeve to prevent a sail from forming as the partially inflated balloon ascends. A tear-strip on the collar tears, allowing the gas bubble to expand as the collar falls away. As the gas bubble expands, a rip-stitch on the reefing sleeve tears allowing the gas bubble to grow. After the balloon has been launched, the launch system will continue to track and receive data as long as the balloon is within range.
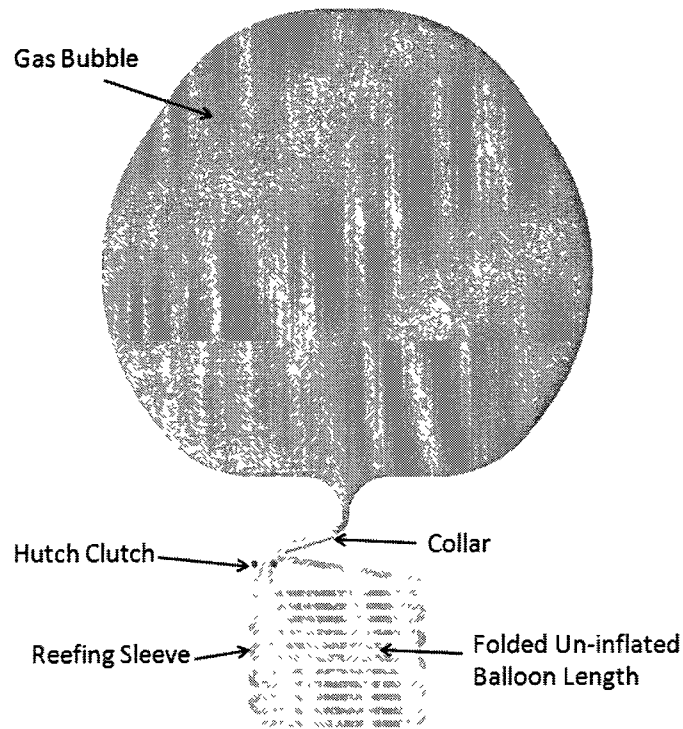
Figure 26: MET Balloon Launch Component Schematic.

CHAPTER 5

BALLOON EXPLORATION SYSTEM

5.1 BALLOON EXPLORATION SYSTEM MEASUREMENT TYPES

In addition to small, short-lived balloon-borne radiosondes, larger balloons, designed to float in the atmosphere for extended periods of time can carry heavy payloads, such as small rovers and other deployable surface instrumentation, over large distances, while providing access to topographical regions that are considered to be too hazardous for any other type of payload deployment. Simultaneously, these heavy balloon systems can expand atmospheric measurements and enable high resolution geological, geochemical, and geophysical surveys spanning distances measured in hundreds or thousands of kilometers. Instruments like particle detectors, mass spectrometers, and gas chromatographs can directly sense the atmosphere to provide high resolution *in situ* measurements of gas composition, isotopes, and dust and aerosol characterization. Remote sensing instruments such as imagers, radars, radiometers, polarimeters, and photometers are able to perform measurements at remote distances (Zubrin et al., 1994).

The scientific needs of planetary geology require measurements of magnetic properties, mineralogy, and imagery. Airborne sensors that can detect atmospheric methane concentrations would be extremely important in pinpointing methane sources (see Mumma et al., 2009) because methane is a short-lived atmospheric constituent and it is produced primarily by biological processes on Earth. Balloon borne payloads can fill a resolution gap between orbiters and surface rovers. Orbiters provide planetary scale measurements with limited resolution. Rovers and landers provide high resolution surface measurements at a local perspective, but over very limited surface ranges from a planetary perspective. The rovers *Sojourner, Spirit,* and *Opportunity* made evident the severe restrictions on the mobility of surface rovers - large areas of Mars are inaccessible by rovers and orbiters. A balloon borne payload can provide surface sensing with

resolution orders of magnitude better than orbiters over a range of hundreds of kilometers and provide access to geographic features that are inaccessible to contemporary rovers and orbiters.

Analysis of magnetic properties with a balloon-borne magnetometer of sufficient resolution could provide understanding of the structure and source of Mars' remnant crustal magnetism (Wright et al., 2004). Local concentrations of ice, hydrated minerals, or deposits on carbonates could be detected by neutronic devices, while electromagnetic sounding using radar altimeters can reveal sub-surface ice layers (Zubrin et al., 1994). Detailed spectral surface measurements can be made using balloon-borne miniature grating and acoustic-optic spectrometers. 3-D image surface mapping can be created from balloon-borne laser altimeter topographic measurements. And, high resolution imaging can be performed from a balloon-borne aerial platform (Wright et al., 2004).

Whatever the instruments, atmospheric density constraints on Mars balloons necessitate the need for lightweight payloads. Lightweight payloads can benefit directly from miniaturization initiatives accomplished through the use of technologies developed for other micro vehicles. In addition, instruments will require sufficient robustness to remain calibrated for extended periods of time (months to years) while providing capability for remote calibration. It is also apparent that scientific balloon payloads require sustained electrical power, which benefits from lightweight, low-power communications systems employing a relay infrastructure, possibly using orbiters, capable of handling the data-rate needs (Cutts and Kerzhanovich, 2001). Long duration payloads will likely require a means to generate power.

5.2 VARIABLE-ALTITUDE LATERAL FLIGHT CONTROL

Depending on the season, the ground track of a balloon free-floating in the Mars atmosphere is generally from east to west, carried by the zonal winds within a given latitude band. Two-way altitude control allows the balloon to descend and ascend in the downwind direction, and has successfully been demonstrated in long duration CMET balloon flights in the

arctic (Voss et al., 2011). Coupling vertical altitude control with horizontal motion created by planetary winds facilitates an aerobot capability for sub-orbital planetary-scale exploration, enabling the investigation of specific features of Mars or even delivery of payloads to distant, even conventionally inaccessible locations, based on entry, descent, and landing constraints. North-south meridional travel is possible utilizing atmospheric circulation winds – Hadley cells and the CO_2 condensation - sublimation cycle that transports carbon dioxide between the poles and equator (see Figure 27). These winds are highly variable and altitude dependent, with alternating north-to-south winds and south-to-north winds depending on the circulation patterns of the cell. The zonal winds, however, are dominant and thus overall balloon trajectories are primarily east-to-west with potentially active north/south lateral adjustments. To provide a balloon with this type of trajectory control requires enabling technologies in buoyancy control, ground track determination, sensing, wind modeling, and path planning.

EQUINOX CIRCULATION

TWO HADLEY CELLS

HEIGHT, km

CO_2 MASS FLUX ⇨

POLAR CAP WINDS

THERMAL TIDES

WEAK PLANETARY-SCALE WAVES

SPRING HEMISPHERE

FALL HEMISPHERE

SOLSTICE CIRCULATION

SINGLE HADLEY CELL

HEIGHT, km

CO_2 MASS FLUX ⇨

WEAK WINDS

THERMAL TIDES

STRONG PLANETARY-SCALE WAVES

-90   0   +90

SUMMER HEMISPHERE

WINTER HEMISPHERE
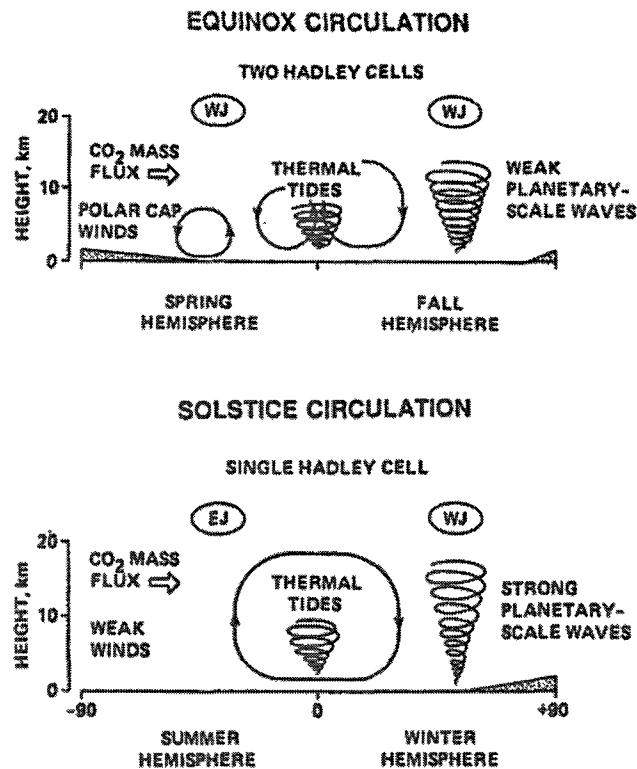
Figure 27: Mars Atmospheric Circulation (Bagenal, 2011).

The oldest method of reversible balloon altitude control controlled the temperature of the lifting gas, and has been a standard navigational procedure employed by hot air balloonists. Heat loss across the balloon envelope is significant, however, and this method is not efficient from an energy standpoint. Exploration balloon altitude control systems must be more energy-efficient with minimal mass loss, while exhibiting predictable performance under varied atmospheric conditions. These systems must be capable of traversing the desired vertical range of the atmosphere, while operating reliably on long duration flights (Voss and Smith, 2003). Potential altitude control systems include the Air Ballast (AB) system. AB systems utilize the high molecular weight of the ambient atmosphere, relative to the lifting gas, as ballast. To descend, ambient atmosphere is pumped into a bladder inside the superpressure balloon (see Figure 28) increasing the system mass. To ascend, the process is reversed. AB systems have been utilized successfully in terrestrial sounding campaigns.
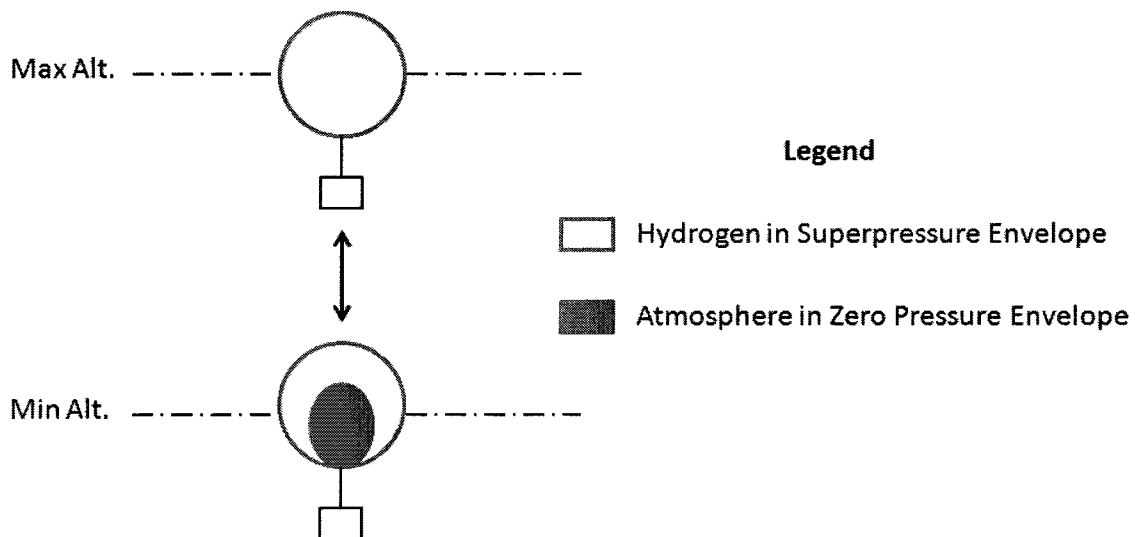
Figure 28: Air Ballast Altitude Control Schematic (Voss and Smith, 2003).

Scientific measurements must be correlated with specific locations on the planet. In addition, for an aerobot to adjust its trajectory to reach a location of interest, the aerobot must be able to determine its own location. On-board sensors are necessary to estimate the aerobot

position relative to planetary coordinates, and the absence of a planetary magnetic field or other global direction information represents a significant challenge. On-board sensors may include a gyro and accelerometers for dead-reckoning navigation, a sun sensor to determine the angle of the sun at a given local time with respect to the balloon platform, a gravity vertical sensor to determine gondola orientation with respect to the local vertical, a radar altimeter to sense the terrain profile to match against existing topographical data and to provide ground velocity data, and/or a camera to image surface topography for correlation with map data to determine the position of the aerobot with respect to specific target sites (Cutts et al., 1995). On-board location determination can be verified regularly through balloon tracking by orbiters, but those data cannot be used by terrestrial ground controllers because of the two-way radio transmission delay. Additionally, balloon hazard avoidance requires that imminent collision of the balloon with high-elevation terrain be detected early enough to permit evasive action.

Detailed knowledge and accurate forecasts of local wind patterns will be essential for effective aerobot navigation. Flight control systems will be required to employ three-dimensional navigation. An on-board engineering atmospheric model utilizing periodic updates from Earth or orbiter spacecraft, and consisting of prevailing wind directions and velocities as a function of altitude, vertical down/up draft, cloud-cover, and day/night insolation will be necessary for autonomous navigation (Cutts et al., 1995). *In situ* data gathered from Mars MET balloons can contribute to this model.

Balloon path planning is a complex motion planning problem requiring short-term path planning and monitoring for obstacle avoidance, as well as more-forward-looking path planning to increase the probability of direct over-flight of the target area, and path planning to maneuver as close as possible to a specific target. The aerobot must be adaptive and capable of updating its wind models on-the-fly. The flight control system must be adaptive enough to respond to both predicted and unexpected favorable wind currents and likewise react to unfavorable wind currents

whenever they are encountered. Maneuvers like precision navigation or equatorial crossing may not be possible.

5.3 EXPLORATION BALLOON DESIGN

Heavy payloads compound the challenge of flying a balloon platform on Mars. Autonomous launches of very large balloons at Mars will be unprecedented. In order to minimize the mass penalty associated with the balloon envelope, a spherical shape is preferable because envelope mass is a smaller fraction of total mass than for other balloon shapes. Long duration flights require super-pressure balloon designs. Mylar, Dartek, and special-purpose composite lay-ups were considered as envelope material candidates. A composite lay-up based on the MABS composite (Rand and Phillips, 2002) was selected because it satisfied the strength requirements while accommodating all of the identified ancillary requirements associated with surface-launched Mars balloon systems. The exploration balloons were designed to float at an altitude of 10 km above MOLA which was considered to be a good compromise between balloon payload performance and altitude-based local surface restrictions. The envelope mass was estimated assuming an areal density of 19.66 g/m^2 for the composite balloon film. Existing manufacturing constraints limit maximum nominal gore widths to 2.75 m; it was thus determined iteratively that 60 gores were required for appropriate envelope volumes. A free lift of 10% was specified in order to provide a slow ascent rate, minimizing the anticipated shock loads associated with an autonomous launch. A MATLAB™ design tool, similar to the one created for the MET balloons, was developed to size the large balloon system and predicted balloon ascent rates and flight trajectories based on local atmospheric conditions and predicted winds, employing the Mars-GRAM 2005 model. The MATLAB™ code is contained in Appendix A 2.

Using the relationship:

$$\rho^* V_{max} - m_b \left(V_{max} \right) - m_{payload} - \rho_g V_{max} = 0 \qquad (38)$$

where $m_b \left(V_{max} \right)$ is the mass of the balloon as a function of maximum balloon volume, V_{max} can

be calculated numerically to determine the mass of the complete balloon system. With the mass

of the complete balloon system fully defined, an iterative approach was developed so that the

required mass of lifting gas and balloon volume converged to provide the required free lift at

launch and a neutrally buoyant balloon at the specified constant-density float altitude.

As with the MET balloons, for a specified free lift ratio, f, the volume of the balloon

necessary to provide the desired free lift could be calculated using Equation (36):

$$V_b = \frac{m_{sys} \left(f + 1 \right)}{\rho_\infty} \qquad (36)$$

and the mass of lifting gas required to provide the necessary volume using Equation (37):

$$m_g = \rho_g V_b \qquad (37)$$

Substituting the lifting gas mass required for launch into the lifting gas term in Equation (38), the

equation becomes:

$$\rho^* V_{max} - m_b \left(V_{max} \right) - m_{payload} - \rho_g V_b = 0 \qquad (39)$$

and a new V_{max} can be calculated. This approach can be iterated until a solution converges that

provide a V_{max} and m_g that produce the required free lift at launch and a neutrally buoyant

balloon at the specified atmospheric float density altitude.

Using Mars-GRAM 2005, with default inputs, seasonal variation of background dust, and the MOLA reference areoid, an atmospheric database was generated, resolved in 5 degree increments of both latitude and longitude, and in 100 m increments in height, on an hour-by-hour basis. Outputs from the Mars-GRAM 2005 model included atmospheric temperature, atmospheric pressure, atmospheric density, albedo, surface temperature, terrain height, north-south (meridional) wind speed, east-west (zonal) wind speed, standard deviation in the wind speed – both north-south and east-west, and the cosine of the local solar zenith angle.

The exploration balloon design and simulation program required the following inputs: (1) balloon payload mass; (2) the number of balloon gores; (3) the free lift ratio desired for a prescribed ascent rate; (4) the gray body radiation properties for the top and bottom halves of the balloon envelope; (5) a nominal convective heat transfer coefficient characterizing natural convection between the lifting gas and the balloon envelope; (6) the desired MOLA float altitude; (7) the assumed MOLA launch altitude; (8) the latitude and longitude of the balloon launch location; (9) the time of the balloon launch in seconds from UTC midnight on the day of launch; and (10) the trajectory simulation time step. Like the weather balloon design tool, the atmospheric database created using the Mars-GRAM 2005 program was referenced to UTC time, while Mars LTST was established through the Mars24 program. Again, the simulation time step had to be small enough to avoid numerical instabilities, especially during the balloon float – a time step of 1 s was used for those calculations. In addition to the balloon-specific inputs, the user had the option of including the standard deviation of wind speed in the trajectory calculations. The standard deviation of local wind speed was considered to be a useful parameter in attempting to bracket simulated balloon flight trajectories. Lastly, an input vector, representing the distance and location of Mars relative to the sun was required. Based on the user inputs, the design tool used a Newton-Raphson algorithm to size the balloon for neutral buoyancy at the desired float altitude based on the methodology just described.

Once the balloon was sized, the program simulated balloon ascent as a function of time, utilizing the specified simulation time step. After ascending to the desired float altitude, the program continued to predict balloon motion and the overall flight trajectory as a function of time. Estimated instantaneous balloon properties were: envelope volume, diameter, projected area for thermal calculations, buoyant force, free lift, envelope superpressure, lifting gas temperature, MOLA height, vertical velocity, vertical acceleration, latitude, and longitude. Like the weather balloon design tool, vertical wind components were ignored, because buoyancy acts as a righting force. For the ascent, the program assumed that the balloon temperature was equal to the ambient temperature at a given altitude. After float altitude was reached, the balloon temperature was estimated using an energy balance of the type described in the BALLOON THERMAL EFFECTS section. Again, the MATLAB™ program created a balloon trajectory output text file.

Prior to balloon trajectory analyses, the sensitivity of balloon design to specified payload mass was investigated to develop a relationship between the payload mass and overall balloon system mass. Assuming the same launch site as the MET balloon calculations, Northeast Amazonis (35°54'N 144°21.6'W -3867 m MOLA height), and a balloon launch during vernal equinox, Ls=0°, overall balloon system mass and fully inflated volume were calculated as functions of payload mass. The sensitivity of balloon size to payload mass is shown in Figure 29, and the influence of payload mass on estimated launch mass is shown in Figure 30.
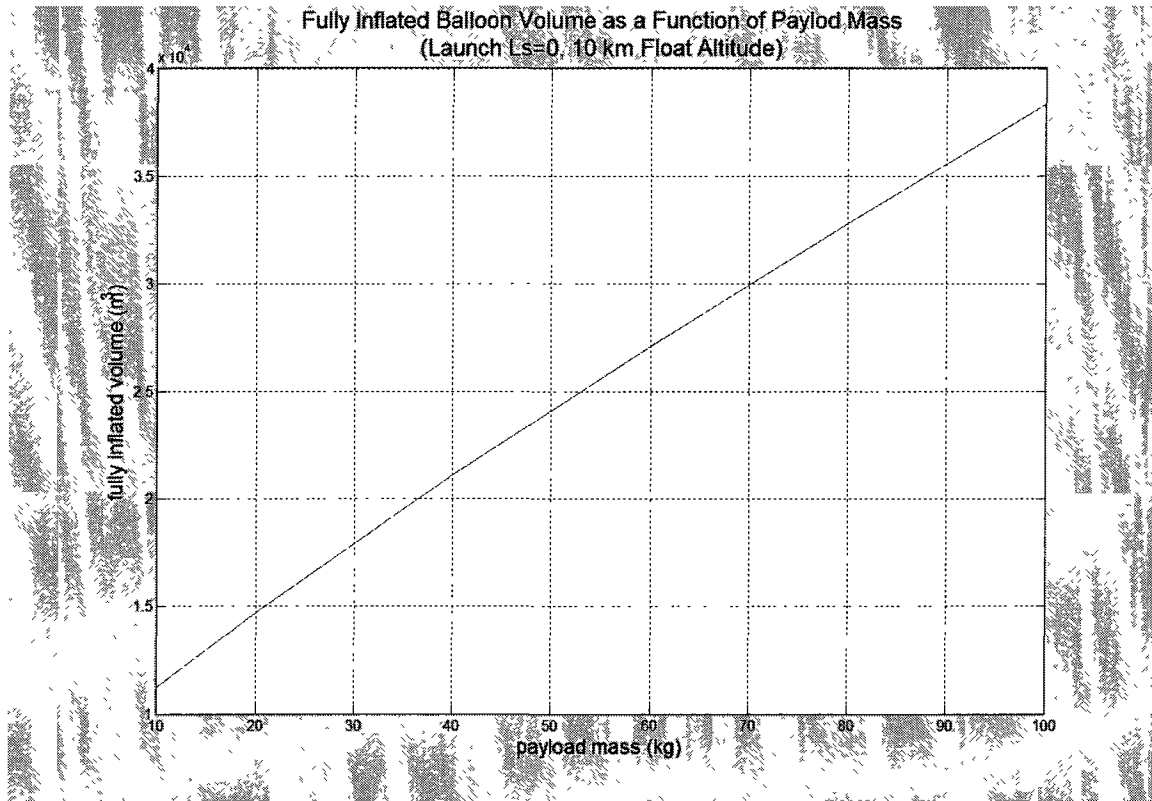
Figure 29: Influence of Payload Mass on Superpressure Balloon Size (Volume at Float Altitude; Seasonal Launch Time Ls=0, ~10 km Float Altitude).

While the required overall system mass and balloon volume were influenced by seasonal launch times, the trends exhibited in these plots can be considered to be representative, regardless of Mars season. Over the range of payload masses considered, total system launch mass could be approximated as a linear function of payload mass. However, as can be seen in both figures, balloon volume and launch mass performance improves as the payload mass is increased. Consequently, secondary considerations such as autonomous launch difficulties associated with increasing envelope size will become controlling. The trajectory simulations assumed the balloon payload mass was 100 kg, since that payload size is capable of transporting a modest deployable surface rover (Mars rover masses have ranged between 10.5 and 180 kg to date) or a significant instrumentation package, including on-board navigation and two-way altitude controls that could enable wind vector flight control.
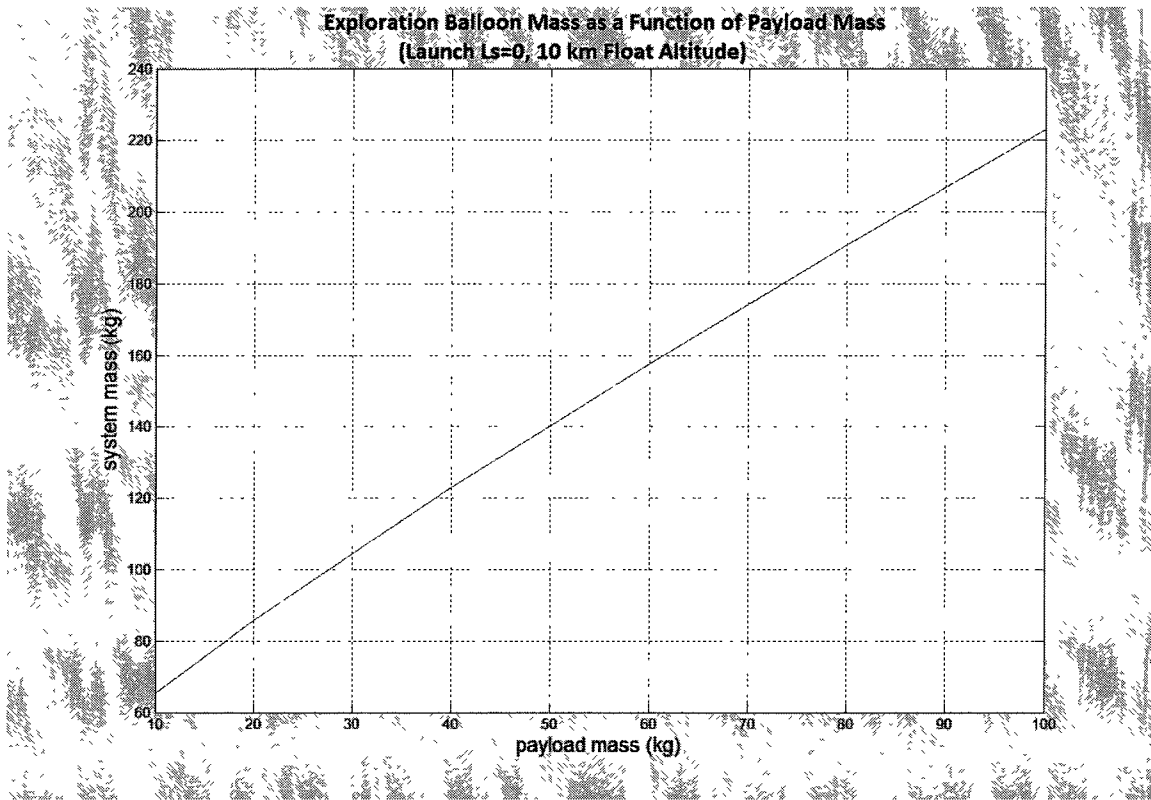
Figure 30: Influence of Payload Mass on Total Superpressure Balloon Launch Mass (Seasonal Launch Time Ls=0, ~10 km Float Altitude).

The thermal performance of the 100 kg payload superpressure balloon was incorporated in the trajectory simulations in order to understand the influence of gray-body balloon film performance on balloon temperature, and thus superpressure, at the upper size limit. For the Northeast Amazonis (35°54'N 144°21.6'W -3867 m MOLA height) launch during vernal equinox, Ls=0°, a parametric study of the influence of ultraviolet absorption (α) and infrared emission (ε) on the top and bottom of the balloon envelope (α_{top}, ε_{top}, α_{bot}, and ε_{bot}) was performed to assess the influence of thermal radiation on balloon temperature and pressure variation during a one-sol diurnal cycle. The results of those simulations are presented in Figures 31 through 33. Figure 31 shows the effect of each of the respective gray-body properties on maximum balloon temperature in the Mars environment. Figures 32 and 33 show the effect on

minimum temperature and the difference between maximum and minimum balloon temperatures respectively.
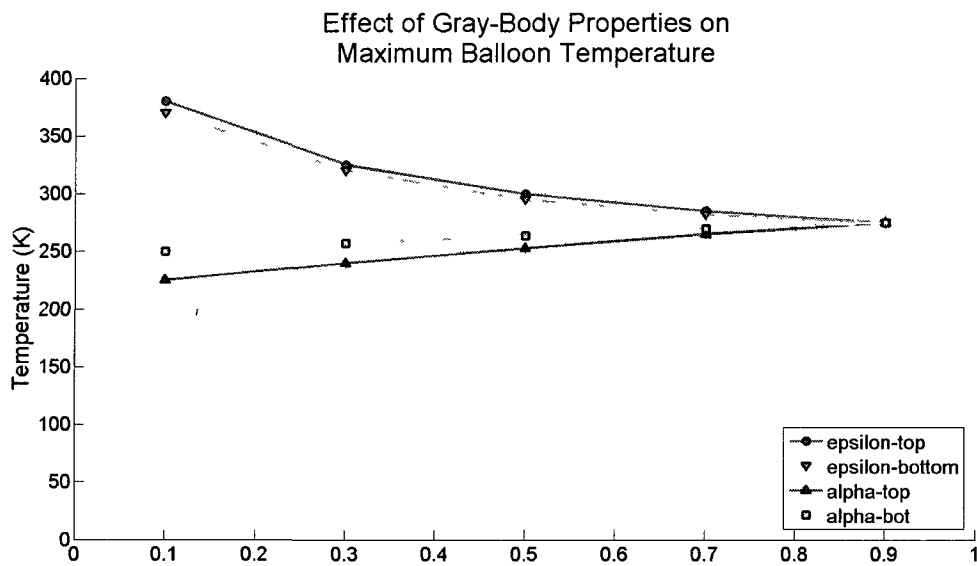
Figure 31: Influence of Gray-Body Envelope Film Properties on Maximum Balloon Temperature Over One Sol.
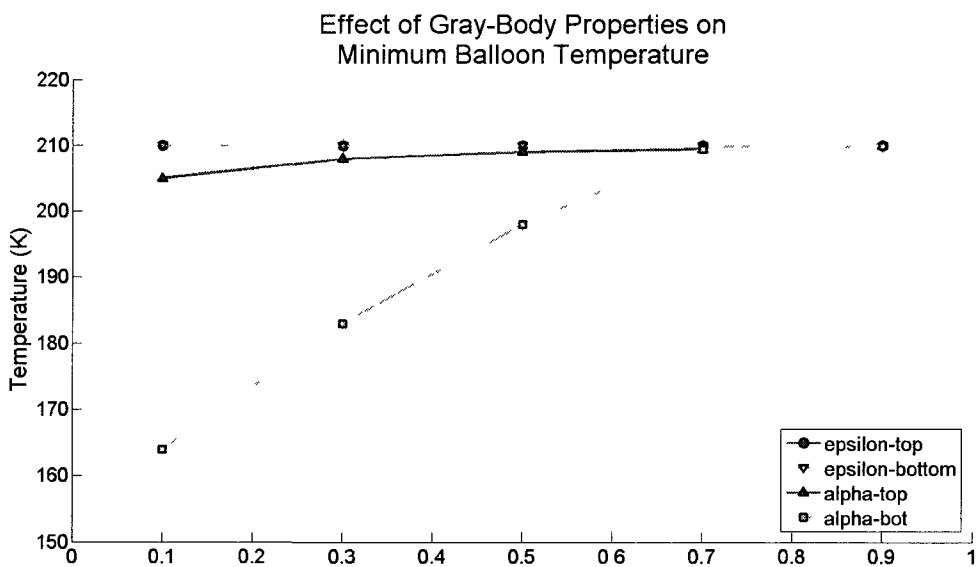
Figure 32: Influence of Gray-Body Envelope Film Properties on Minimum Balloon Temperature Over One Sol.

Effect of Gray-Body Properties on
Balloon Δ T
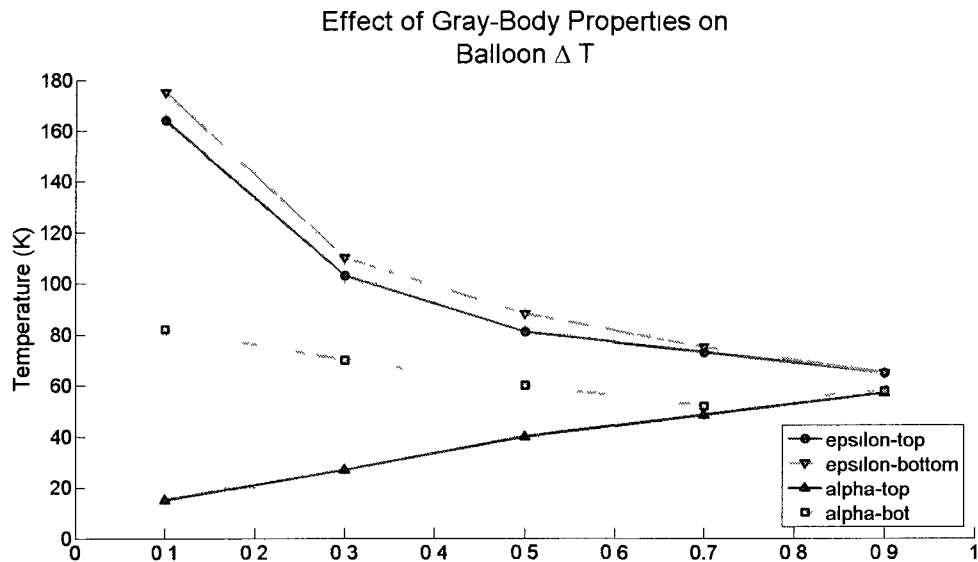
Figure 33: Effect of Film Optical Properties on Balloon Diurnal ΔT.

It is desirable to minimize the diurnal ΔT while minimizing the maximum balloon

temperature (and balloon superpressure) by maximizing the minimum balloon temperature at a

specific constant density altitude. Based on the simulations, selective coatings on the upper

balloon film hemisphere with a nominal ultraviolet absorptivity of 0.1 and infrared emissivity of

0.9 was considered to be optimal. (Based on the ultraviolet vs. infrared selective coating

properties represented in Figure 34, silver FEP-teflon is capable of producing the desired

performance.) The diurnal temperature history for a selective coating balloon of this type is

shown in Figure 35, starting from local solar noon.

As was the case for the MET balloon launch simulations, exploration (100 kg), long-

duration balloon system launches were simulated using the MATLAB™ design tools, for Ls=0°,

90°, 180°, 270° respectively. Based on a plot of surface winds made from Mars GRAM 2005

predictions (Figure 36), it was determined that average wind speeds tend to be lower in late

morning to early afternoon LTST. Therefore, exploration balloon launches were assumed to

occur at local solar noon.
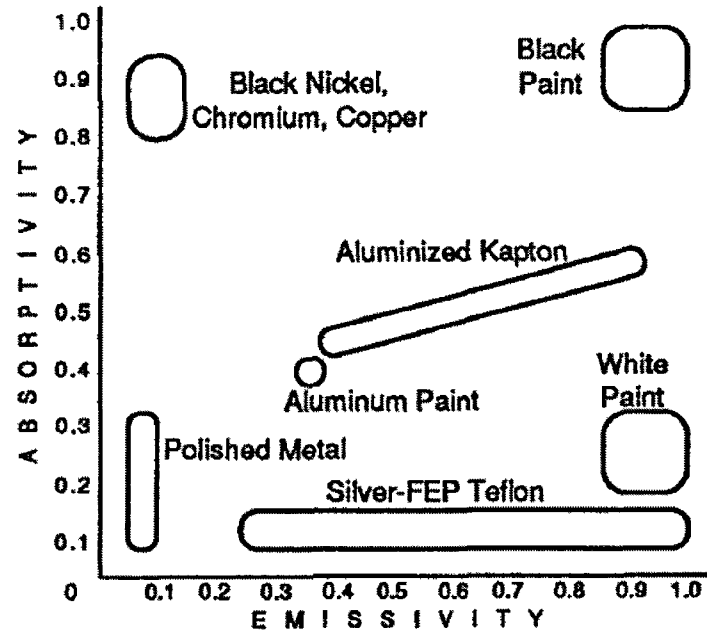
Figure 34: Optical Properties of Common Surface Finishes (Cathey, 1996).
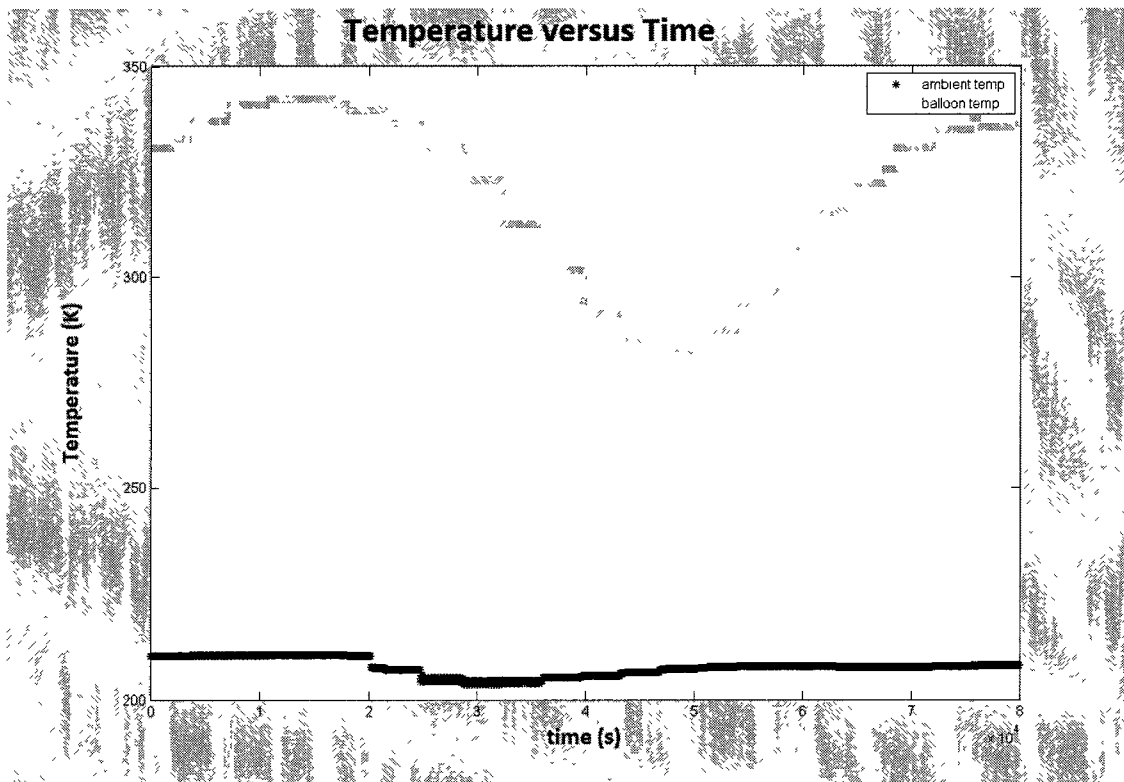
Figure 35: Comparison Between Ambient and Balloon Temperature Histories During One Sol - Noon to Noon ($L_s = 0°$).
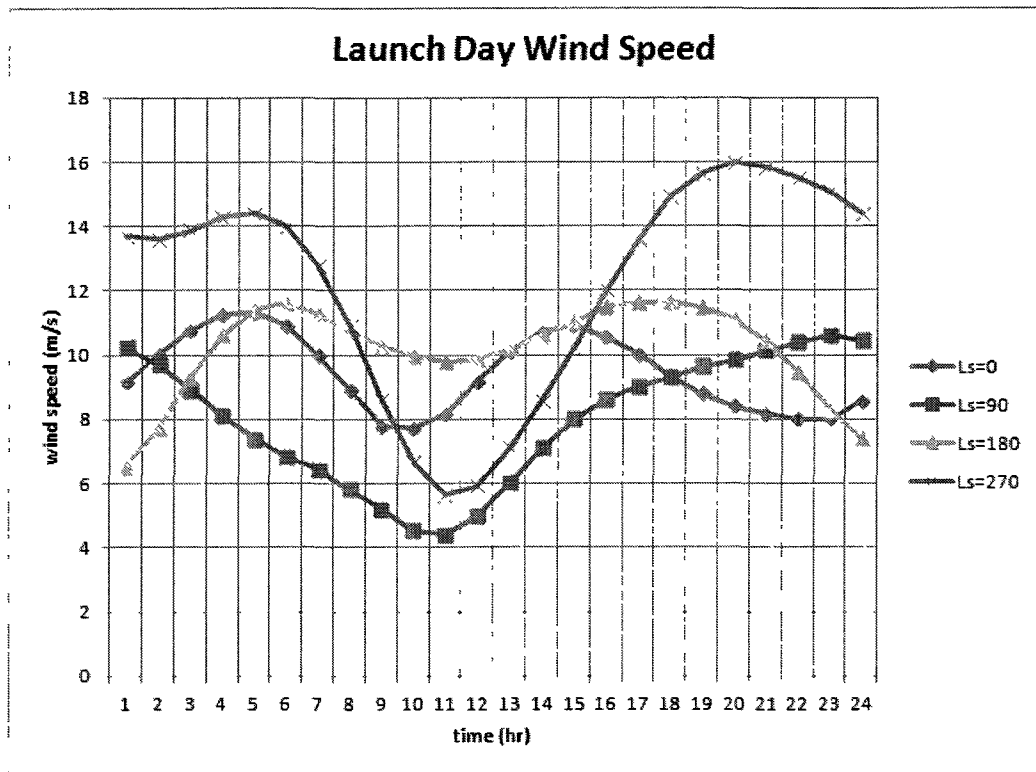
Figure 36: Launch Day Surface Wind Speed Profiles.

The sensitivity of the exploration balloon design to seasonal environmental conditions is summarized in Table 10. Like the MET balloon, atmospheric conditions require somewhat larger balloon systems for launches during autumnal equinox in the northern hemisphere. For this case, the required balloon volume was 45000 m^3 with a total system mass of 236 kg. The increase in required volume (up to 28% larger, compared with a winter solstice launch) could be significant since larger balloons will be more difficult to launch autonomously. However, the increased performance requirement for the autumnal equinox launch only translates to a 9 % increase in estimated overall system mass. A more-detailed study of autonomous balloon launch systems may illuminate substantially greater complexity associated with the 44.1 m diameter balloon, compared with the smaller diameter balloons required during other Mars seasons. However, it is probable that a single balloon size and launch system can be selected that can transport 100 kg or larger payloads at any time of the year, or that a smaller balloon size is found to be optimal based

on launch complexity and thus the payload will be 100 kg or less, depending on the time of launch.   Thus, the exploration balloon system will have "launch constraints".

Ls	0°	90°	180°	270°
Fully Inflated Volume (m³)	38300	38800	45000	35200
Fully Inflated Diameter (m)	41.8	42.0	44.1	40.7
Launch Volume (m³)	11200	15400	13800	9510
Launch Diameter (m)	27.8	30.8	29.7	26.2
Initial Hydrogen Mass (kg)	12.3	12.3	13.0	12.0
Balloon Mass (kg)	112	113	124	106
System Mass (kg)	223	224	236	217

Table 10: Exploration Balloon Sensitivity to Launch Season.

Simulated flight trajectories are displayed in Figures 37 through 58. Figures 37, 42, 47, and 52 show the nominal ground tracks for a balloon flight duration of 20 sols. Figures 38, 43, 48, and 53 show these same ground tracks overlaying a MOLA plot of Mars to provide reference to geographic features. During a 20-sol mission, the balloon can nearly circumnavigate the planet twice, after a summer solstice launch; nearly four times after a winter solstice launch. Additionally, like the MET balloons, a balloon launched during summer solstice results in an east to west flight trajectory while launches during the other three seasons produce west to east flight trajectories. Figures 39, 44, 49, and 54 show the nominal flight altitude histories for a 20-sol deployment. Generally, the float altitude remains fairly constant with only slightly more variation for the "summer solstice" and "winter solstice" balloons. Also, it can be seen that the constant density altitude decreases with time for these two scenarios due to seasonal atmospheric changes. Figures 40, 45, 50, and 55 show nominal ground track along with ground tracks associated with the +/- standard deviation of the wind speeds from the Mars-GRAM 2005 model to provide a reference of the error associated with the nominal trajectories. For clarity, only 10-sol trajectories are shown. It can be seen from these plots that the standard deviation-based wind uncertainty adjustments can produce quite different trajectory predictions. This shows the

potential to cover a significant portion of the Martian surface with a single mission, and also

justifies the inclusion of two-way altitude control as a means for lateral flight trajectory control.

The general trend is that the winds including positive standard deviation direct the balloon

poleward, while the negative standard deviation components steer the balloon in the opposite

direction. Figures 41, 46, 51, and 56 show the nominal altitude histories, along with those

associated with the +/- standard deviation of the wind speeds from the Mars-GRAM 2005 model

to provide a reference of the error associated with the nominal profiles. Again, for clarity, only

10 sols are shown. The expect wind variations from "nominal" can lead to significantly different

altitude histories with a balloon floating at altitudes of less than 8 km or as great as 11 km. This

resulted from the fact that the altitude corresponding to the specified constant density is lower for

trajectories nearer the poles and higher for trajectories nearer the equator. This is verified since

the balloon volume remains constant over the entire flight for all standard deviation scenarios and

therefore maintains its superpressure so that the change in altitude is necessarily a result of a

change in the atmospheric constant density altitude. Lastly, Figure 57 shows the ground tracks of

each of the four scenarios for a single circumnavigation overlaying a MOLA plot of Mars. Figure

58 shows a close up of the four trajectories from launch with hourly meter marks.
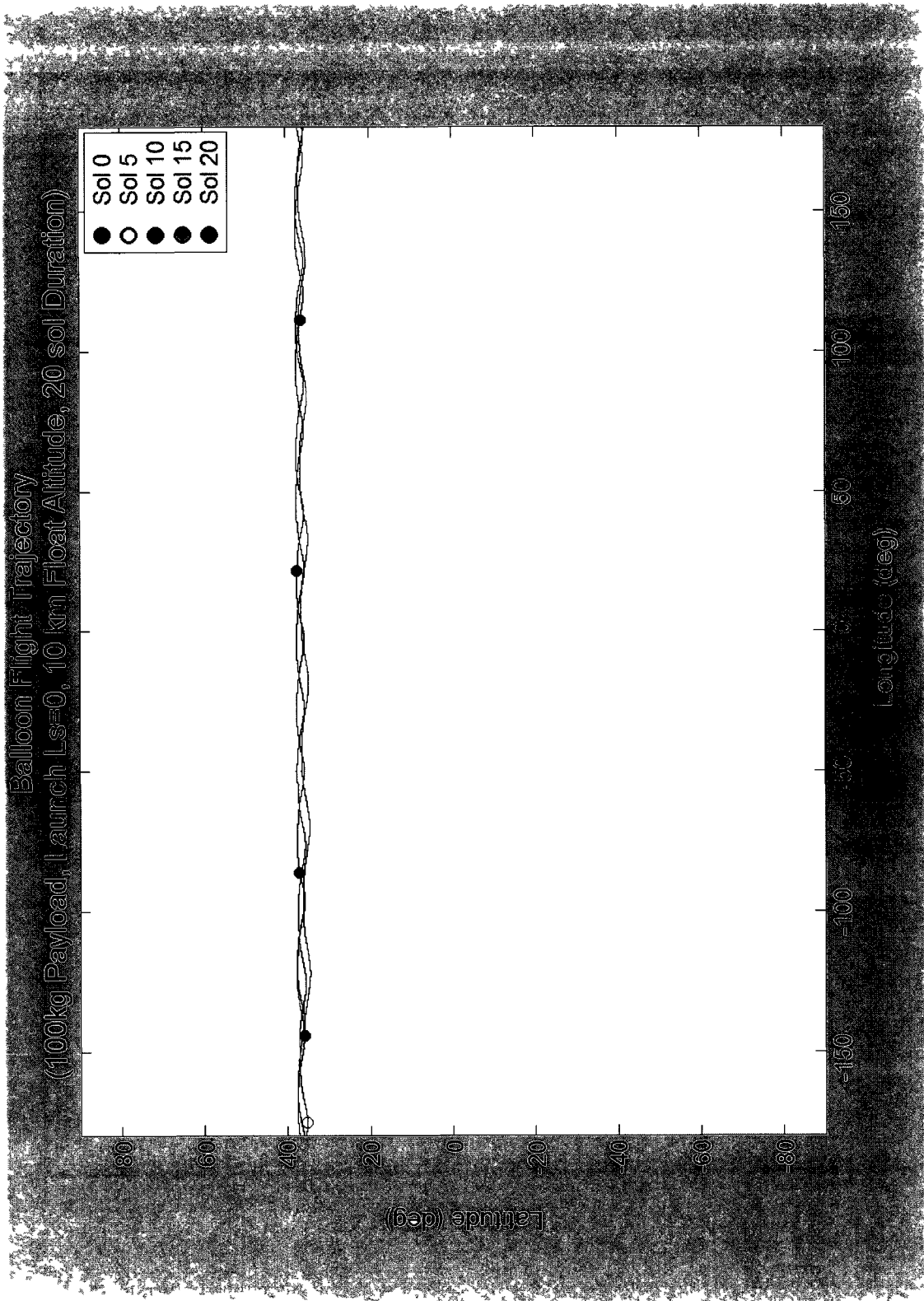
Figure 37: Exploration Balloon Ground Track
(Launch Ls=0, ~10 km Float Altitude, 20 sol Flight)

Figure 38: MOLA Overlay of Exploration Balloon Ground Track
(Launch Ls=0, ~10 km Float Altitude, 20 sol Flight).
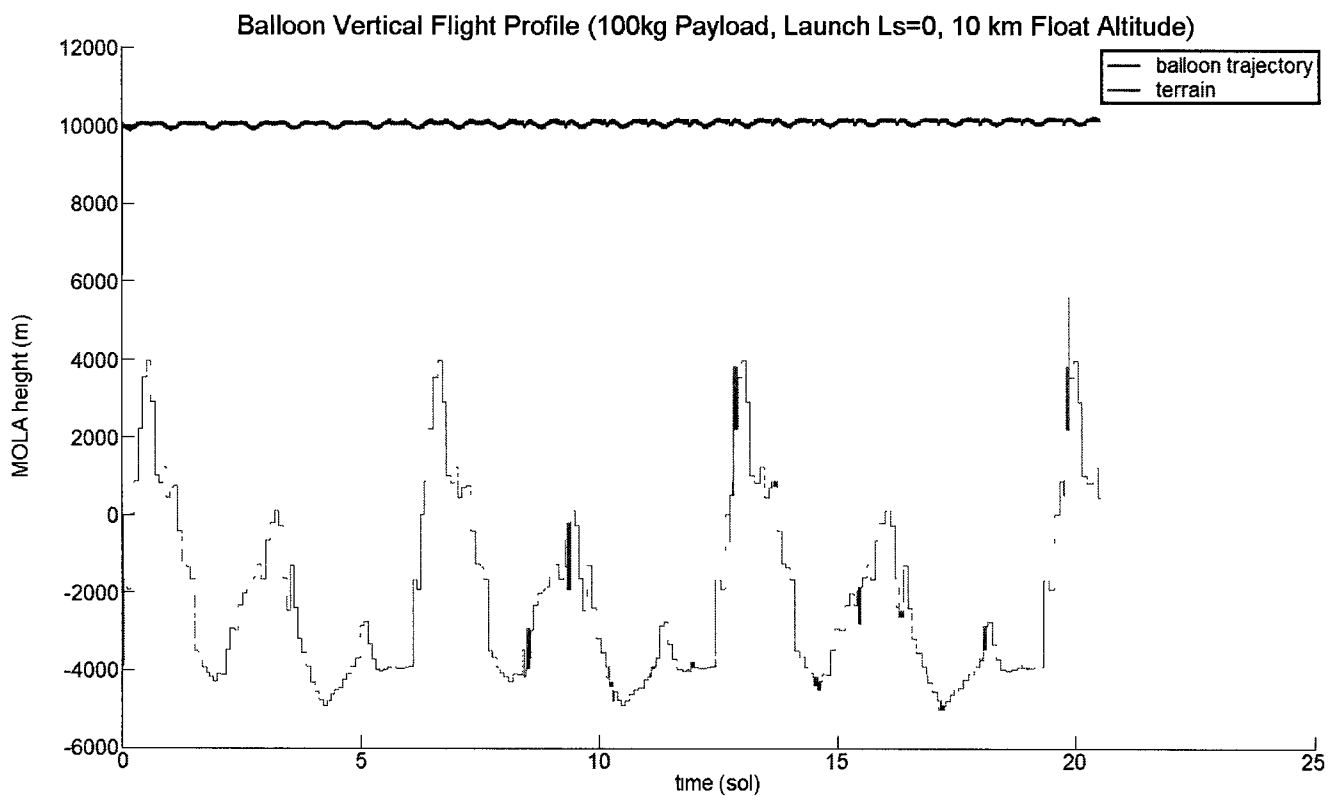
Figure 39: Exploration Balloon Float Altitude History
(Launch Ls=0, ~ 10 km Float Altitude, 20 sol Flight).
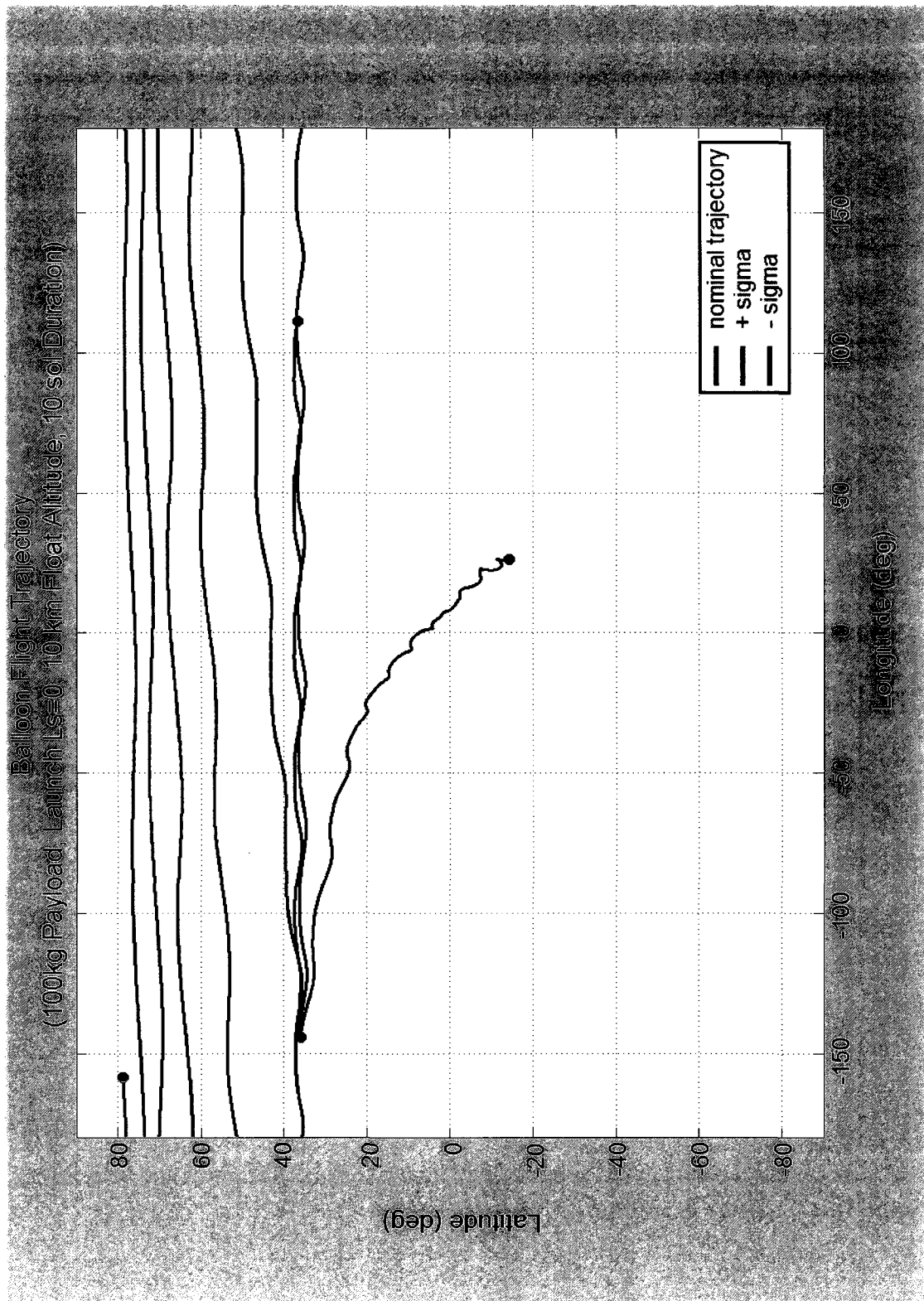
Figure 40: Exploration Balloon Ground Track with Wind Standard Deviation (Launch Ls=0, ~10 km Float Altitude, 10 sol Flight).
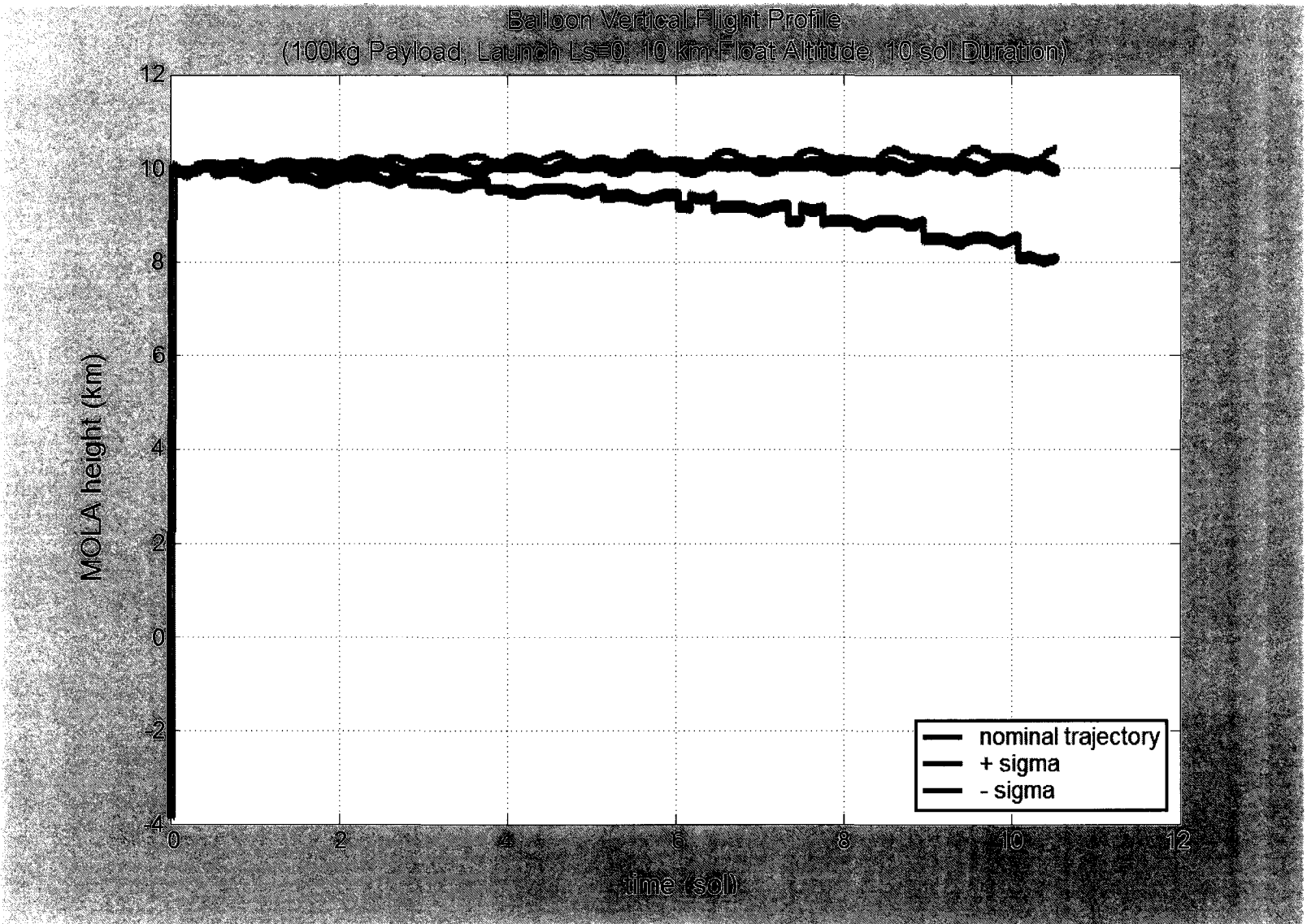
Figure 41: Exploration Balloon Vertical Flight Profile with Wind Standard Deviation (Launch Ls=0, ~10 km Float Altitude, 20 sol Flight).
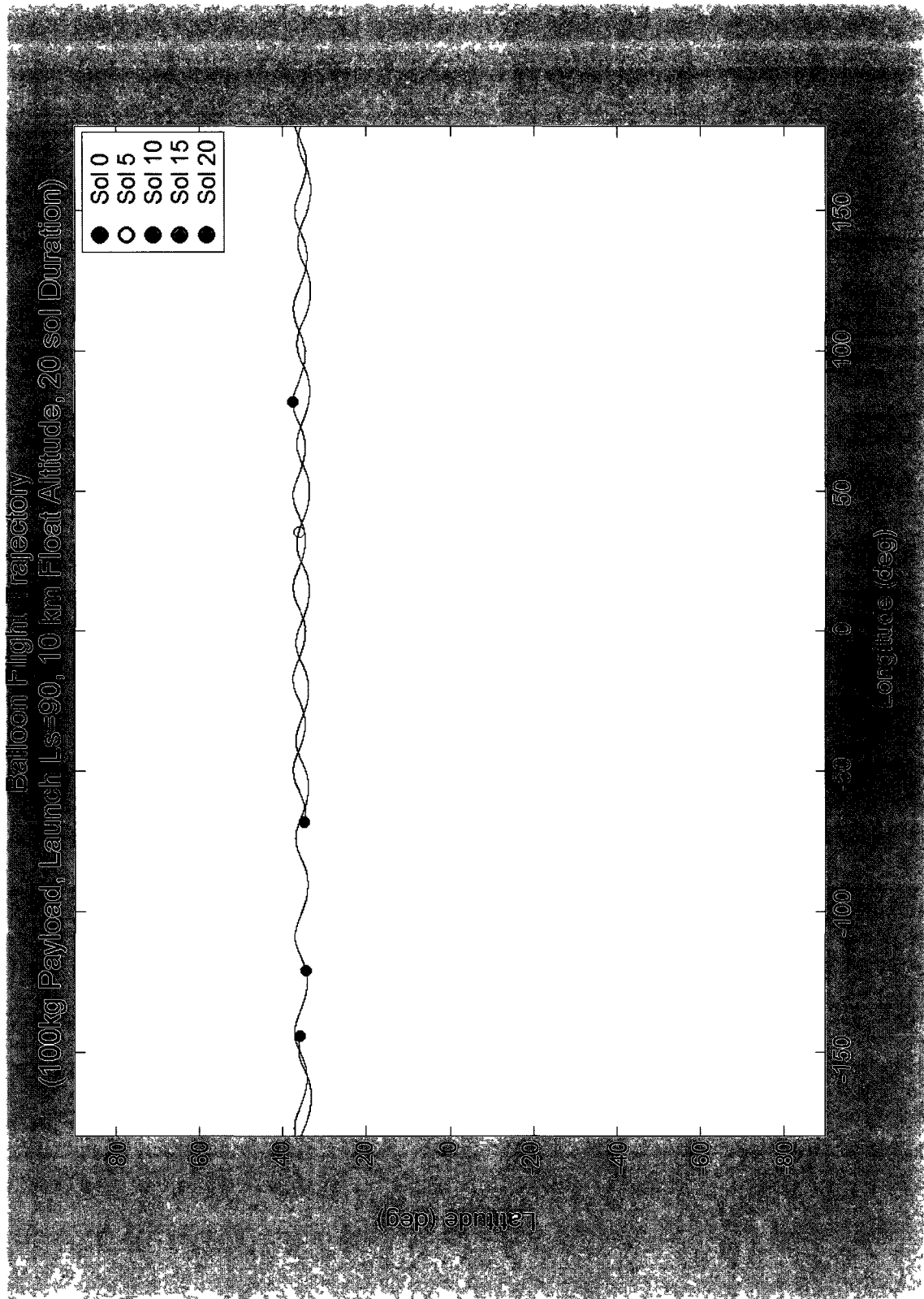
Figure 42: Exploration Balloon Ground Track
(Launch Ls=90, ~10 km Float Altitude, 20 sol Flight)

Figure 43: MOLA Overlay of Exploration Balloon Ground Track
(Launch Ls=90, ~10 km Float Altitude, 20 sol Flight).
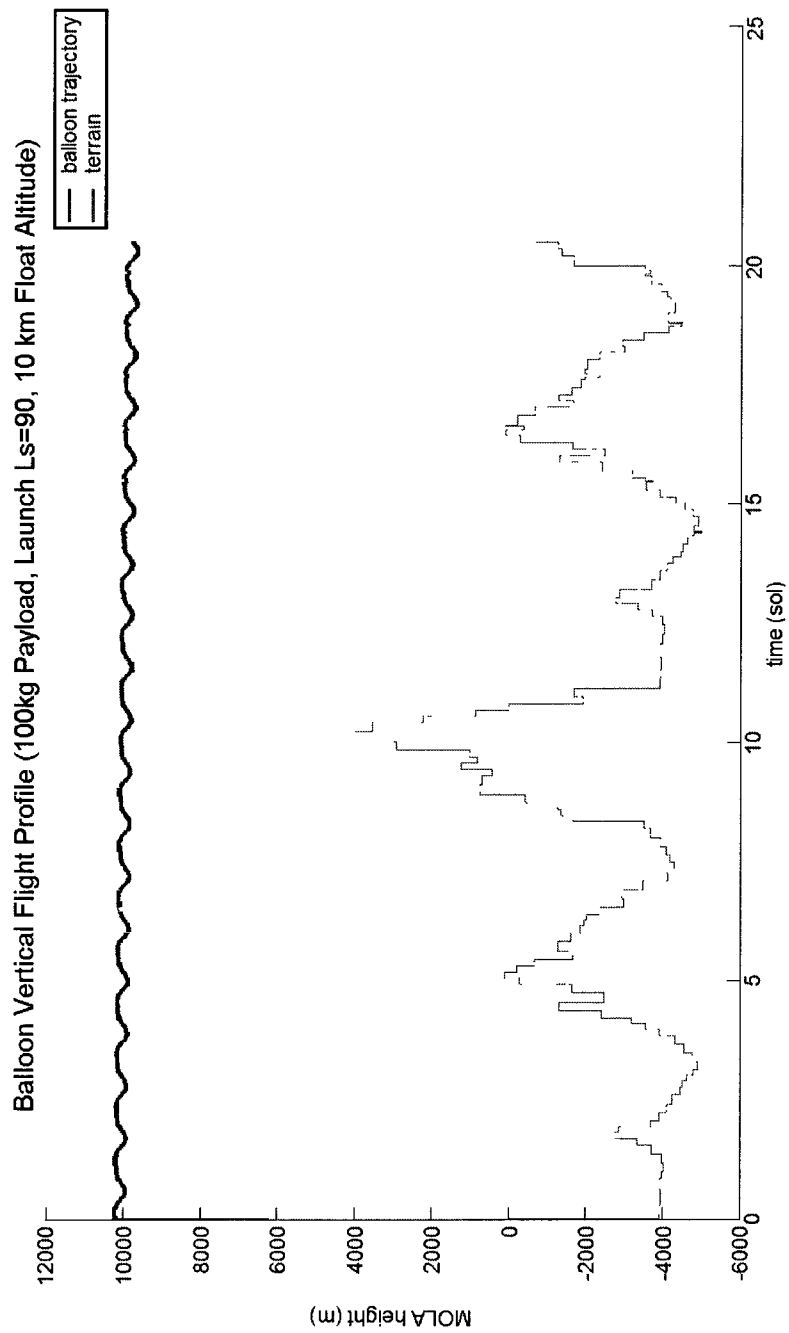
Figure 44: Exploration Balloon Vertical Flight Profile
(Launch Ls=90, ~10 km Float Altitude, 20 sol Flight).
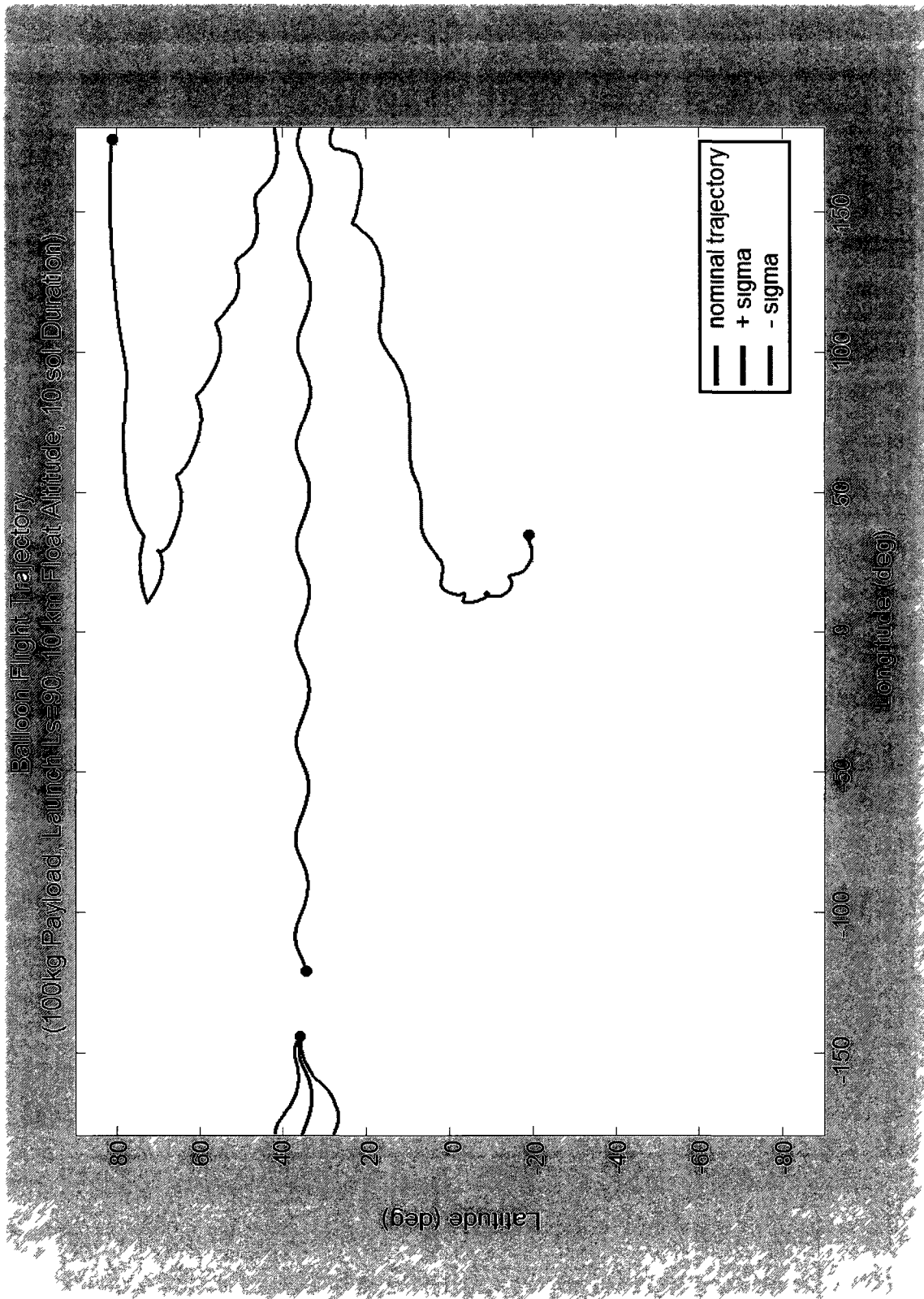
Figure 45: Exploration Balloon Ground Track with Wind Standard Deviation
(Launch Ls=90, ~10 km Float Altitude, 10 sol Flight)
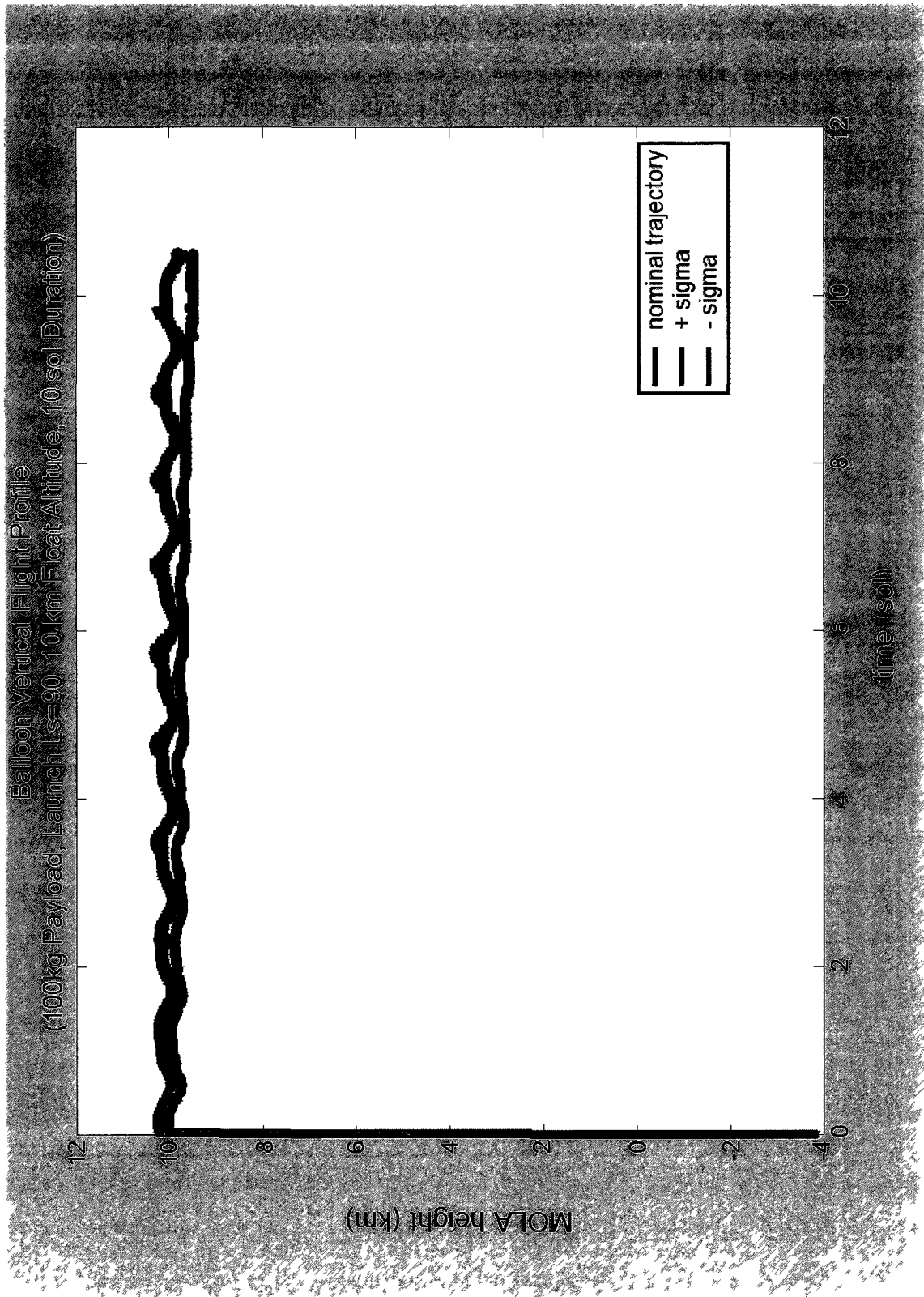
Figure 46: Exploration Balloon Vertical Flight Profile with Wind Standard Deviation
(Launch Ls=90, ~10 km Float Altitude, 20 sol Flight)
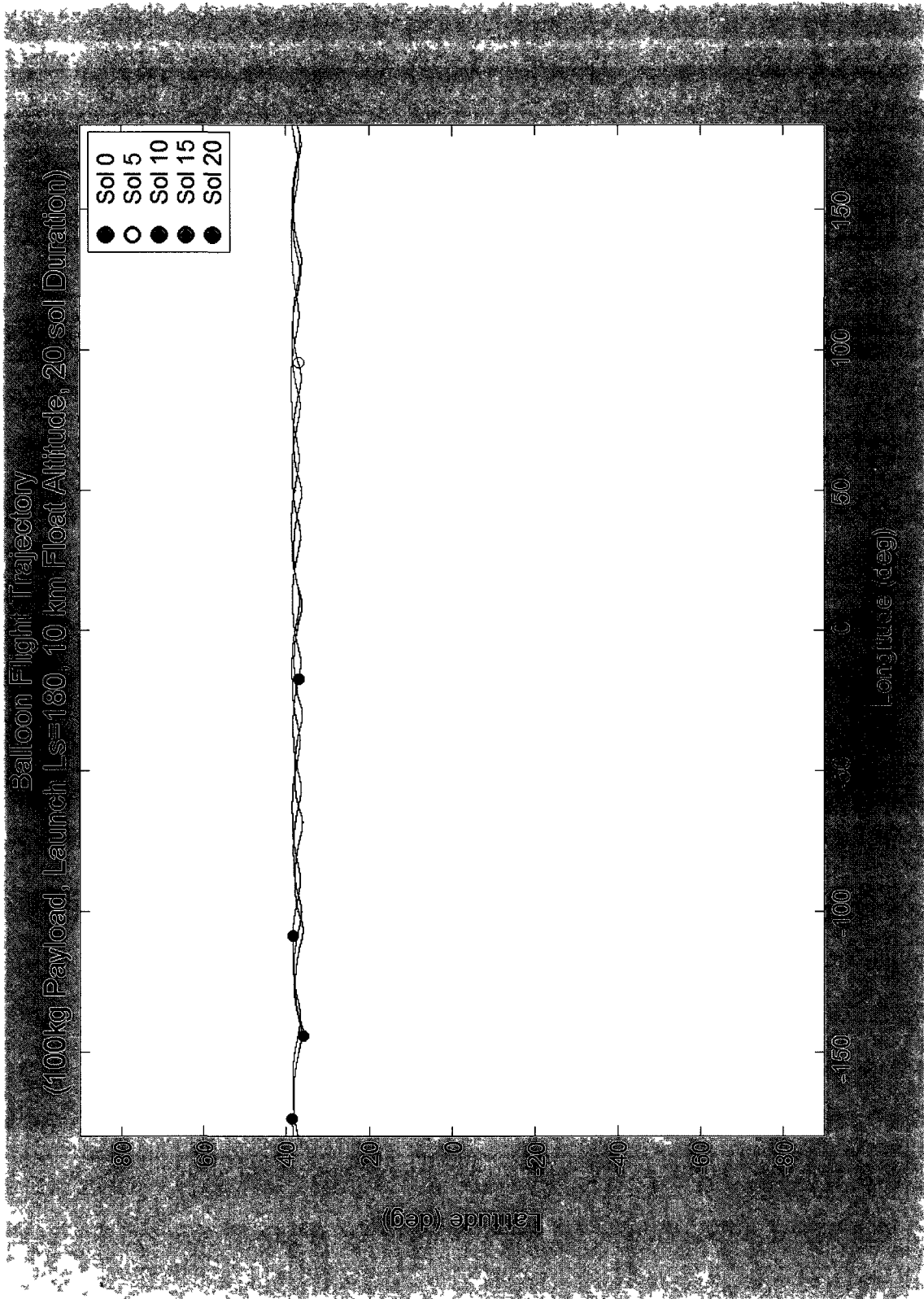
Figure 47: Exploration Balloon Ground Track
(Launch Ls=180, ~10 km Float Altitude, 20 sol Flight)

Figure 48: MOLA Overlay of Exploration Balloon Ground Track
(Launch Ls=180, ~10 km Float Altitude, 20 sol Flight).
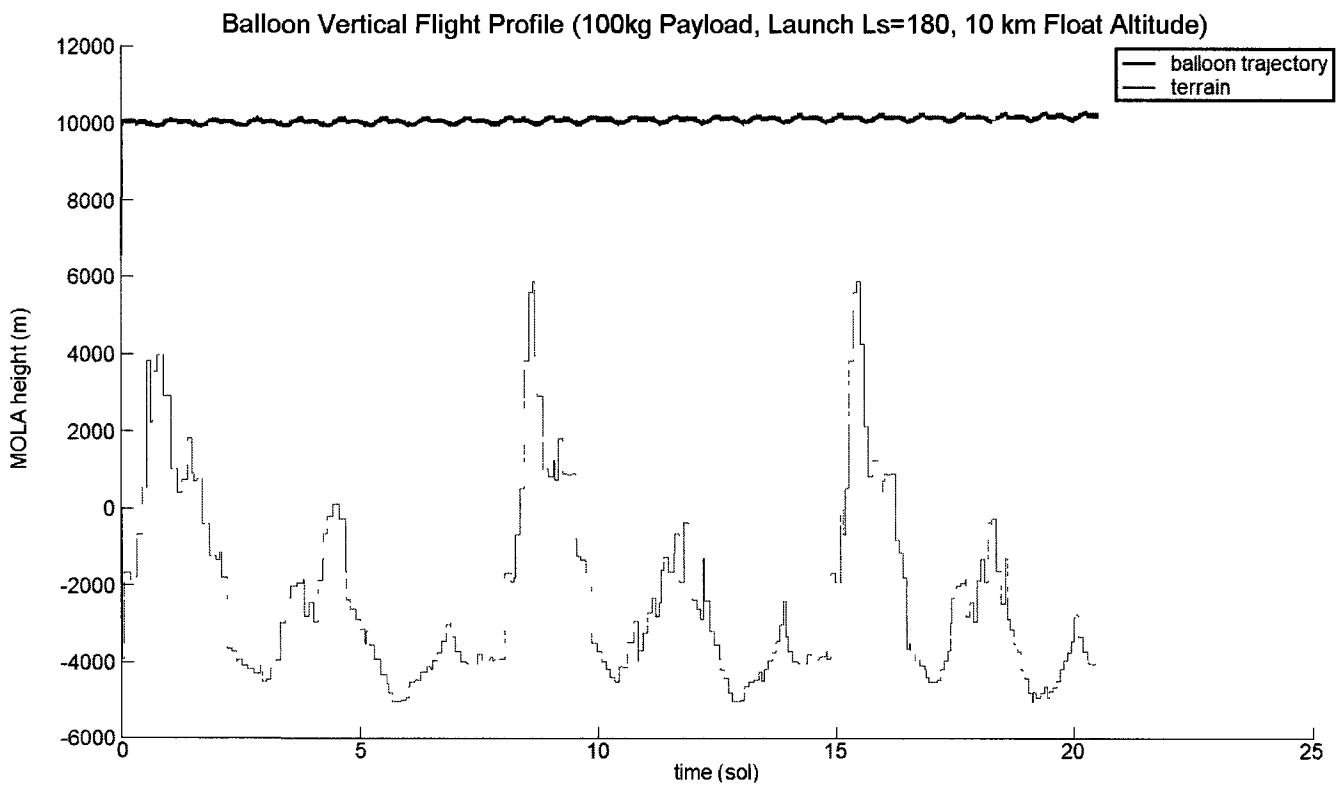
Figure 49: Exploration Balloon Vertical Flight Profile (Launch Ls=180, ~10 km Float Altitude, 20 sol Flight).
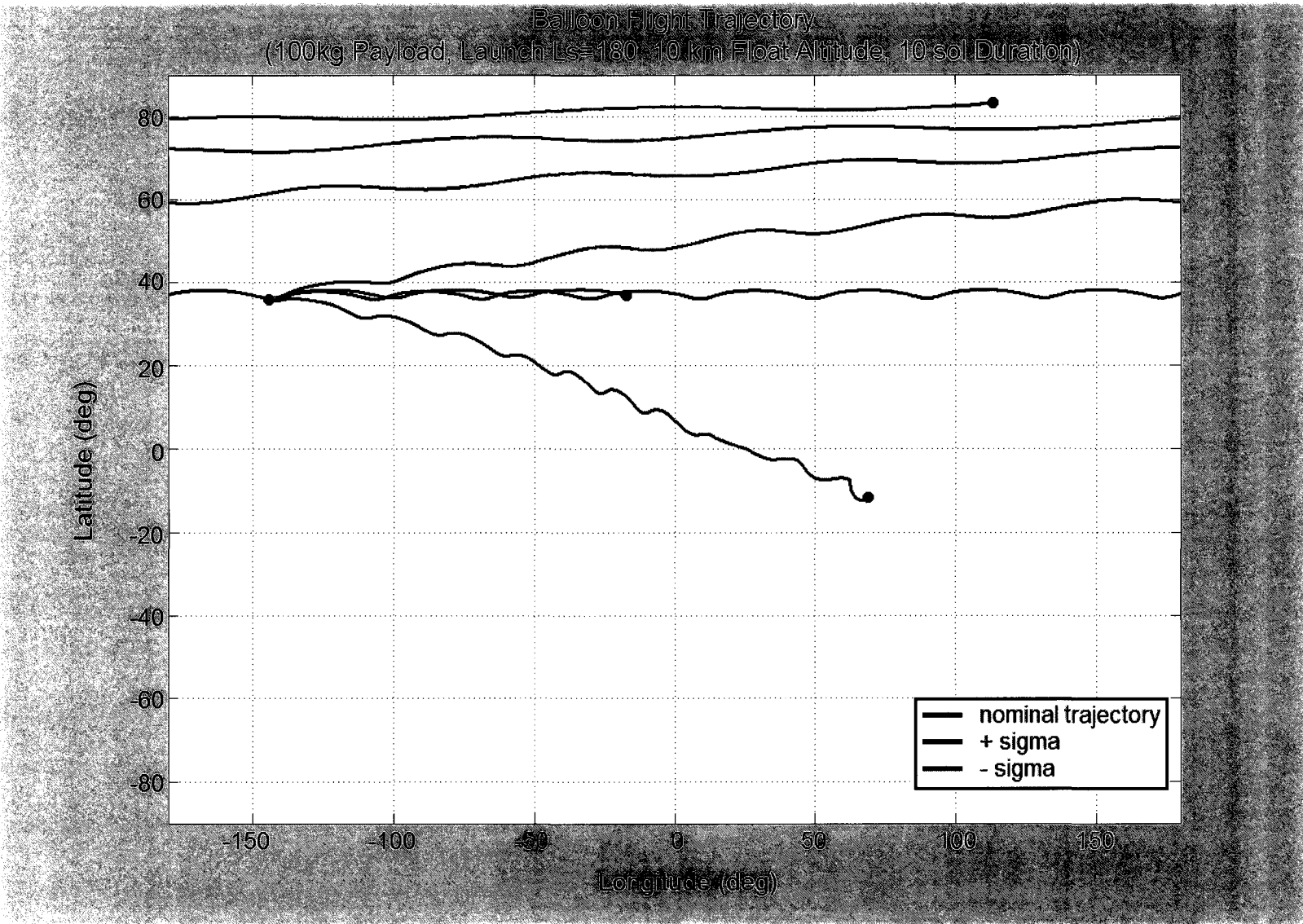
Figure 50: Exploration Balloon Ground Track with Wind Standard Deviation (Launch Ls=180, ~10 km Float Altitude, 10 sol Flight).
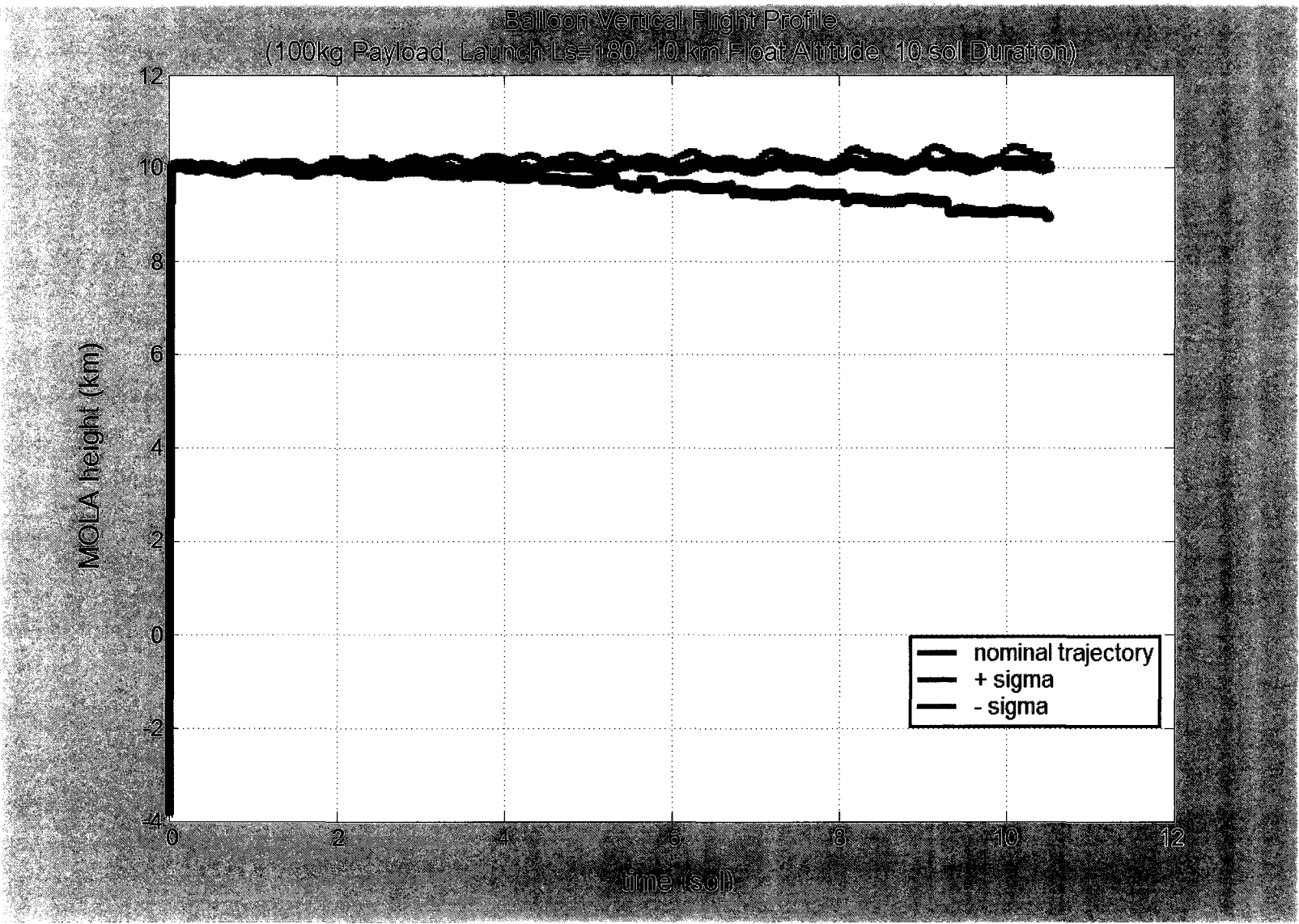
Figure 51: Exploration Balloon Vertical Flight Profile with Wind Standard Deviation (Launch Ls=180, ~10 km Float Altitude, 20 sol Flight).
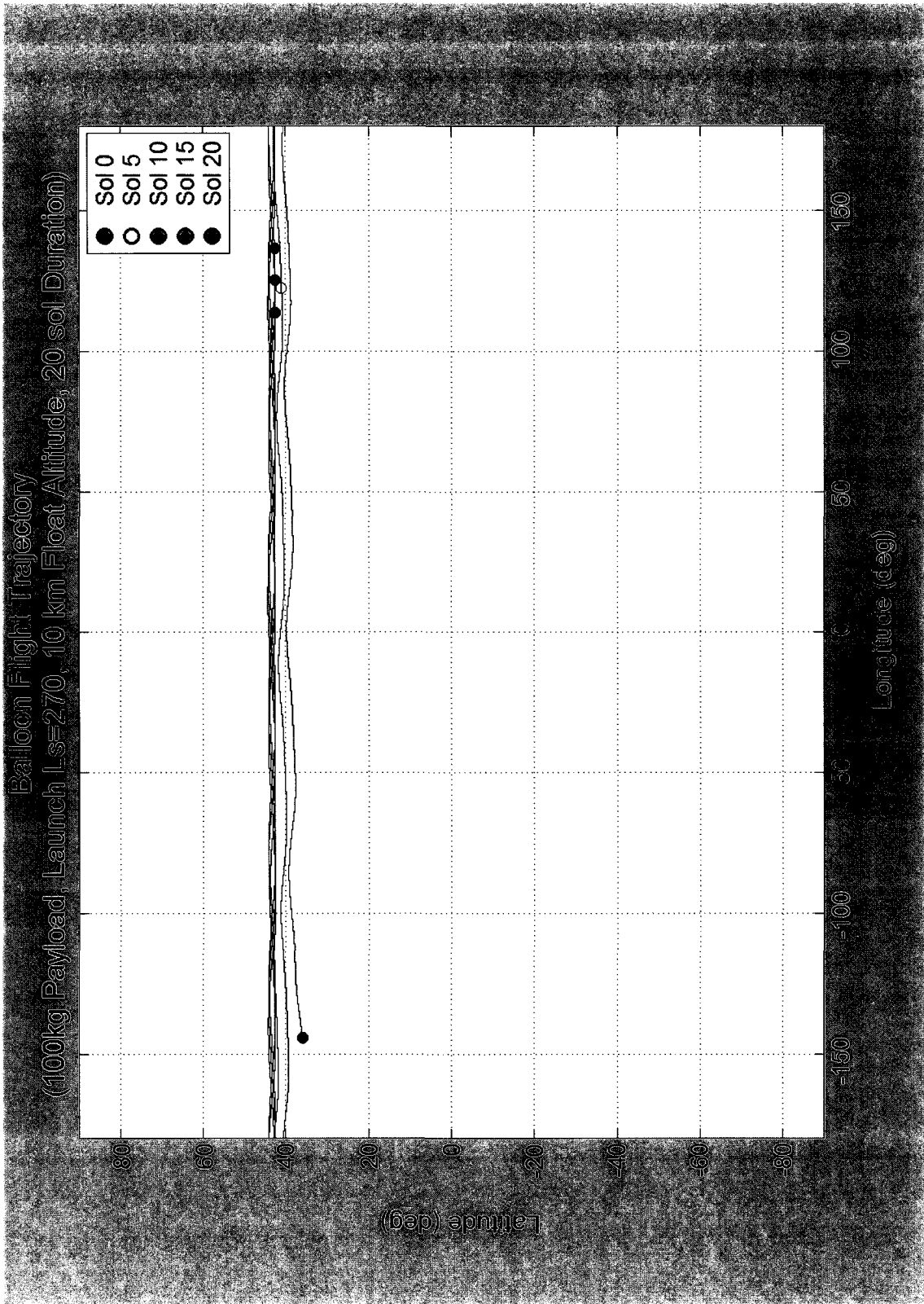
Figure 52: Exploration Balloon Ground Track
(Launch Ls=270, ~10 km Float Altitude, 20 sol Flight).

Figure 53: MOLA Overlay of Exploration Balloon Ground Track
(Launch Ls=270, ~10 km Float Altitude, 20 sol Flight).
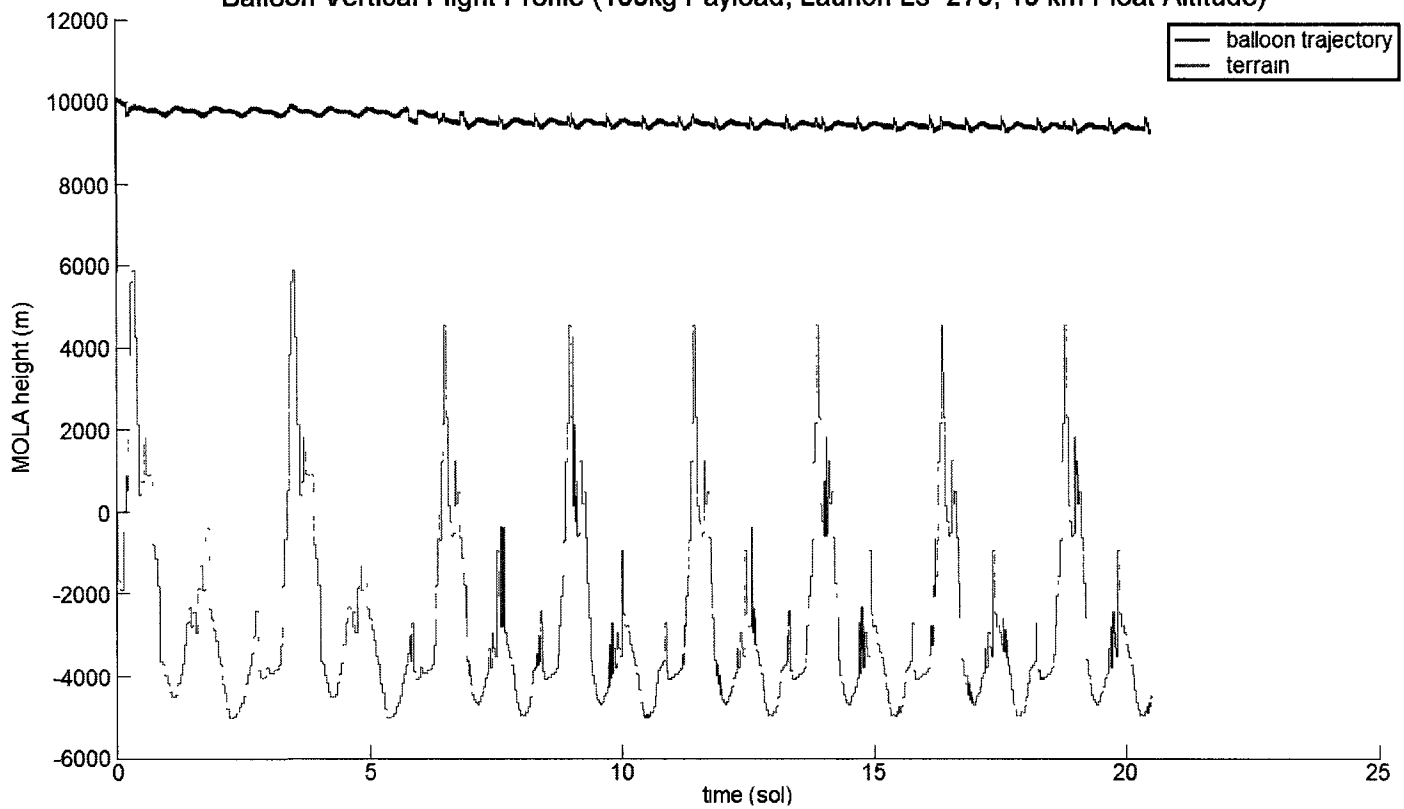
Figure 54: Exploration Balloon Vertical Flight Profile (Launch Ls=270, ~10 km Float Altitude, 20 sol Flight).
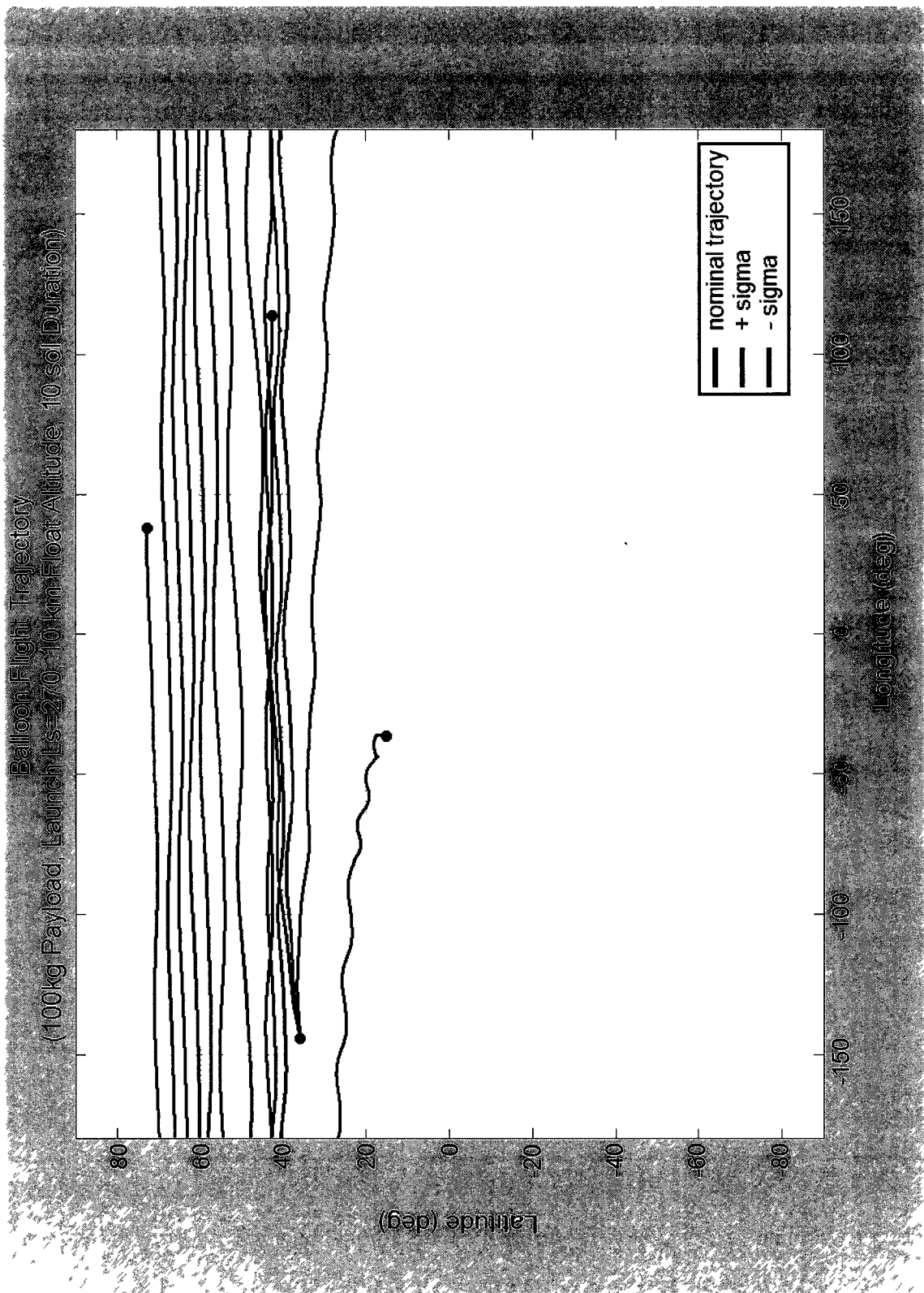
Figure 55: Exploration Balloon Ground Track with Wind Standard Deviation
(Launch Ls=270, ~10 km Float Altitude, 10 sol Flight).
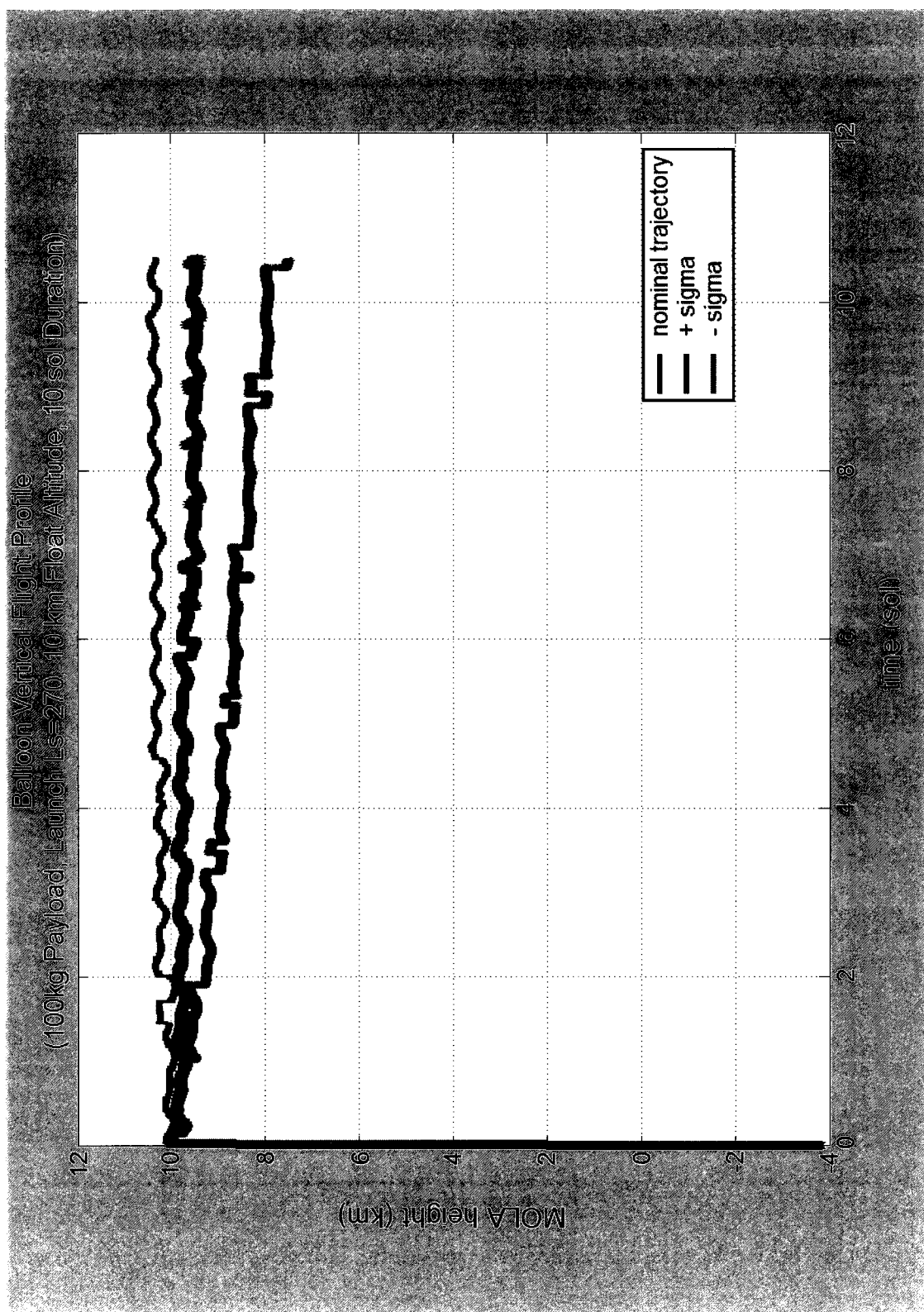
Figure 56: Exploration Balloon Vertical Flight Profile with Wind Standard Deviation (Launch Ls=270, ~10 km Float Altitude, 20 sol Flight).

Exploration Balloon Circumnavigation Times

Launch Ls=0
Launch Ls=90
Launch Ls=180
Launch Ls=270
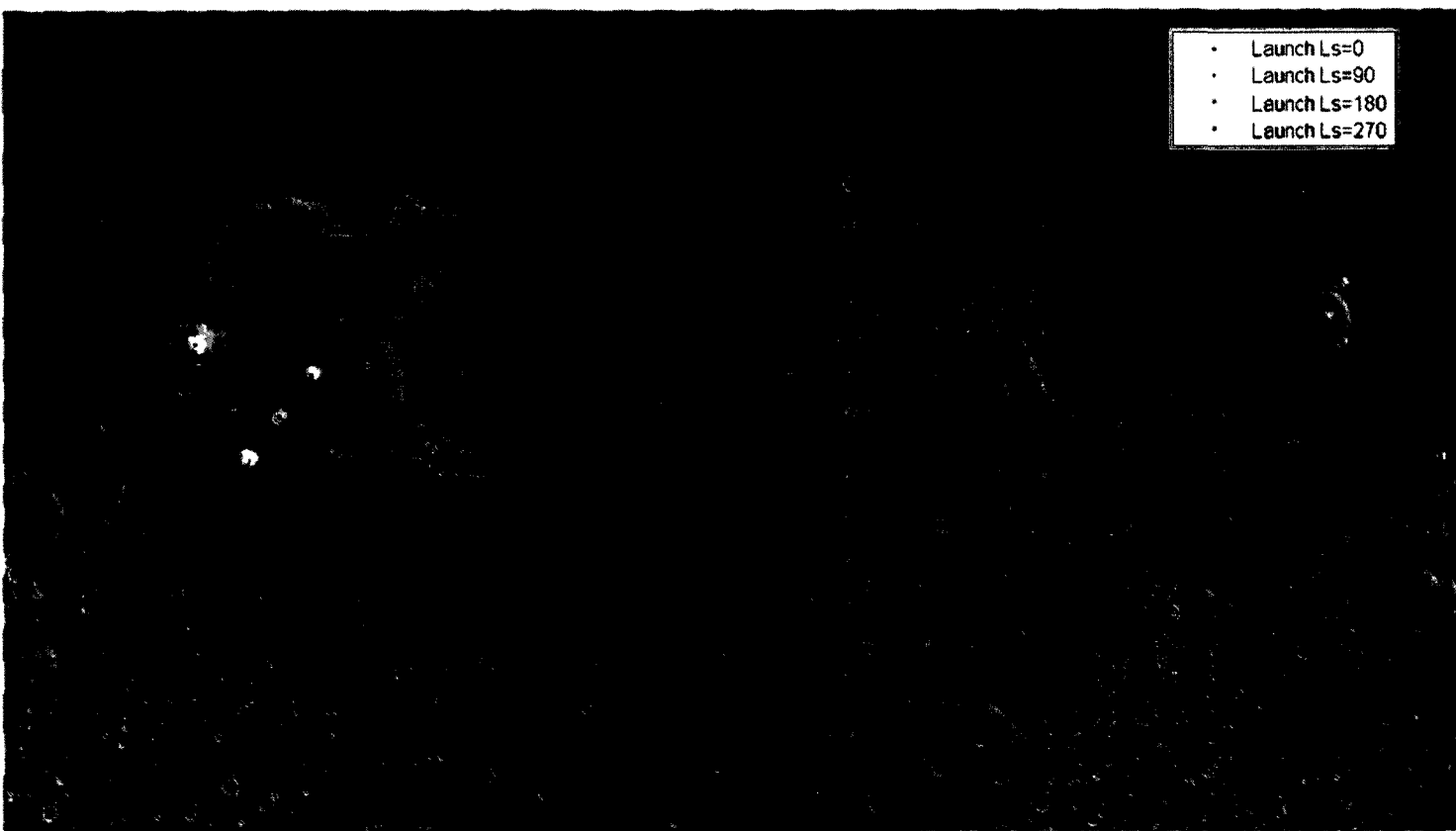
flight time for 1 revolution:
Ls=0: 6.1 sol
Ls=90: 11.2 sol
Ls=180: 8.0
Ls=270: 3.2 sol

Figure 57: Seasonal Sensitivity of Exploration Balloon Circumnavigation Times (~10 km float altitude).
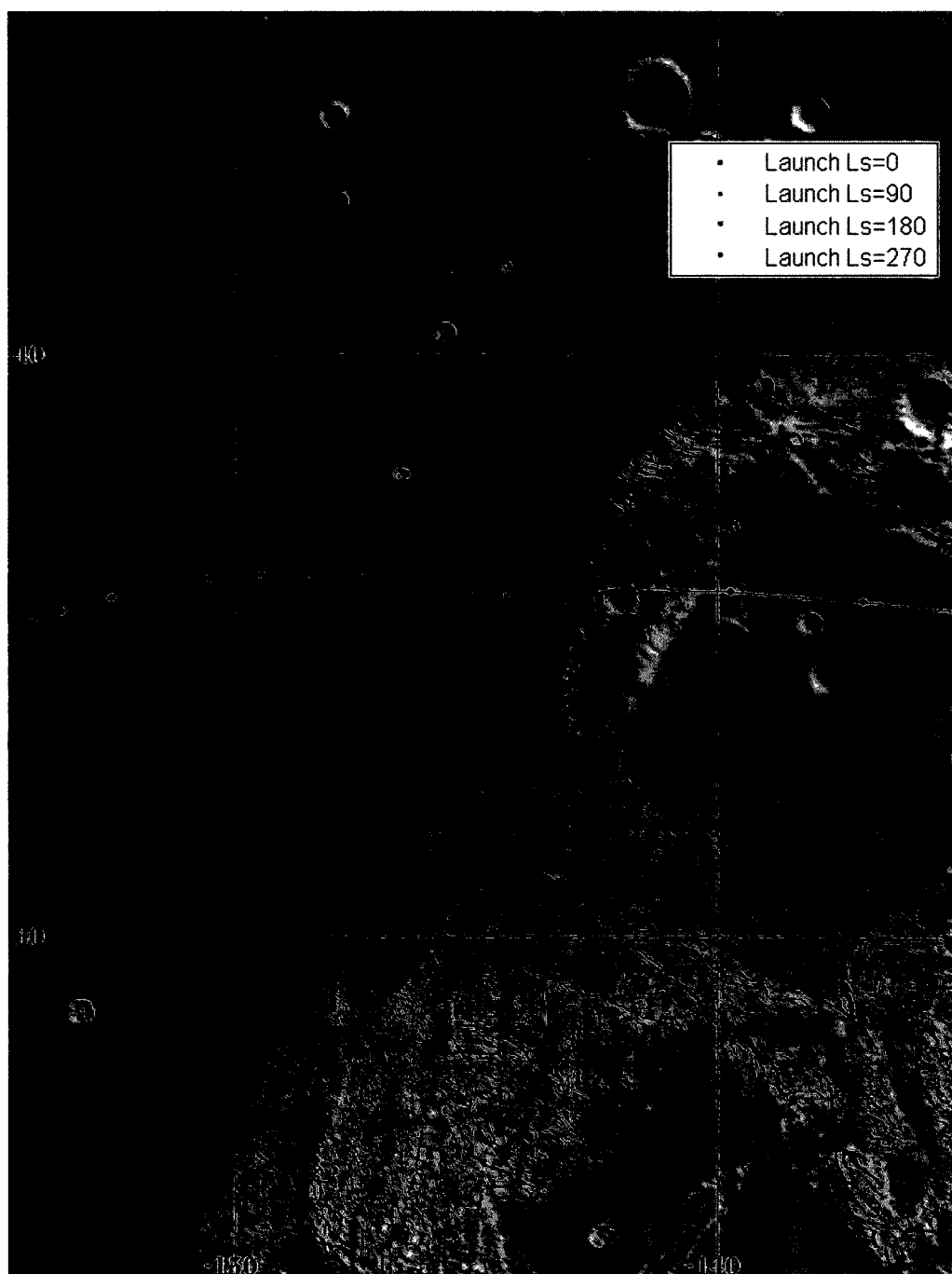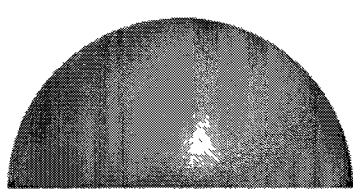
Figure 58: Close-up of Exploration Balloon Ground Trajectories Showing Hourly Progression of Balloon Ground Track.

5.4 EXPLORATION BALLOON SYSTEM SUMMARY

The exploration balloon system consists of the balloon-envelope, seams, end fittings, an inflation tube; a payload gondola; and the payload suspension system. It is designed to carry a generic 100 kg gondola, including payload, to a nominal 10 km constant density altitude for the duration of the balloon flight. Sufficient variation in the seasonal Martian atmospheric conditions produce slightly different design specifications as indicated in Figure 59, summarizing the overall characteristics.

	Exploration Balloon-1	Exploration Balloon-2
Geometry:	Spherical	Spherical
Volume (m3):	38800	35200
Diameter (m):	42.0	40.7
# of gores:	60	60
Balloon Mass (kg):	113	106
Lifting Gas:	Hydrogen	Hydrogen
Gas Mass (kg):	12.3	11.9
Payload Mass (kg):	100	100
System Mass (kg):	225	218
Material:	MABS Composite	MABS Composite
Material Strength (N/m):	>2500	>2500
Coating:	Top: Silver FEP-teflon	Top: Silver FEP-teflon

Figure 59: Exploration Balloon System Design Summary.

The Exploration Balloon-1 balloon envelope is sized for an Ls=0° or Ls=90° launch northern hemisphere vernal equinox and summer solstice, whereas the Exploration Balloon-2 balloon envelope is sized for an Ls=270° launch.. Based on these system estimates, the possible increased risk associated with higher surface wind speeds during an autumnal equinox launch coupled with the increase in overall system mass make a balloon launch during this period less attractive than other launch opportunities.

The balloons are inflated through an inflation tube located in the upper hemisphere of the balloon and each balloon is packed by folding. It is estimated, based on the four evaluated design

scenarios, that the balloon volume at launch from a launch site located at Northeast Amazonis (35°54'N 144°21.6'W) will be between 9510 m^3 and 15400 m^3 (26.2 m < diameter < 30.8 m).

5.5 EXPLORATION BALLOON LAUNCH SYSTEM

The exploration balloon launch system must be capable of launching at least three exploration balloons and is expected to utilize the common MET balloon launch system. The functional flow block diagram for exploration balloon launch operations is depicted in Figure 60. When an exploration balloon system launch command is initiated, the launch system first checks the local ambient conditions versus go / no-go conditions. The resulting condition is transmitted to the Earth monitoring station. If the local conditions are within the specified launch constraints, the launch system activates the system radar and UHF receiver and sequentially performs appropriate system checks.

After successful system checkout, the launch system rotates to place the payload down-wind of the lander, deploys the inflatable launch cone, and extends the payload on the jib boom in a similar fashion to the MET balloons. With the payload activated and checked out, the inflation cone will be fully inflated, and the launcher will be oriented in the correct configuration. Subsequently, the exploration balloon solenoid valve and the balloon solenoid valve will be opened to initiate inflation. As with the MET balloons, with these valves confirmed open, the main solenoid valve is opened and the balloon begins to fill, slowly at first and then at a higher rate, controlled by the control valve.

Similar to the MET balloon launch configuration presented in Chapter IV, the balloon will be held in place in the launcher by a hutch clutch with the inflation bubble constrained by a collar with a tear strip. The payload is held in place with clamps. Once sufficient lifting gas mass is supplied to the inflation bubble, the hutch clutch and clamps holding the payload will release and the balloon can begin to rise, lifting the un-inflated portion of the envelope, wrapped in a reefing sleeve, so that it can unfold as it unfurls. The wind carries the balloon away from the

lander, snatching the payload away as it ascends. As the gas bubble expands, the tear-strip on the

collar tears, allowing the gas bubble to further expand as the collar falls away. As the balloon

ascends, the gas bubble continues to expand, tearing a rip-stitch on the reefing sleeve. After the

balloon has been launched, the launch system will continue to track and receive data as long as

the balloon is within range.
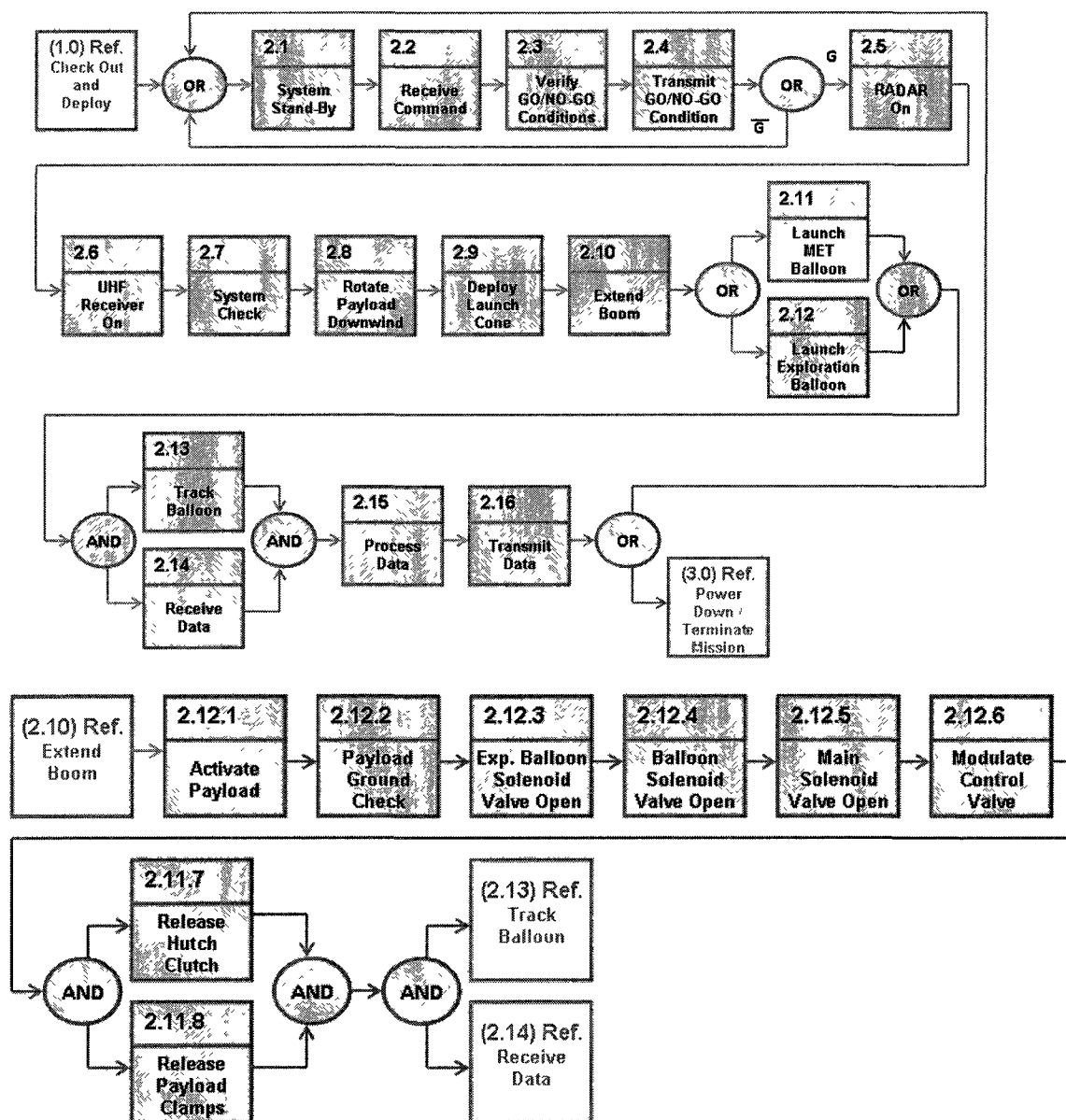
Figure 60: Exploration Balloon System Launch Functional Flow Block Diagram.

CHAPTER 6

CONCLUSIONS AND RECOMMENDATIONS

A measurement gap exists between orbiters and surface rovers and landers. MEPAG has prioritized the understanding of Mars atmosphere and climate and the preparation for human exploration of Mars through understanding of the variation of atmospheric properties between the surface and 90 km. The similarity of the Martian atmosphere between 0 and 20 km and the upper stratosphere of Earth make balloons a viable option, with long heritage of successful flights in Earth's atmosphere. Inflatable aerial vehicles can provide planetary scale *in situ* measurements with resolution orders of magnitude greater than orbiters, including scientifically interesting terrain that is either inaccessible or hazardous to rovers and landers. Large aerial platforms also offer the capability to deploy surface probes or rovers to regions inaccessible due to limitations on existing EDL systems.

To date, several missions have been proposed utilizing aerial vehicles capable of operating in the Mars atmosphere. These designs all utilized balloons deployed during entry, but have proven difficult due to mass limitations on the balloon, the thin Mars atmosphere, limitations in balloon envelope technology, and forces experienced by the balloon during aerial deployment. Permanent robotic outposts on the surface could utilize locally-derived hydrogen as a lifting gas for balloon systems and may simplify the inflation and launch of aerial vehicles while simultaneously allowing for a long duration deployment campaign.

Advances in ultra-thin balloon film technology by JAXA have resulted in balloon material with a successful flight heritage in a relevant operating environment. The Vaisala radiosonde has a long successful heritage of use in Earth's atmosphere and the temperature, pressure, and humidity sensors also have a heritage of Mars application. A complement of 26 zero pressure MET balloons with Vaisala derived radiosondes, will provide for a launch every

eighteen degrees of solar longitude with one launch day each Mars season including one morning and evening launch and two spare balloons. These weather balloons can provide year round *in situ* vertical profile atmospheric measurements of pressure, temperature, humidity, and wind speed up to 20 km altitude, for verification and calibration of global circulation models.

Building on material developments of past Mars balloon mission studies, it is possible to fabricate a spherical superpressure balloon from a composite created during the 2001 Mars-Aerobot/Balloon System project of sufficient size and strength to carry a 100 kg payload at an altitude of nominally 10 km above the Mars reference surface. Depending on the season, trajectory calculations have predicted the balloon can circumnavigate the planet more than three times during a 20 sol mission. The thin atmosphere makes these balloons quite large (35200 m^3 – 38800 m^3) even at launch with estimated launch diameters ranging from 26.2 m to 30.8 m. While balloon trajectories are primarily east-west within a narrow latitude band, the inclusion of altitude control on exploration balloons may take advantage of north-south circulatory winds created by CO_2 condensation – sublimation cycles and Hadley cells which are variable and altitude dependent. And while maneuvers like precision navigation or equatorial crossing may not be possible, this may allow sufficient lateral control to enable the investigation of specific features of Mars or even delivery of payloads to locations that are inaccessible to entry, descent, and landing systems.

Much work remains to be done. Both the MET balloon and exploration balloon materials have been successfully designed, fabricated, and tested in previous studies. More work and testing is necessary, however, for optimization and understanding of how the material will respond to the Earth-Mars transit environment and Mars surface and flight environments. This thesis has shown that a surface launcher is feasible, but more work is necessary to mature the design including modeling and testing of the launch and inflation systems. Mars global wind models indicate that altitude-dependent, time-varying wind speed and direction can potentially be exploited by adjusting the balloon float altitude. Mars' dusty atmosphere should enable an on-

board LIDAR system to monitor altitude-dependent, relative wind conditions and enable float altitude-based flight path control. That possibility should be explored to the extent that feasibility can be demonstrated and flight control limitations are identified. Additionally, this thesis made a very top level thermal analysis of the exploration system balloon to validate the capability of the balloon to maintain a constant density altitude and withstand the resulting superpressure. A more rigorous thermal analysis would provide a much more accurate picture of the balloon thermal and pressure environment and go a long way towards balloon design optimization. This analysis assumed a 2021/2022 balloon mission. There is still sufficient time for the necessary work to occur to make inflatable aerobots a viable option for planetary exploration in this time frame and contribute to a manned Mars landing in the 2030's.

LITERATURE CITED

Alexander, M., NASA/TM-2001-210935 Mars transportation environment definition document. 2001.

Bagenal, F., Class 16 - Earth, Venus, Mars - Dynamics 2. Web. 1 Oct. 2011. http://lasp.colorado.edu/~bagenal/3720/CLASS16/16EVM-Dyn2.html.

Balme, M., Greeley, R. Dust devils on Earth and Mars. Rev. Geophys. 44 (RG3003), doi:10.1029/2005RG000188, 2006.

Barlow, N. Mars: An Introduction to its Interior, Surface, and Atmosphere. Cambridge Planetary Science, Cambridge, UK. 2008.

Beaty, D.W., Snook, K., Allen, C.C., Eppler, D., Farrell, W.M., Heldmann, J., Metzger, P., Peach, L., Wagner, S.A., Zeitlin, C. An analysis of the precursor measurements of Mars needed to reduce the risk of the first human missions to Mars. (Unpublished white paper, 77 p., posted June, 2005 by the Mars Exploration Program Analysis Group (MEPAG)) http://mepag.jpl.nasa.gov/reports/index.html.

Byrne, S., Dundas, C.M., Kennedy, M.R., Mellon, M.T., McEwen, A.S., Cull, S.C., Dauber, I.J., Shean, D.E., Seelos, K.D., Murchie, B.A., Cantor, R.E., Arvidson, K.S., Edgett, A., Reufer, N., Thomas, N., Harrison, T.N., Posiolova, L.V., Seelos, F.P. Distribution of mid-latitude ground ice on Mars from new impact craters. Science 325 (5948), 1674-1676, 2009.

Calladine, C.R. Stability of the Endeavour Balloon, buckling of structures. Elsevier Science Publishers, Amsterdam, 133–149, 1988.

Cathey, H.M. Advances in thermal analysis of scientific balloons. AIAA 34th Sciences Meeting and Exhibit, Reno, NV, 1996.

Cattermole, P.J. Mars: the mystery unfolds. Cambridge University Press, Cambirdge, UK. 2008.

Clark, I.G., Hutchings, A.L., Tanner, C.L., Braun, R.D. Supersonic inflatable aerodynamic decelerators for use on future robotic missions to Mars. J. Spacecraft Rockets 46 (2), 340-352, 2009.

Cutts, J.A., Kerzhanovich, Viktor V. Martian aerobot missions: first two generations. IEEE Aerospace 2001Conference, Big Sky, MT, 2001.

Cutts, J.A., Neck, K.T., Jones, J.A., Guillermo, R., Balaram, J., Powell, G.E., Synott, S.P. Aerovehicles for planetary exploration. IEEE International Conference on Robotics & Automation, Pasadena, CA. 1995.

Davies, D.W. The relative humidity of Mar's atmosphere. J. Geophys. Res. 84, 8335-8340, 1979.

Greeley, R., Christensen, P.R., Cantrell, J., Clark, B.C., Price, R.S., Zubrin, R.M., Cutts, J.A., Oberto, R.E., Haberle, R.M., Malin, M.C. The Mars Aerial Platform concept", AIAA 34th Aerospace Sciences Meeting, Reno, NV, 1996.

Harri, A.M., Siili, T., Pirjola, R., Pellinen, R. Aspects of atmospheric science and instrumentation for Martian missions. Adv. Space Res. 16 (6), 615-622, 1995.

Harrison, L., Loofbourow. Practical Spectroscopy. Prentice Hall, New York, NY. 1948.

Heun, M. K., Cathey Jr. H.M., Haberle, R. Mars balloon trajectory model for Mars geoscience aerobot development, AIAA International Balloon Technology Conference, San Francisco, CA, 1997.

Hourdin, F.; Le Van, Phu, Forget, F., Talagrand, O. Meteorological variability and the annual surface pressure cycle on Mars. J. Atmos.Sci. 50, 3625-40, 1993.

Jones, J.A., Saunders, S., Blamont, J., Yavrouian, A. Balloons for controlled roving/landing on Mars. Acta Astronaut. 45, 293-300, 1999.

Justh, H. L., Justus, C.G., Keller, V.W. Global reference atmospheric models, including thermospheres, for Mars, Venus and Earth. Collection of Technical Papers – AIAA/AAS Astrodynamics Specialist Conference 2, 988-992, 2006.

Justh, H.L., C.G. Justus, Mars Global Reference Atmospheric Model (Mars-GRAM 2005) applications for Mars Science Laboratory. Seventh International Conference on Mars, Pasadena, CA, 2007.

Justus, C.G., Johnson, D.L. NASA/TM-2001-210961 Mars Global Reference Atmospheric Model 2001 Version (Mars-GRAM 2001): Users Guide. 2001.

Justus, C.G., James, B.F., Bougher, S.W., Bridger, A.F.C, Haberle, R.M., Murphy, J.R., Engel, S. Mars-GRAM 2000: A Mars atmospheric model for engineering applications. Adv. Space Res. 29, 193-202. 2002.

Kezhanovich, V.V., Cutts, J.A., Cooper, H.W., Hall, J.L., McDonald, B.A., Pauken, M.T., White, C.V., Yavrouian, A.H., Castano, A., Cathey Jr., H.M., Faibrother, D.A., Smith, I.S. Shreves, C.M., Lachenmeier, T., Rainwater, E., Smith, M., Breakthrough in Mars balloon technology. Adv. Space Res. 33, 1836-1841, 2004.

Lavoie, S. PIA02816: Mars Albedo. 17 Jan. 2001. Web. 1 Oct. 2011. http://photojournal.jpl.nasa.gov/catalog/PIA02816.

Letrenne, G., Nouel, F., Dubourg, V. French Long Duration Balloon activity: the InfraRed Montgolfiere (MIR) - The Superpressure Balloon (BPS). AIAA International Balloon Technology Conference, Norfolk, VA, 1999.

Mathieu, F., Forget F., Mustard J. Water ice at low to midlatitudes on Mars. J. Geophys. Res. - Planets 115, doi: 10.1029/2010JE003584, 2010.

MEPAG. Mars scientific goals, objectives, investigations, and priorities: 2008. (Unpublished white paper, 37 p., posted September, 2008 by the Mars Exploration Program Analysis Group (MEPAG)) http://mepag.jpl.nasa.gov/reports/index.html.

Mumma, M.J., Villanueva, G.L., Novak, R.E., Hewagama, T., Bonev, B.P., DiSanti, M.A., Mandell, A.M., Smith, M.D. Strong release of methane on Mars in northern summer 2003. Science 323, 1041-1045, 2009.

Lavoie, S. PIA02816: Mars Albedo. 17 Jan. 2001. Web. 1 Oct. 2011. http://photojournal.jpl.nasa.gov/catalog/PIA02816.

Neumann, G. The Mars Orbiter Laser Altimeter. 1 Jan. 2007. Web. 30 Sep 2011. http://mola.gsfc.nasa.gov/ .

Nock, K.T., Balaram, J., Heun, M.K., Smith, I.S., Camber, T. Mars 2001 Aerobot/Balloon system overview. AIAA International Balloon Technology Conference, San Francisco, CA, 1997.

Rand, J. L., Crenshaw, J. R. Superpressure balloon design. Adv. Space Res. 17, 5-13, 1996.

Rand, J. L., Phillips, M. L., Grant, D. A. An ultra lightweight superpressure balloon material. AIAA International Balloon Technology Conference, Norfolk, VA. 1999.

Rand, J. L., Phillips, M. L. A superpressure balloon for Mars observations. Adv. Space Res. 30, 1245-1250, 2002.

Ruff, S.W., Christensen, P.R. Bright and dark regions on Mars: Particle size and mineralogical characteristics based on Thermal Emission Spectrometer data. J. Geophys. Res. 107, doi:10.1029/2001JE001580, 2002.

Sagdeev, R.Z., Linkin, V.M., Blamont, J. E., and Preston, R. A., The VEGA Venus balloon experiment. Science 231 (4744), 1407-1408, 1986.

Saito, Y., Yamagami, T., Matsuzaka, Y., Namiki, M., Ohta, S., Toriumi, M., Yokota, R., Makino, F., Matsumoto, T., Hirosawa, H. High altitude balloons with ultra thin polyethylene films. Adv. Space Res. 30, 1159-1165, 2002.

Saito, Y., Iijima, I., Izutsu, N., Kawasaki, T., Matsuzaka, Y., Namiki, M., Toriumi, M., Yamagami, T., Ichimura, K., Kobayashi, T., Matsushima, K., Nakada, T., Development of a 2.8 μm film for scientific balloons. Adv. Space Res. 37, 2026-2032, 2006.

Savijärvi, H., Sili, T. The Martian slope winds and the nocturnal PBL Jet. J. Atmos. Sci. 50, 77-88, 1993.

Schmunk, R.B. Mars24 Sunclock – Time on Mars. 5 Aug. 2008. Web. 5 May 2011. http://www.giss.nasa.gov/tools/mars24/.

Seely, L., Zimmerman, M., McLaughlin, J. The use of Zylon fibers in ULDB tendons. Adv. Space Res. 37, 1736-1740, 2004.

Sinclair, P.C. General characteristics of dust devils. J. Appl. Meteorol. 8, 32-45, 1969.

Smalley, J.H. Balloon Design Considerations. Scientific Ballooning Handbook, NCAR Technical Note, NCAR-TN/IA-99. 1975.

Smith, I. S., H. Cathey, S. Raque, M. Said, Simpson J., The Mars 2001 Balloon design, AIAA International Balloon Technology Conference, San Francisco, CA, 1997.

Smith, M.S., Rainwater, E.L. Development of the elastica shape for pressurized balloons. Japan Society for Aeronautical and Space Sciences and ISTS. 2002.

Smith, M. S., Rainwater, E. L. Optimum design for superpressure balloons. Adv. Space Res. 33, 1688-1693. 2004.

Stanzel, C., Pätzold, M., Williams, D.A., Whelley, P. L., Greeley, R., Neukum, G., the HRSC Co-Investigator Team. Dust devil speeds, directions of motion and general characteristics observed by the Mars Express High Resolution Stereo Camera. Icarus 197, 39-51, 2008.

Steltzner, A., Desai, P. N., Lee, W. J., and Bruno, R. The Mars Exploration Rovers entry descent and landing and the use of aerodynamic decelerators, AIAA Aerodynamic Decelerator Systems Technology Conference and Seminar, Washington, DC, 2003.

Szwast, M.A., Richardson, M.I., Vasavada, A.R. Surface dust redistribution on Mars as observed by the Mars Global Surveyor and Viking Orbiters. J. Geophys. Res. (111), doi:10.1029/2005JE002485, 2006.

Tarrieu, C. Status of the Mars 96 aerostat development. 44th Congress of the International Astronautical Federation, Graz, Austria, 1993.

Tillman, J.E., Martian meteorology and dust storms from Viking observations, in: McKay, C.P. (Ed.), The Case for Mars II, Volume 62, Science and Technology Series, American Astronautical Society, San Diego, CA, 1985.

Tillman, J.E. Mars global atmospheric oscillations: annually synchronized, transient normal-mode oscillations and the triggering of global dust storms. J. Geophys. Res. 93 (D8), 9433-9451, 1988.

Voss, Paul; Smith, Mike; Altitude Control of Planetary Balloons; AIAA's 3rd Annual Aviation Technology, Integration, and Operation (ATIO) Technical Conference; Denver, CO; 2003.

Voss, P.B., Hole, L.R., Mentzoni, A., Helbling, E.F., Johnston, H.G., Roberts, T.J., Controllable meteorological balloons for arctic research. 11th AIAA Aviation Technology, Integration, and Operations (ATIO) Conference, including the AIAA Balloon Systems Conference and 19th AIAA Lighter-Than-Air Systems Conference, Virginia Beach, VA, 2011.

Wright, H.S., Levine, J.S., Croom, M.A., Edwards, W.C., Qualls, Garry D., Gasbarre, J.F. Measurements from an aerial vehicle: a new tool for planetary exploration. Instruments, Science, and Methods for Geospace and Planetary Remote Sensing Conference, Honolulu, HI, 2004.

Yajima, N, Izutsu, N., Imamura, T., Abe, T. Scientific Ballooning: Technology and Applications of Exploration Balloons Floating in the Stratosphere and the Atmospheres of Other Planets;. Springer, New York, NY, 2009.

Yamagami, T., Saito, Y., Matsuzaka, Y., Namiki, M., Toriumi, M., Yokota, R., Hirosawa, H., Matsushima, K., Development of the highest altitude balloon. Adv. Space Res. 33, 1653-1659, 2004.

Zubrin, R.M., Price, S., Gamber, T., Clark, B., Cantrell, J. The Mars aerial platform mission. Space Technol. 14, 261-267, 1994.

Zurek, R. W. Diurnal tide in the Martian atmosphere. J. Atmos. Sci. 33, 321-337, 1976.

APPENDIX A 1

MET BALLOON DESIGN TOOL

```
%*********************************************************************
% MABL_WEATHER (Mars Autonomous Balloon Launcher) predicts the flight
% of a weather ballon in Mar's atmosphere.  The program utilizes the
% Newton-Raphson method to find the balloon volume that would provide
% neutral buoyancy at the maximum altitude.  It calculates the
% necessary mass of gas required to provide the desired free lift with
% the calculated balloon size.  Then, iterations of these calculations
% are done to converge on a balloon volume and lifting gas mass for the
% desired float altitude and free lift.  Once the physical balloon
% parameters are set, MABL_WEATHER calculates the balloon flight
% profile.
%
%          BALLOON ASCENT ASSUMPTIONS:
%          - atmospheric characterization for the initial balloon ascent
%            is based on a vertical atmospheric characterization of the
%            launch site by the Mars_GRAM_05 program
%          - balloon temperature is equal to the atmospheric temperature
%            at a given altitude - this shouldn't matter since the balloon
%            is zero pressure balloon
%          - because of the righting force from balloon buoyancy, vertical
%            winds are ignored
%          - the program will input the following text files based on the
%            output generated from the Mars_GRAM_05 program:
%                    - launch_atm.txt
%
%          USER INPUTS:
%          - max_altitude: the desired maximum altitude in meters (the
%            initial program assumption is 20km.  If the altitude differs
%            from this, changes may be required in the Mars_GRAM_05
%            database requirements to allow for this.
%          - m_payload: the desired payload mass in kg
%          - free_lift: the free lift as a percentage greater than neutral
%            buoynacy entered as a decimal (i.e. enter 0.10 for 10%)
%          - launch_height: the desired launch altitude in meters
%            above/below the MOLA reference areoid surface altitude
%          - LAT_start: the starting latitude for balloon launch
%          - LON_start: the starting longitude for balloon launch (E is +)
%          - delta_t: the time step
%
%          PROGRAMMER:
%          Sean Hancock
%
%          LAST UPDATED:
%          4/10/11
%
%*********************************************************************

clear
clc
```

```
%%%%%%%%%%%%%%%%%%%%%%%%%%%%%%%%%%%%%%%%%%%%%%%%%%%%%%%%%%%%%%%%%%%%%%%
% define input parameters - these are the parameters the user should
% change to fit mission requirements
%%%%%%%%%%%%%%%%%%%%%%%%%%%%%%%%%%%%%%%%%%%%%%%%%%%%%%%%%%%%%%%%%%%%%%%


max_alt = 20000;
% desired float altitude (m)
launch_height = -3864;
% launch MOLA height (m)


m_payload = 0.155;
% payload mass (kg)
m_reef_sleave = 0.050;
free_lift = 0.021;
% free lift ratio (Free Lift / Weight)


t_start = 0;
% launch time (s) from UTC midnight
delta_t = 1;
% time step (s) (for the float portion, this will be mulitplied by 60)


launch_lat = 35.9;
% N is positive
launch_lon = -144.36;
% E is positive


%%%%%%%%%%%%%%%%%%%%%%%%%%%%%%%%%%%%%%%%%%%%%%%%%%%%%%%%%%%%%%%%%%%%%%%
% initialize parameters - these are the constants to be used in
% calculations
%%%%%%%%%%%%%%%%%%%%%%%%%%%%%%%%%%%%%%%%%%%%%%%%%%%%%%%%%%%%%%%%%%%%%%%


g = 3.7;
% gravity constant of Mars (kg-m/s^2)
Cd = 0.8;
% assumes a constant drag coefficient despite percent of inflation
R_gas = 4.12;
% ideal gas constant for hydrogen (kJ/kg/K)
h(1) = launch_height;
% height (m)
total_dist = 0;
% total ground track distance traveled (km)


%%%%%%%%%%%%%%%%%%%%%%%%%%%%%%%%%%%%%%%%%%%%%%%%%%%%%%%%%%%%%%%%%%%%%%%
% import atmospheric profile for balloon ascent
% ***THE NAME OF THE TEXT FILE WILL NEED TO MATCH THE textread
% COMMAND***
%        L_MOLAhgt = MOLA height (km)
%        L_rho = atmospheirc density (kg/m^3)
%        L_P = atmospheric pressure (Pa)
%        L_T = atmospheric temperture (K)
%        L_Ewind = east wind (m/s)
%        L_Nwing = north wind (m/s)
%%%%%%%%%%%%%%%%%%%%%%%%%%%%%%%%%%%%%%%%%%%%%%%%%%%%%%%%%%%%%%%%%%%%%%%
```

```
[L_MOLAhgt L_rho L_P L_T L_Ewind L_Nwind]=textread('launch_atm.txt','%f
%f %f %f %f %f');
L_P = L_P/1000;
% convert pressure to kPa


%%%%%%%%%%%%%%%%%%%%%%%%%%%%%%%%%%%%%%%%%%%%%%%%%%%%%%%%%%%%%%%%%%%%%
% define atmospheric conditions at balloon launch
%%%%%%%%%%%%%%%%%%%%%%%%%%%%%%%%%%%%%%%%%%%%%%%%%%%%%%%%%%%%%%%%%%%%%


for CNT=1:length(L_MOLAhgt)
    if round(h(1)/100)/10==L_MOLAhgt(CNT)
        i=CNT;
% find location in database corresponding to launch alt.
    end
end


%%%%%%%%%%%%%%%%%%%%%%%%%%%%%%%%%%%%%%%%%%%%%%%%%%%%%%%%%%%%%%%%%%%%%
% define atmospheric conditions at max altitude
%%%%%%%%%%%%%%%%%%%%%%%%%%%%%%%%%%%%%%%%%%%%%%%%%%%%%%%%%%%%%%%%%%%%%


for CNT=1:length(L_MOLAhgt)
    if round(max_alt/100)/10==L_MOLAhgt(CNT)
        I=CNT;
% find location in database corresponding to max alt.
    end
end


%%%%%%%%%%%%%%%%%%%%%%%%%%%%%%%%%%%%%%%%%%%%%%%%%%%%%%%%%%%%%%%%%%%%%
% define balloon lifting gas conditions for balloon sizing - it is
% assumed for simplicity that the lifting gas is at thermal equlibirium
% with the ambient atmosphere
%%%%%%%%%%%%%%%%%%%%%%%%%%%%%%%%%%%%%%%%%%%%%%%%%%%%%%%%%%%%%%%%%%%%%


rho_gas = L_P(I)/R_gas/L_T(I);
% hydrogen density at max altitude (kg/m^3)
rho_gas_start = L_P(i)/R_gas/L_T(i);
% hydrogen density at launch altitude (kg/m^3)


%%%%%%%%%%%%%%%%%%%%%%%%%%%%%%%%%%%%%%%%%%%%%%%%%%%%%%%%%%%%%%%%%%%%%
% calculate balloon size - this calculates the required volume of a
% balloon to float a payload of the mass entered above at the float
% altitude entered above.  This code assumes the volume is such that a
% force balance of the balloon results in an equilibrium where the
% buoyant force equal the weight of the combined balloon system.
%%%%%%%%%%%%%%%%%%%%%%%%%%%%%%%%%%%%%%%%%%%%%%%%%%%%%%%%%%%%%%%%%%%%%


%%%Newton Raphson Method - IT SHOULD BE NOTED x1 WILL NEED TO BE %%%
%%%             PICKED SO THAT THE SOLUTION CONVERGES            %%%
fn='(m_payload+m_reef_sleave+(0.023*x^(2/3))+(rho_gas*x))/L_rho(I)-x';
gn=diff(fn);
x1=41200;
x=x1;
n=0;
while abs(eval(fn)) > 1.e-6
  x=x1;g1=eval(gn);
```

```
   x=x1;f1=eval(fn);
   x2=x1-f1/g1;
   x1=x2;
   x=x1;
   n=n+1;
   f=eval(fn);
end

V_bal = x;
% balloon volume (m^3)
m_bal = 0.023*x^(2/3);
% balloon mass (kg)
D_bal = 2*((3/4)*V_bal/pi)^(1/3);
% diameter of balloon (m)

%%%%%%%%%%%%%%%%%%%%%%%%%%%%%%%%%%%%%%%%%%%%%%%%%%%%%%%%%%%%%%%%%%%%
% calculate mass of gas required to give desired free lift at launch
%%%%%%%%%%%%%%%%%%%%%%%%%%%%%%%%%%%%%%%%%%%%%%%%%%%%%%%%%%%%%%%%%%%%

m_gas = rho_gas*V_bal;
% mass of gas required for neutral buoyancy at float based on this
V_bal (kg)
m_sys = m_payload + m_bal + m_gas;
% total system mass (kg)

V_start = (free_lift+1)*m_sys/L_rho(i);
% required volume of balloon at launch (m^3)
D_start = 2*((3/4)*V_start/pi)^(1/3);
% diameter of balloon at launch (m)
m_gas = rho_gas_start*V_start;
% new mass of lifting gas based on free lift(kg)

%%%%%%%%%%%%%%%%%%%%%%%%%%%%%%%%%%%%%%%%%%%%%%%%%%%%%%%%%%%%%%%%%%%%
% iterate balloon volume calculation so that an equilibrium exists at
% the desired float altitude with the required mass of give to give the
% desired lift at launch
%%%%%%%%%%%%%%%%%%%%%%%%%%%%%%%%%%%%%%%%%%%%%%%%%%%%%%%%%%%%%%%%%%%%

%%%Newton Raphson Method - IT SHOULD BE NOTED x1 WILL NEED TO BE %%%
%%%           PICKED SO THAT THE SOLUTION CONVERGES              %%%
= 1;
%initialize convergence criteria
while abs(delta) > 0.001
    V_start_old = V_start;
    fn='(m_payload+(0.023*x^(2/3))+m_gas)/L_rho(I)-x';
    gn=diff(fn);
    x1=41200;
    x=x1;
    n=0;
    while abs(eval(fn)) > 1.e-6
        x=x1;g1=eval(gn);
        x=x1;f1=eval(fn);
        x2=x1-f1/g1;
        x1=x2;
        x=x1;
        n=n+1;
```

```
        f=eval(fn);
    end


    V_bal = x;
% balloon volume (m^3)
    m_bal = 0.023*x^(2/3);
% balloon mass (kg)
    D_bal = 2*((3/4)*V_bal/pi)^(1/3);
% diameter of balloon (m)


    m_gas = rho_gas*V_bal;
% mass of gas required for neutral buoyancy at float based on this
% V_bal (kg)
    m_sys = m_payload + m_bal + m_gas;
% total system mass (kg)


    V_start = (free_lift+1)*m_sys/L_rho(i);
% required volume of balloon at launch (m^3)
    D_start = 2*((3/4)*V_start/pi)^(1/3);
% diameter of balloon at launch (m)
    m_gas = rho_gas_start*V_start;
% new mass of lifting gas based on free lift(kg)


    delta = V_start_old - V_start;
% calculate convergence
end


fprintf('******************\n')
fprintf('***FINAL RESULTS***\n')
fprintf('******************\n')


V_bal
D_bal
V_start
D_start
m_gas
m_bal
m_bal_sys = m_bal + m_gas
% mass of balloon system (kg)
m_sys
% mass of balloon and payload (kg)
W = m_sys*g;
% weight of total flight system (N)


m_gas_START = m_gas;


%%%%%%%%%%%%%%%%%%%%%%%%%%%%%%%%%%%%%%%%%%%%%%%%%%%%%%%%%%%%%%%%%%%%%%%%%%%%
% calculate balloon ascent properties as a function of time
%%%%%%%%%%%%%%%%%%%%%%%%%%%%%%%%%%%%%%%%%%%%%%%%%%%%%%%%%%%%%%%%%%%%%%%%%%%%


%%%atmospheric properties%%%
T(1) = L_T(i);
% initial ambient temp. (K)
P(1) = L_P(i);
% initial ambient pressure (kPa)
```

```
rho(1) = L_rho(i);
% initial ambient density (kg/m^3)
Ewind(1) = L_Ewind(i);
% initial east wind (m/s)
Nwind(1) = L_Nwind(i);
% initial north wind (m/s)

%%%balloon properties%%%
V(1) = V_start;
% initial volume (m^3)
d(1) = 2*((3/4)*V(1)/pi)^(1/3);
% balloon diameter (m)
S(1) = pi*d(1)*d(1)/4;
% balloon projected area (m^2)

%%%flight properties%%%
t(1) = 0;
% sets initial time to zero (s)
Fb(1) = (rho(1)*V(1))*g;
% buoyant force of balloon(N)
F(1) = Fb(1) - W;
% free lift of balloon (N)
height(1) = launch_height;
% sets initial height to launch height (m)
u(1) = 0;
% initial velocity is zero (m/s)
a(1) = Fb(1)/m_sys - g - (1/2)*rho(1)*(u(1)^2)*Cd*S(1)/m_sys;
% initial acceleration (m/s^2)

%%%balloon loacation%%%
LAT(1) = launch_lat;
% N is positive
LON(1) = launch_lon;
% E is positive

%%%calculate balloon ascent%%%

cnt = 1;
% time counter for balloon ascent
while h(cnt) < max_alt
    cnt = cnt +1;
% increments counter
    t(cnt) = t(cnt-1)+delta_t;
% time (s)
    u(cnt) = u(cnt-1) + a(cnt-1)*delta_t;
% velocity (m/s)
    height(cnt) = height(cnt-1) + u(cnt-1)*delta_t;
% height (m)
    h(cnt) = round(height(cnt));
% height round to nearest meter

%%%atmospheric properties%%%
    for CNT=1:length(L_MOLAhgt)
        if round(h(cnt)/100)/10==L_MOLAhgt(CNT)
% rounding height to nearest km for weather database
```

```
            i=CNT;
% find location in database corresponding to current alt.
        end
    end
    T(cnt) = L_T(i);
% ambient temperature (K)
    P(cnt) = L_P(i);
% ambient pressure (kPa)
    rho(cnt) = L_rho(i);
% ambient density (kg/m^3)
    Ewind(cnt) = L_Ewind(i);
% ambient east wind (m/s)
    Nwind(cnt) = L_Nwind(i);
% ambient north wind (m/s)


%%%balloon properties%%%
    V(cnt) = m_gas*R_gas*T(cnt)/P(cnt);
% balloon volume (m^3)
    if V(cnt)>V_bal
% constrains balloon volume to maximum inflated volume
        V(cnt) = V_bal;
    end
    d(cnt) = 2*((3/4)*V(cnt)/pi)^(1/3);
% balloon diameter (m)
    S(cnt) = pi*d(cnt)*d(cnt)/4;
% balloon projected area (m^2)
    if V(cnt) == V_bal
        m_gas = P(cnt)*V(cnt)/R_gas/T(cnt);
    end

    if m_gas > m_gas_START
        cnt
        V(cnt)
        P(cnt)
        m_gas
        pause(1)
    end


    m_sys = m_payload + m_bal + m_gas;
% total system mass (kg)
    W = m_sys*g;
% weight of total flight system (N)


%%%flight properties%%%
    Fb(cnt) = (rho(cnt)*V(cnt))*g;
% buoyant force of balloon(N)
    F(cnt) = Fb(cnt) - W;
% free lift of balloon (N)
    if u(cnt)>=0
        D(cnt) = rho(cnt)*(u(cnt)^2)*Cd*S(cnt)/2;
% drag (N)
    end
    if u(cnt)<0
        D(cnt) = -rho(cnt)*(u(cnt)^2)*Cd*S(cnt)/2;
% drag (N)
    end
```

```
    a(cnt) = Fb(cnt)/m_sys - g - D(cnt)/m_sys;
% balloon acceleration (m/s^2)


%%%change in latitude%%%
    Ndist = Nwind(cnt-1)*delta_t/1000;
% distance traveled (km) N-S (N is +)
    phi = Ndist/(3376.20+(height(cnt)/1000));
% assumes reference ellipsoid polar radius of 3376.20km (in radians)
    delta_LAT = phi*180/pi;
% converts change in latitude to degrees
    LAT(cnt) = LAT(cnt-1) + delta_LAT;


%%%change in longitude%%%
    Edist = Ewind(cnt-1)*delta_t/1000;
% distance traveled (km) E-W (E is +)
    theta = Edist/((3396.19+(height(cnt)/1000))*cos(LAT(cnt-
1)*pi/180));    % assumes reference ellipsoid equatorial radius of
3396.19km (in radians)
    delta_LON = theta*180/pi;
% converts change in longitude to degrees
    LON(cnt) = LON(cnt-1) + delta_LON;
    if LON(cnt)<=-180
        LON(cnt)=LON(cnt)+360;
    end
    if LON(cnt)>180
        LON(cnt)=LON(cnt)-360;
    end


%%%ground track distance%%%
    total_dist = total_dist + sqrt(Ndist^2+Edist^2);
% total ground track distance traveled (km)


end


%%%%%%%%%%%%%%%%%%%%%%%%%%%%%%%%%%%%%%%%%%%%%%%%%%%%%%%%%%%%%%%%%%%%%%
% write results data to text file
%%%%%%%%%%%%%%%%%%%%%%%%%%%%%%%%%%%%%%%%%%%%%%%%%%%%%%%%%%%%%%%%%%%%%%

%open the file to write to with write permission
fid = fopen('RESULTS.txt','wt');
for i=1:length(t)
        fprintf(fid,'%8.5f %8.5f %8.5f %8.5f %8.5f %8.5f \r\n', t(i),
V(i), height(i), u(i), LAT(i), LON(i));
end
fclose(fid);


fid = fopen('SUMMARY.txt','wt');
fprintf(fid,'Fully Inflated Volume (m^3): %8.5f \r\n', V_bal);
fprintf(fid,'Fully Inflated Diameter (m): %8.5f \r\n', D_bal);
fprintf(fid,'Launch Volume (m^3): %8.5f \r\n', V_start);
fprintf(fid,'Launch Diameter (m): %8.5f \r\n', D_start);
fprintf(fid,'Initial Hydrogen Mass (kg): %8.5f \r\n', m_gas);
fprintf(fid,'Balloon Mass (kg): %8.5f \r\n', m_bal);
fprintf(fid,'System Mass (kg): %8.5f \r\n', m_sys);
fclose(fid);
```

```
%%%%%%%%%%%%%%%%%%%%%%%%%%%%%%%%%%%%%%%%%%%%%%%%%%%%%%%%%%%%%%%%%%%%%%%%%%%
% end
%%%%%%%%%%%%%%%%%%%%%%%%%%%%%%%%%%%%%%%%%%%%%%%%%%%%%%%%%%%%%%%%%%%%%%%%%%%
```

APPENDIX A 2

EXPLORATION SYSTEM DESIGN TOOL

```
%*******************************************************************
% MABL (Mars Autonomous Balloon Launcher) predicts the flight of a
% super-pressure balloon in Mar's atmosphere.  The program utilizes the
% Newton-Raphson method to find the balloon volume that would provide
% neutral buoyancy at the float altitude.  It calculates the necessary
% mass of gas required to provide the desired free lift with the
% calculated balloon size at launch.  Once the physical balloon
% parameters are set, MABL calculates the balloon flight profile.
%
% The program is set up to calculate the flight profile for a flight of
% <= 30 days.  This constraint is based upon references to the
% atmospheric database.  Any deviation from this will require changes
% in the code and also in the Mars_GRAM_05 database created.
%
% The program is broken into two main sections. The first calculates
% the balloon ascent profile, including sizing the balloon.  The second
% calculates the balloon float profile.
%
%       BALLOON ASCENT ASSUMPTIONS:
%       - atmospheric characterization for the initial balloon ascent
%         is based on a vertical atmospheric characterization of the
%         launch site by the Mars_GRAM_05 program (requires input .txt
%         file)
%       - balloon temperature is equal to the atmospheric temperature
%         at a given altitude
%       - because of the righting force from balloon buoyancy, vertical
%         winds are ignored
%       - the program will input the following text files based on the
%         output generated from the Mars_GRAM_05 program:
%               - launch_atm.txt
%
%       BALLOON FLOAT ASSUMPTIONS:
%       - atmospheric characterization is based on output from the
%         Mars_GRAM_05 program.  A Mars_GRAM_05 run is required with a
%         5 deg resolution for both latitude and longitude for -90 to
%         90 deg latitude, -180 to 180 deg longitude, and 7.5 km to 11
%         km MOLA altitude. (requires input .txt files)
%       - it is assumed that the Mars_GRAM_05 database is created for
%         the appropriate time frame and that the first day (UTC time)
%         in the database corresponds to the balloon launch day.
%       - the program will input the following text files based on the
%         output generated from the Mars_GRAM_05 program:
%               - albedo.txt
%               - Ewind.txt
%               - Nwind.txt
%               - lat.txt
%               - lon.txt
%               - MOLAhgt.txt
%               - T.txt
%               - P.txt
```

```
%                    - rho.txt
%                    - TERhgt.txt
%                    - Ls.txt
%
%        USER INPUTS:
%        - max_alt: the desired float altitude in meters (the initial
%          program assumption is 10km.  If the altitude differs from
%          this, changes will be required in the Mars_GRAM_05 database
%          requirements to allow for this.
%        - launch_height: this is the altitude the lander is launching
%          from and is relative to the MOLA aeroid
%        - m_payload: the desired payload mass in kg
%        - N_gore: the number of gores in the balloon as an input
%          parameter
%        - free_lift: the free lift ratio (Free Lift (kg) / Total mass
%          (kg))
%        - t_start: launch time (s) from UTC midnight (the number of
%          seconds that have passed since UTC midnight on the launch day
%        - delta_t: the time step (there is an option to increase the
%          time step in the float section)
%        - sol_max: the desired end time in sols (assume launch day
%          sol=1)
%        - launch_lat: the starting latitude for balloon launch (N is +)
%        - launch_lon: the starting longitude for balloon launch (E is
%          +)
%
%        PROGRAMMER:
%        Sean Hancock
%
%        LAST UPDATED:
%        8/12/11
%
%*******************************************************************************

clear
clc


%%%%%%%%%%%%%%%%%%%%%%%%%%%%%%%%%%%%%%%%%%%%%%%%%%%%%%%%%%%%%%%%%%%%%%%%%%%%%%%
% define input parameters - these are the parameters the user should
% change to fit mission requirements
%
% pos_sigma and neg_sigma should not be set to "1" simultaneously
%%%%%%%%%%%%%%%%%%%%%%%%%%%%%%%%%%%%%%%%%%%%%%%%%%%%%%%%%%%%%%%%%%%%%%%%%%%%%%%


max_alt = 10000;
% desired float altitude (m)
launch_height = -3864;
% launch MOLA height (m)

m_payload = 100.5;
% payload mass (kg)
Ngore = 60;
% number of gores in balloon
free_lift = 0.1;
% free lift ratio (Free Lift / Weight)
```

```
t_start = 43200;
% launch time (s) from UTC midnight on day of launch
delta_t = 1;
% time step (s)
sol_max = 20;
% end time (sol)


launch_lat = 35.9;
% N is positive
launch_lon = -144.3;
% E is positive


alpha_top = 1.0;
% balloon top surface solar absorptivity
epsilon_top = 1.0;
% balloon top surface infrared emissivity/absorptivity
alpha_bot = 1.0;
% balloon bottom surface solar absorptivity
epsilon_bot = 1.0;
% balloon botttom surface infrared emissivity/absorptivity


pos_sigma = 0;
% set to "1" to utilize positive standard deviation on the wind
neg_sigma = 0;
% set to "1" to utilize negative standard deviation on the wind
mult_sigma = 1;
% multiplier to sigma (# of standard deviations to include)


D_sun = [1.510; 1.512; 1.515; 1.517; 1.519; 1.522; 1.524; 1.526; 1.528;
        1.530; 1.532; 1.534; 1.536; 1.538; 1.540; 1.542; 1.543; 1.545;
        1.547; 1.548; 1.550; 1.551; 1.553; 1.554; 1.555; 1.557; 1.558;
        1.559; 1.560; 1.561; 1.562; 1.563];
% distance of Mars from sun (AU)


%%%%%%%%%%%%%%%%%%%%%%%%%%%%%%%%%%%%%%%%%%%%%%%%%%%%%%%%%%%%%%%%%%%%%%%%%%
% initialize parameters - these are the constants to be used in
% calculations
%%%%%%%%%%%%%%%%%%%%%%%%%%%%%%%%%%%%%%%%%%%%%%%%%%%%%%%%%%%%%%%%%%%%%%%%%%


g = 3.7;
% gravity constant of Mars (m/s^2)
Cd = 0.8;
% assumes a constant drag coefficient despite percent of inflation
R_gas = 4.12;
% ideal gas constant for hydrogen (kJ/kg/K)
sigma = 5.67051E-08;
% Steffan Boltzman Constant (W/m^2/K^4)
R_aeroid = 3396;
% reference aeroid radius(km)
P_sun = 3.8E26;
% power output from sun (W)


h(1) = launch_height;
% height (m)
```

```
%%%%%%%%%%%%%%%%%%%%%%%%%%%%%%%%%%%%%%%%%%%%%%%%%%%%%%%%%%%%%%%%%%%%%%
%%%%%%%%%%%%%%%%%%%%%%%%%%%%%%%%%%%%%%%%%%%%%%%%%%%%%%%%%%%%%%%%%%%%%%
%%%                          BALLOON ASCENT
%%%
%%%%%%%%%%%%%%%%%%%%%%%%%%%%%%%%%%%%%%%%%%%%%%%%%%%%%%%%%%%%%%%%%%%%%%
%%%%%%%%%%%%%%%%%%%%%%%%%%%%%%%%%%%%%%%%%%%%%%%%%%%%%%%%%%%%%%%%%%%%%%


%%%%%%%%%%%%%%%%%%%%%%%%%%%%%%%%%%%%%%%%%%%%%%%%%%%%%%%%%%%%%%%%%%%%%%
% import atmospheric profile for balloon ascent
% ***THE NAME OF THE TEXT FILE WILL NEED TO MATCH THE textread
% COMMAND***
%       L_MOLAhgt = MOLA height (m)
%       L_rho = atmospheirc density (kg/m^3)
%       L_P = atmospheric pressure (Pa)
%       L_T = atmospheric temperture (K)
%       L_Ewind = east wind (m/s)
%       L_Nwing = north wind (m/s)
%       L_SigU = standard deviation in wind (m/s)
%       L_mu0 = cosine of solar zenith angle
%%%%%%%%%%%%%%%%%%%%%%%%%%%%%%%%%%%%%%%%%%%%%%%%%%%%%%%%%%%%%%%%%%%%%%


[L_MOLAhgt L_rho L_P L_T L_Ewind L_Nwind L_SigU
L_mu0]=textread('launch_atm.txt','%f %f %f %f %f %f %f %f');
L_P = L_P/1000;
% convert pressure to kPa


%%%%%%%%%%%%%%%%%%%%%%%%%%%%%%%%%%%%%%%%%%%%%%%%%%%%%%%%%%%%%%%%%%%%%%
% define atmospheric conditions at balloon launch
%%%%%%%%%%%%%%%%%%%%%%%%%%%%%%%%%%%%%%%%%%%%%%%%%%%%%%%%%%%%%%%%%%%%%%


launch_hour = floor(t_start/3600);
% time step of Mars ascent database (24 timesteps - i.e. current UTC
hour)
launch_CNT_start = launch_hour*161;
% point in ascent database corresponding to start of current UTC hour
launch_CNT_end = (launch_hour+1)*161;
% point in ascent database corresponding to start of next UTC hour


for CNT=launch_CNT_start:launch_CNT_end
    if round(h(1)/100)/10==L_MOLAhgt(CNT)
        i=CNT;
% find location in database corresponding to launch alt.
    end
    if L_MOLAhgt(CNT)==(max_alt/1000)
        float_i=CNT;
% find location in database corresponding to float alt.
    end
end


%%%%%%%%%%%%%%%%%%%%%%%%%%%%%%%%%%%%%%%%%%%%%%%%%%%%%%%%%%%%%%%%%%%%%%
% define balloon lifting gas conditions for balloon sizing - it is
% assumed for simplicity that the lifting gas is at thermal equilibrium
% with the ambient atmosphere
%%%%%%%%%%%%%%%%%%%%%%%%%%%%%%%%%%%%%%%%%%%%%%%%%%%%%%%%%%%%%%%%%%%%%%
```

```
rho_gas = L_P(float_i)/R_gas/L_T(float_i);
% hydrogen density at float altitude (kg/m^3)
rho_gas_start = L_P(i)/R_gas/L_T(i);
% hydrogen density at launch altitude (kg/m^3)


%%%%%%%%%%%%%%%%%%%%%%%%%%%%%%%%%%%%%%%%%%%%%%%%%%%%%%%%%%%%%%%%%%%%%%
% calculate balloon size - this calculates the required volume of a
% balloon to float a payload of the mass entered above at the float
% altitude entered above.  This code assumes the volume is such that a
% force balance of the balloon results in an equilibrium where the
% buoyant force equals the weight of the combined balloon system.  The
% mass of the balloon (in kg) is assumed to be described by the
% equation:
%    m_bal = 0.095*V_bal^(2/3) + 0.011*((Ngore+1)/1000)*V_bal^(1/3) +
%    4.2
% which describes the film mass, the tape mass, and the fitting mass
%%%%%%%%%%%%%%%%%%%%%%%%%%%%%%%%%%%%%%%%%%%%%%%%%%%%%%%%%%%%%%%%%%%%%%

%%% Newton Raphson Method - IT SHOULD BE NOTED x1 WILL NEED TO BE %%%
%%%              PICKED SO THAT THE SOLUTION CONVERGES            %%%
fn='(m_payload + (0.095*x^(2/3)+0.011*((Ngore+1)/1000)*x^(1/3)+4.2) +
(rho_gas*x))/L_rho(float_i) - x';
gn=diff(fn);
x1=41200;
% initial volume guess
x=x1;
n=0;
while abs(eval(fn)) > 1.e-6
  x=x1;g1=eval(gn);
  x=x1;f1=eval(fn);
  x2=x1-f1/g1;
  x1=x2;
  x=x1;
  n=n+1;
  f=eval(fn);
end


V_bal = x;
% fully inflated balloon volume (m^3)
D_bal = 2*((3/4)*V_bal/pi)^(1/3);
% diameter of fully inflated balloon based on V_bal (m)
m_bal = 0.095*V_bal^(2/3) + 0.011*((Ngore+1)/1000)*V_bal^(1/3) + 4.2;
% balloon mass based on V_bal (kg)


m_gas = rho_gas*V_bal;
% mass of gas required for neutral buoyancy at float based on this
V_bal (kg)
m_sys = m_payload + m_bal + m_gas;
% total system mass (kg)
W = m_sys*g;
% total system weight (N)


V_start = (free_lift+1)*m_sys/L_rho(i);
% required volume of gas bubble at launch (m^3)
D_start = 2*((3/4)*V_start/pi)^(1/3);
% diameter of balloon at launch (m)
```

```
%%%%%%%%%%%%%%%%%%%%%%%%%%%%%%%%%%%%%%%%%%%%%%%%%%%%%%%%%%%%%%%%%%%%%
% iterate balloon volume calculation so that an equilibrium exists at
% the desired float altitude with the required mass of lifting gas to
% give the desired free lift at launch
%%%%%%%%%%%%%%%%%%%%%%%%%%%%%%%%%%%%%%%%%%%%%%%%%%%%%%%%%%%%%%%%%%%%%

%%% Newton Raphson Method - IT SHOULD BE NOTED x1 WILL NEED TO BE %%%
%%%            PICKED SO THAT THE SOLUTION CONVERGES              %%%
delta = 1;
%initialize convergence criteria
while abs(delta) > 0.001
    V_bal_old = V_bal;

    m_gas = rho_gas*V_bal;
% mass of gas required for neutral buoyancy at float based on V_bal
%(kg)
    m_sys = m_payload + m_bal + m_gas;
% total system mass (kg)

    V_start = (free_lift+1)*m_sys/L_rho(i);
% required volume of balloon at launch (m^3)
    D_start = 2*((3/4)*V_start/pi)^(1/3);
% diameter of balloon at launch (m)

    fn='(m_payload + (0.095*x^(2/3)+0.011*((Ngore+1)/1000)*x^(1/3)+4.2)
+ m_gas)/L_rho(float_i)-x';
    gn=diff(fn);
    x1=41200;
    x=x1;
    n=0;
    while abs(eval(fn)) > 1.e-6
        x=x1;g1=eval(gn);
        x=x1;f1=eval(fn);
        x2=x1-f1/g1;
        x1=x2;
        x=x1;
        n=n+1;
        f=eval(fn);
    end

    V_bal = x;
% current balloon volume (m^3)
    m_bal = 0.095*V_bal^(2/3) + 0.011*((Ngore+1)/1000)*V_bal^(1/3)+4.2;
% current balloon mass based on V_bal(kg)
    D_bal = 2*((3/4)*V_bal/pi)^(1/3);
% current diameter of balloon based on V_bal (m)

    m_gas = rho_gas*V_bal;
% mass of gas required for neutral buoyancy at float based on this
% V_bal (kg)
    m_sys = m_payload + m_bal + m_gas;
% total system mass (kg)
```

```
    V_start = (free_lift+1)*m_sys/L_rho(i);
% required volume of balloon at launch (m^3)
    D_start = 2*((3/4)*V_start/pi)^(1/3);
% diameter of balloon at launch (m)
    m_gas = rho_gas_start*V_start;
% new mass of lifting gas based on free lift(kg)


    delta = V_bal_old - V_bal;
% calculate convergence

end


W = m_sys*g;
% weight of total flight system (N)
Fb = L_rho(float_i)*V_bal*g;
% buoyant force at float altitude (N)
F = Fb-W;
% system free lift at float altitude (N)


FREE_LIFT_RATIO = F/W;
% calculated free lift ratio


fprintf('******************\n')
fprintf('***FINAL RESULTS***\n')
fprintf('*******************\n')
fprintf('Fully Inflated Balloon Volume (m^3) V_bal: %f\n',V_bal)
fprintf('Fully Inflated Balloon Diameter (m) D_bal: %f\n',D_bal)
fprintf('Initial Balloon Volume at Launch (m^3) V_start: %f\n',V_start)
fprintf('Initial Balloon Diameter at Launch (m) D_start: %f\n',D_start)
fprintf('Balloon Mass (kg) m_bal: %f\n',m_bal)
fprintf('Hydrogen Inflation Gas Mass (kg) m_gas: %f\n',m_gas)
fprintf('Total Exploration Balloon System Mass (kg) m_sys: %f\n',m_sys)
fprintf('Total Exploration Balloon System Weigth (N) W: %f\n',W)
fprintf('Buoyant Force at Float Altitude (N): %f\n',Fb)
fprintf('Free Lift at Float Altitude (N): %f\n',F)
fprintf('Free Lift Ratio at Float Altitude: %f\n',FREE_LIFT_RATIO)
fprintf('Free Lift Ratio at Float Launch: %f\n',(L_rho(i)*V_start*g-
W)/W)
fprintf('\n\n')


%%%%%%%%%%%%%%%%%%%%%%%%%%%%%%%%%%%%%%%%%%%%%%%%%%%%%%%%%%%%%%%%%%%%%
% calculate balloon ascent properties as a function of time - because
% of the duration of the ascent, it is assumed for simplicity that the
% lifting gas is at thermal equilibrium with the ambient atmosphere
%%%%%%%%%%%%%%%%%%%%%%%%%%%%%%%%%%%%%%%%%%%%%%%%%%%%%%%%%%%%%%%%%%%%%


%%%initial launch - atmospheric properties%%%
P(1) = L_P(i);
% initial ambient pressure (kPa)
T(1) = L_T(i);
% initial ambient temp. (K)
rho(1) = L_rho(i);
% initial ambient density (kg/m^3)
Ewind(1) = L_Ewind(i);
% initial east wind (m/s)
```

```
Nwind(1) = L_Nwind(i);
% initial north wind (m/s)
SigU(1) = L_SigU(i);
% initial wind standard deviation (m/s)
mu0(1) = L_mu0(i);
% initial cosine of the solar zenith angle

%%%initial launch - account for standard deviation in wind%%%
if pos_sigma == 1
    Ewind(1) = Ewind(1)+SigU(1)*mult_sigma;
% initial east wind + standard deviation (m/s)
    Nwind(1) = Nwind(1)+SigU(1)*mult_sigma;
% initial north wind + standard deviation (m/s)
end
if neg_sigma == 1
    Ewind(1) = Ewind(1)-SigU(1)*mult_sigma;
% initial east wind - standard deviation (m/s)
    Nwind(1) = Nwind(1)-SigU(1)*mult_sigma;
% initial north wind - standard deviation (m/s)
end

%%%initial launch - balloon properties%%%
V(1) = V_start;
% initial volume (m^3)
d(1) = 2*((3/4)*V(1)/pi)^(1/3);
% balloon diameter (m)
S(1) = pi*d(1)*d(1)/4;
% balloon projected area (m^2)
P_gas(1) = P(1);
% balloon/hydrogen pressure (kPa) (zero pressure, P_gas = P)
T_gas(1) = T(1);
% balloon/hydrogen temperature (K) (assume T_gas = T for ascent,
% simplification)
if V(1) == V_bal
    P_gas(1) = m_gas*R_gas*T(1)/V(1);
% calculates superpressure if balloon is fully inflated
end
delta_P(1) = P_gas(1)-P(1);
% balloon super-pressure (kPa)

%%%initial launch - flight properties%%%
t(1) = 0;
% sets initial time to zero (s)
Fb(1) = (rho(1)*V(1))*g;
% buoyant force of balloon(N)
F(1) = Fb(1) - W;
% free lift of balloon (N)
height(1) = launch_height;
% sets initial height to launch height (m)
u(1) = 0;
% initial velocity is zero (m/s)
a(1) = Fb(1)/m_sys - g - (1/2)*rho(1)*(u(1)^2)*Cd*S(1)/m_sys;
% initial acceleration (m/s^2)

%%%initial launch - balloon location%%%
```

```
LAT(1) = launch_lat;
% N is positive
LON(1) = launch_lon;
% E is positive

%%%calculate balloon ascent%%%
cnt = 1;
% time counter for balloon ascent
while h(cnt) < max_alt
    cnt = cnt +1;
% increments counter
    t(cnt) = t(cnt-1)+delta_t;
% time (s)
    u(cnt) = u(cnt-1) + a(cnt-1)*delta_t;
% velocity (m/s)
    height(cnt) = height(cnt-1) + u(cnt-1)*delta_t;
% height (m)
    h(cnt) = round(height(cnt));
% height round to nearest meter

%%%ascent - atmospheric properties%%%
    for CNT=1:length(L_MOLAhgt)
        if round(h(cnt)/100)/10==L_MOLAhgt(CNT)
% rounding height to nearest km for weather database
            i=CNT;
% find location in database corresponding to current alt.
        end
    end
    T(cnt) = L_T(i);
% ambient temperature (K)
    P(cnt) = L_P(i);
% ambient pressure (kPa)
    rho(cnt) = L_rho(i);
% ambient density (kg/m^3)
    Ewind(cnt) = L_Ewind(i);
% ambient east wind (m/s)
    Nwind(cnt) = L_Nwind(i);
% ambient north wind (m/s)
    SigU(cnt) = L_SigU(i);
% wind standard deviation (m/s)
    mu0(cnt) = L_mu0(i);
% local cosine of the solar zenith angle

%%%ascent - account for standard deviation in wind%%%
    if pos_sigma == 1
        Ewind(cnt) = Ewind(cnt)+SigU(cnt)*mult_sigma;
% east wind + standard deviation (m/s)
        if LAT(cnt-1) < 90
            Nwind(cnt) = Nwind(cnt)+SigU(cnt)*mult_sigma;
% north wind + standard deviation (m/s)
        end
    end
    if neg_sigma == 1
        Ewind(cnt) = Ewind(cnt)-SigU(cnt)*mult_sigma;
% east wind - standard deviation (m/s)
        if LAT(cnt-1) > -90
```

```
                Nwind(cnt) = Nwind(cnt)-SigU(cnt)*mult_sigma;
% north wind - standard deviation (m/s)
        end
    end


%%%ascent - balloon thermal properties%%%
    H(cnt) = (height(cnt)/1000)/R_aeroid;
% ratio of altitude to planetary radius
    T_gas(cnt) = T(cnt);
% hydrogen inlfation gas temperature (K) - equal to ambient for ascent


%%%ascent - balloon properties%%%
    V(cnt) = m_gas*R_gas*T_gas(cnt)/P(cnt);
% balloon volume (m^3)
    if V(cnt)>V_bal
% constrains balloon volume to maximum inflated volume
        V(cnt) = V_bal;
    end
    d(cnt) = 2*((3/4)*V(cnt)/pi)^(1/3);
% balloon diameter (m)
    S(cnt) = pi*d(cnt)*d(cnt)/4;
% balloon projected area (m^2)
    A_proj(cnt) = pi*d(cnt-1)*d(cnt-1)/4;
% projected area of balloon (m^2)
    A_surf(cnt) = pi*d(cnt-1)*d(cnt-1);
% surface area of balloon
    P_gas(cnt) =  P(cnt);
% balloon pressure (kPa)
    if V(cnt) == V_bal
        P_gas(cnt) = m_gas*R_gas*T_gas(cnt)/V(cnt);
    end
    delta_P(cnt) = P_gas(cnt)-P(cnt);
% balloon super-pressure (kPa)


%%%ascent - flight properties%%%
    Fb(cnt) = (rho(cnt)*V(cnt))*g;
% buoyant force of balloon(N)
    F(cnt) = Fb(cnt) - W;
% free lift of balloon (N)
    if u(cnt)>=0
        D(cnt) = rho(cnt)*(u(cnt)^2)*Cd*S(cnt)/2;
% drag (N)
    end
    if u(cnt)<0
        D(cnt) = -rho(cnt)*(u(cnt)^2)*Cd*S(cnt)/2;
% drag (N)
    end
    a(cnt) = Fb(cnt)/m_sys - g - D(cnt)/m_sys;
% balloon acceleration (m/s^2)


%%%ascent - change in latitude%%%
    Ndist = Nwind(cnt-1)*delta_t/1000;
% distance traveled (km) N-S (N is +)
    phi = Ndist/(3376.20+(height(cnt)/1000));
% assumes reference ellipsoid polar radius of 3376.20km (in radians)
```

```
delta_LAT = phi*180/pi;
% converts change in latitude to degrees
LAT(cnt) = LAT(cnt-1) + delta_LAT;
if LAT(cnt)>90
    LAT(cnt)=90;
end
if LAT(cnt)<-90
    LAT(cnt)=-90;
end

%%%change in longitude%%%
Edist = Ewind(cnt-1)*delta_t/1000;
% distance traveled (km) E-W (E is +
theta = Edist/((3396.19+height(cnt)/1000))*cos(LAT(cnt-
1)*(pi/180));
% assumes reference ellipsoid equatorial radius of 3396.19km (in
% radians)
delta_LON = theta*180/pi;
% converts change in longitude to degrees
LON(cnt) = LON(cnt-1) + delta_LON;
if LON(cnt)=>-180
    LON(cnt)=LON(cnt)+360;
end
if LON(cnt)>180
    LON(cnt)=LON(cnt)-360;
end
end

end

fprintf('***BALLOON ASCENT COMPLETE***\n\n',);


%%%%%%%%%%%%%%%%%%%%%%%%%%%%%%%%%%%%%%%%%%%%%%%%%%%%%%%%%%%%%%%%%
%%%%%%%%%%%%%%%%%%%%%%%%%%%%%%%%%%%%%%%%%%%%%%%%%%%%%%%%%%%%%%%%%
%%%%
%%%                    BALLOON FLOAT                        %%%
%%%
%%%%%%%%%%%%%%%%%%%%%%%%%%%%%%%%%%%%%%%%%%%%%%%%%%%%%%%%%%%%%%%%%
%%%%%%%%%%%%%%%%%%%%%%%%%%%%%%%%%%%%%%%%%%%%%%%%%%%%%%%%%%%%%%%%%

%%%%%%%%%%%%%%%%%%%%%%%%%%%%%%%%%%%%%%%%%%%%%%%%%%%%%%%%%%%%%%%%%
% import atmospheric profile for balloon float
%***THE NAME OF THE TEXT FILES WILL NEED TO MATCH THE textread
%***COMMAND
% F_T = atmospheric temperature (K)
% F_P = atmospheric pressure (initially Pa converted to kPa)
% F_rho = atmospheric density (kg/m^3)
% F_MOLAhgt = MOLA height (km)
% F_Ls = solar longitude (degrees)
% F_lat = latitude (degrees)
% F_lon = longitude (degrees)
% F_Ewind = east wind (m/s)
% F_Nwind = north wind (m/s)
% F_TERhgt = terrain height (km) relative to MOLA aeroid
% F_Tgrnd = local surface temperature (K)
% F_SigU = standard deviation in wind (m/s)
% F_mu0 = cosine of solar zenith angle
```

```
%
% It should be noted that the Mars_GRAM_05 output data is arranged
% according to UTC time with 24 hr days.  Time conversion from UTC time
% to local solar time is not included in this program and will need to
% utilize a secondary method.
%%%%%%%%%%%%%%%%%%%%%%%%%%%%%%%%%%%%%%%%%%%%%%%%%%%%%%%%%%%%%%%%%%%%%%%%%%

F_albedo = textread('albedo.txt','%f');
F_T = textread('T.txt','%f');
F_P = textread('P.txt','%f');
F_P = F_P/1000;
% convert pressure to kPa
F_rho = textread('rho.txt','%f');
F_MOLAhgt = textread('MOLAhgt.txt','%f');
F_lat = textread('LAT.txt','%f');
F_lon = textread('LON.txt','%f');
F_Ewind = textread('Ewind.txt','%f');
F_Nwind = textread('Nwind.txt','%f');
F_TERhgt = textread('TERhgt.txt','%f');
F_Tgrnd = textread('Tgrnd.txt','%f');
F_SigU = textread('SigU.txt','%f');
F_mu0 = textread('mu0.txt','%f');

%%%convert longitude database from W+ to E+%%%
for i=1:length(F_lon)
    if F_lon(i)<180
        F_lon(i)=-F_lon(i);
    else
        F_lon(i)=-F_lon(i)+360;
    end
end

%%%%%%%%%%%%%%%%%%%%%%%%%%%%%%%%%%%%%%%%%%%%%%%%%%%%%%%%%%%%%%%%%%%%%%%%%%
% calculate float properties as a function of time
%%%%%%%%%%%%%%%%%%%%%%%%%%%%%%%%%%%%%%%%%%%%%%%%%%%%%%%%%%%%%%%%%%%%%%%%%%

fprintf('***BALLOON FLOAT START***\n\n')

%%%set balloon float calculation initial criteria%%%
sol = ceil((t(cnt)-t_start)/88775.24409);
% number of sols since balloon is launched
%%%%%%%%%%%%%%%%%%%%%%%%%%
delta_t = delta_t*10;
% increases time step for 10x coarser resolution during float
%%%%%%%%%%%%%%%%%%%%%%%%%
fprintf('delta_t change over:\n')

%%%initialize balloon film temps for thermal calculations %%%
T_bal_top = T_gas(cnt);
% assumes at end of float T_gas is equal to ambient T and
T_bal_bot = T_gas(cnt);
% no difference between top and bottom of balloon (there will

% be a small discontinuity in balloon temp here)
while sol<(sol_max+1)
    cnt = cnt+1;
```

```
%%%locate balloon properties in atmospheric database%%%
    sol = floor((t(cnt-1)+t_start)/88775.24409);
% number of sols since balloon launch sol - starting sol is sol 0
    day = floor((t(cnt-1)+t_start)/86400);
% number of days since balloon luanch (for location in database)
    time = floor((((t(cnt-1)+t_start) - day*86400)/3600);
% time step of Mars atmosphere database (24 timesteps per day - i.e.
% current UTC hour)
    current_height = round(height(cnt-1)/100)/10;
% converts to km and rounds to nearest tenth to match database

%%%code to speed up sorting through database%%%
    cnt_start = (day)*2400000 + (time)*100000 + 10*(current_height-
7.5)*2701 + 1;

%%%calculate balloon float%%%
    t(cnt) = t(cnt-1)+delta_t;
% time (s)
    u(cnt) = u(cnt-1) + a(cnt-1)*delta_t;
% vertical velocity (m/s)
    height(cnt) = height(cnt-1) + u(cnt-1)*delta_t;
% height (m)
    h(cnt) = round(height(cnt));
% height round to nearest meter

%%%local planetary and atmospheric properties%%%
    found = 0;
    i = cnt_start - 1;
    round(height(cnt-1)/100)/10;
    round(LAT(cnt-1)/5)*5;
    lonCOMP = round(LON(cnt-1)/5)*5;
% longitude value to compare against database
    if lonCOMP<=-180
        lonCOMP=lonCOMP+360;
    end
    if lonCOMP>180
        lonCOMP=lonCOMP-360;
    end
    while found == 0
        i = i+1;
        i = int32(i);
%this is to fix an error that kept saying index must be positive
%integer
        if F_MOLAhgt(i) == round(height(cnt-1)/100)/10
            if F_lat(i) == (round(LAT(cnt-1)/5)*5)
                if F_lon(i) == lonCOMP
                    albedo(cnt) = F_albedo(i);
% local planetary albedo
                    T(cnt) = F_T(i);
% ambient temperature (K)
                    P(cnt) = F_P(i);
% ambient pressure (kPa)
                    rho(cnt) = F_rho(i);
% ambient density (kg/m^3)
```

```
                            Ewind(cnt) = F_Ewind(i);
% ambient east wind (m/s)
                            Nwind(cnt) = F_Nwind(i);
% ambient north wind (m/s)
                            TERhgt(cnt) = F_TERhgt(i);
% local MOLA terain height (km)
                            Tgrnd(cnt) = F_Tgrnd(i);
% surface temperature (K)
                            SigU(cnt) = F_SigU(i);
% wind standard deviation (m/s)
                            mu0(cnt) = F_mu0(i);
% local cosine of the solar zenith angle
                        found = 1;
                    end
                end
            end
        end


%%%balloon float - account for standard deviation in wind%%%
    if pos_sigma == 1
        Ewind(cnt) = Ewind(cnt)+SigU(cnt)*mult_sigma;
% east wind + standard deviation (m/s)
        if LAT(cnt-1) < 90
            Nwind(cnt) = Nwind(cnt)+SigU(cnt)*mult_sigma;
% north wind + standard deviation (m/s)
        end
    end
    if neg_sigma == 1
        Ewind(cnt) = Ewind(cnt)-SigU(cnt)*mult_sigma;
% east wind - standard deviation (m/s)
        if LAT(cnt-1) > -90
            Nwind(cnt) = Nwind(cnt)-SigU(cnt)*mult_sigma;
% north wind - standard deviation (m/s)
        end
    end


%%%balloon thermal properties%%%

%*** define properties of lifting gas from table ***
%***      based on temperature of lifting gas     ***
    T_gas(cnt) = T_gas(cnt-1);
% hydrogen inlfation gas temperature
    T_table_check = T_gas(cnt)/50;
% code to round T_gas to nearest 50
    T_table_check = ceil(T_table_check);
    T_table_check = T_table_check*50
    if T_table_check == 150
        lambda = 0.129
% hydrogen thermal conductivity (W/m-K)
        mu = 5.56E-6
% hydrogen viscosity (kg/m-s)
        Pr = 0.70;
% hydrogen Prandtl Number
    end
    if T_table_check == 200
```

```
        lambda = 0.157
% hydrogen thermal conductivity (W/m-K)
        mu = 6.78E-6
% hydrogen viscosity (kg/m-s)
        Pr = 0.70;
% hydrogen Prandtl Number
    end
    if T_table_check == 250
        lambda = 0.176
% hydrogen thermal conductivity (W/m-K)
        mu = 7.90E-6
% hydrogen viscosity (kg/m-s)
        Pr = 0.69;
% hydrogen Prandtl Number
    end
    if T_table_check == 300
        lambda = 0.194
% hydrogen thermal conductivity (W/m-K)
        mu = 8.95E-6
% hydrogen viscosity (kg/m-s)
        Pr = 0.69;
% hydrogen Prandtl Number
    end
    del_Tbal = abs(T_bal_top-T_gas(cnt-1));
% difference in temp between balloon film and lifting gas (K)
    Gr = g*(rho_g(cnt-1)^2)*(del_Tbal)*((d(cnt-1)/2)^3)/T_gas(cnt-
1)/mu/mu;
% Grashof number
    if (Gr*Pr) < 2E7
        Nu = 0.54*(Gr*Pr)^(1/4);
% Nusselt number
    else
        Nu = 0.135*(Gr*Pr)^(1/3);
% Nusselt number
    end
    h_conv = Nu*lambda/d(cnt-1)
% convective heat transfer coefficient (W/m^2-K)

    gas_Temp_check = 1;
    while abs(gas_Temp_check) > 1.e-2
        I_sun =
P_sun/4/pi/(D_sun(day+1)*149598200000)/(D_sun(day+1)*149598200000);%
Solar Constant (W/m^2)

%%% T_bal_top %%%
%%% Newton Raphson Method - IT SHOULD BE NOTED x1 WILL NEED TO BE %%%
%%%             PICKED SO THAT THE SOLUTION CONVERGES             %%%
        fn='(3.1416*d(cnt-1)*d(cnt-
1)/2)*((1+mu0(cnt))*alpha_top*I_sun*(albedo(cnt)+1)/4 +
h_conv*(T_gas(cnt)-x) - sigma*epsilon_top*(x^4-20^4))';
        gn=diff(fn);
        x1=T_gas(cnt);
% initial balloon top film temperature guess
        x=x1;
        n=0;
        while abs(eval(fn)) > 1.e-6
```

```
            x=x1;g1=eval(gn);
            x=x1;f1=eval(fn);
            x2=x1-f1/g1;
            x1=x2;
            x=x1;
            n=n+1;
            f=eval(fn);
        end
        T_bal_top = x;


%%% T_bal_bot %%%
%%% Newton Raphson Method - IT SHOULD BE NOTED x1 WILL NEED TO BE %%%
%%%            PICKED SO THAT THE SOLUTION CONVERGES             %%%
        fn='(3.1416*d(cnt-1)*d(cnt-1)/2)*((1-
mu0(cnt))*alpha_bot*I_sun*(albedo(cnt)+1)/4 + h_conv*(T_gas(cnt)-x) -
sigma*epsilon_bot*(x^4 - Tgrnd(cnt)^4))';
        gn=diff(fn);
        x1=T_gas(cnt);
% initial balloon bottom film temperature guess
        x=x1;
        n=0;
        while abs(eval(fn)) > 1.e-6
            x=x1;g1=eval(gn);
            x=x1;f1=eval(fn);
            x2=x1-f1/g1;
            x1=x2;
            x=x1;
            n=n+1;
            f=eval(fn);
        end
        T_bal_bot = x;

        T_gas_old = T_gas(cnt);
        T_gas(cnt) = (T_bal_top+T_bal_bot)/2;
        gas_Temp_check = T_gas_old - T_gas(cnt);
    end


%%%balloon properties%%%
    V(cnt) = m_gas*R_gas*T_gas(cnt)/P(cnt);
% balloon volume (m^3)
    if V(cnt)>V_bal
% constrains balloon volume to maximum inflated volume
        V(cnt) = V_bal;
    end
    d(cnt) = 2*((3/4)*V(cnt)/pi)^(1/3);
% balloon diameter (m)
    S(cnt) = pi*d(cnt)*d(cnt)/4;
% balloon projected area (m^2)
    P_gas(cnt) =  P(cnt);
% balloon pressure (kPa)
    if V(cnt) == V_bal
        P_gas(cnt) = m_gas*R_gas*T_gas(cnt)/V(cnt);
    end
    delta_P(cnt) = P_gas(cnt)-P(cnt);
% balloon super-pressure (kPa)
```

```
%%%flight properties%%%
    Fb(cnt) = (rho(cnt)*V(cnt))*g;
% buoyant force of balloon(N)
    F(cnt) = Fb(cnt) - W;
% free lift of balloon (N)
    if u(cnt)>=0
        D(cnt) = rho(cnt)*(u(cnt)^2)*Cd*S(cnt)/2;
% drag (N)
    end
    if u(cnt)<0
        D(cnt) = -rho(cnt)*(u(cnt)^2)*Cd*S(cnt)/2;
% drag (N)
    end
    a(cnt) = Fb(cnt)/m_sys - g - D(cnt)/m_sys;
% balloon acceleration (m/s^2)

%%%change in latitude%%%
    Ndist = Nwind(cnt-1)*delta_t/1000;
% distance traveled (km) N-S (N is +)
    phi = Ndist/(3376.20+(height(cnt)/1000));
% assumes reference ellipsoid polar radius of 3376.20km (in radians)
    delta_LAT = phi*180/pi;
% converts change in latitude to degrees
    LAT(cnt) = LAT(cnt-1) + delta_LAT;
    if LAT(cnt)>90
        LAT(cnt)=90;
    end
    if LAT(cnt)<-90
        LAT(cnt)=-90;
    end

%%%change in longitude%%%
    Edist = Ewind(cnt-1)*delta_t/1000;
% distance traveled (km) E-W (E is +)
    theta = Edist/((3396.19+(height(cnt)/1000))*cos(LAT(cnt-
1)*pi/180));
% assumes reference ellipsoid equatorial radius of 3396.19km (in
% radians)
    delta_LON = theta*180/pi;
% converts change in longitude to degrees
    LON(cnt) = LON(cnt-1) + delta_LON;
    if LON(cnt)<=-180
        LON(cnt)=LON(cnt)+360;
    end
    if LON(cnt)>180
        LON(cnt)=LON(cnt)-360;
    end

end

%%%%%%%%%%%%%%%%%%%%%%%%%%%%%%%%%%%%%%%%%%%%%%%%%%%%%%%%%%%%%%%%%%%%%%%
% write results to file
%%%%%%%%%%%%%%%%%%%%%%%%%%%%%%%%%%%%%%%%%%%%%%%%%%%%%%%%%%%%%%%%%%%%%%%

RESULTS = [t' height' TERhgt' V' u' rho' T' P' T_gas' P_gas' delta_P'
LAT' LON'];
```

```
%open the file to write to with write permission
fid = fopen('MABL_output.txt','wt');
for i=1:length(RESULTS)
    fprintf(fid,'%8.5f %8.5f %8.5f %8.5f %8.5f %8.5f %8.5f %8.5f %8.5f
%8.5f %8.5f %8.5f %8.5f\r\n', RESULTS(i,:));
end
fclose(fid);


%%%%%%%%%%%%%%%%%%%%%%%%%%%%%%%%%%%%%%%%%%%%%%%%%%%%%%%%%%%%%%%%%%%%%%%%%%%
% end
%%%%%%%%%%%%%%%%%%%%%%%%%%%%%%%%%%%%%%%%%%%%%%%%%%%%%%%%%%%%%%%%%%%%%%%%%%%
```

VITA

Sean Michael Hancock

Department of Mechanical and Aerospace Engineering

Old Dominion University

Norfolk, VA

EDUCATION

B.S. Mechanical Engineering, Old Dominion University, May, 2008

HONORS AND AWARDS

NASA ESMD Systems Engineering Paper Competition 3rd Place:

"Sustainable Mars Sample Return"

ODU Faculty Award for Academic Excellence in Engineering

ODU Faculty Award in Mechanical Engineering

Tau Beta Pi Engineering Honor Society

ASSOCIATION MEMBERSHIPS

American Institute of Aeronautics and Astronautics

Aircraft Owners and Pilots Association

PROFESSIONAL EXPERIENCE

Senior Engineer – SSAI contracted to NASA Langley Research Center

Hampton, VA, May 1010 to Present

Plant Engineer - ALCOA POWER AND PROPULSION,

Hampton, VA, June 2008 to May 2010

Application/Sales Engineer - UNICON SERVICES, INC.

Vienna, VA, September 2004 to June 2008

RESEARCH EXPERIENCE

Balloon Systems for Robotic Bases on Mars – Old Dominion University

Hypersonic Inflatable Aerodynamic Decelerators – SSAI / NASA LaRC

ISRU CO_2 Powered Rocket Test Stand – Old Dominion University

Parametric CFD Study of Microaerodynamic Drag Generators – Old Dominion University